Quarterly Newsletter

Editorial – January 2008

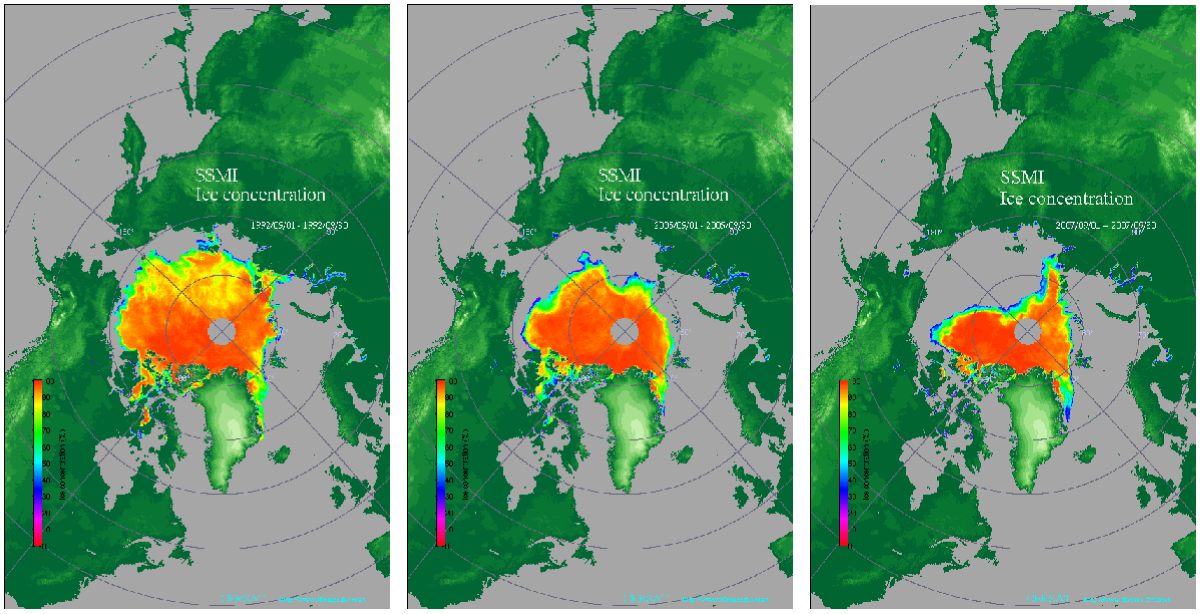

September monthly mean sea ice concentration (%) in the Arctic Ocean in 1992 (left), 2005 (middle) and 2007 (right). Arctic Ocean sea ice is receding: 1.5 millions of km2 of ice area have been melting during the summer of 2007 in comparison with the former 2005 summer minimum.

Credits: Ifremer/CERSAT, ftp://ftp.ifremer.fr/ifremer/cersat/products/gridded/psi-concentration

Greetings all,

As we, in the northern hemisphere in Toulouse, go further into the winter and the cold, the Mercator-Ocean newsletter goes towards even higher latitudes. The 2007-2008 International Polar Year (IPY) which started last March, marks the opportunity for us to review the state of the art on Polar research. The 2007-2008 IPY emphasizes the need to capture the contemporary and significant changes occurring in Polar Regions. It provides a crucial benchmark for detecting and understanding changes in comparison with past and future data sets and will improve the observational system for a better monitoring of polar areas.

The 2007-2008 IPY celebrates respectively the 125th, 75th and 50th anniversaries of the first and second IPYs and first IGY. Indeed, the first IPY took place in 1882-1883 and its key concept was that geophysical phenomena could not be surveyed by one nation alone and that it would require a coordinated international effort. Twelve countries participated, and fifteen expeditions to the poles were completed (13 to the Arctic, and 2 to the Antarctic). The second IPY took place in 1932-1933 and investigated the global implications of the newly discovered "Jet Stream" and to what extent Polar observations could improve weather forecasts. Forty nations participated and forty permanent observation stations were established in the Arctic. In Antarctica, the U.S.A. established the first research station inland from Antarctica's coast. The International Geophysical Year

(IGY) then took place in 1957-58 and celebrated the 75th and 25th anniversaries of the first and second IPYs. A notable political result founded during the IGY was the ratification of the Antarctic Treaty in 1961.

This newsletter is introduced by an article by Gascard, who presents the DAMOCLES program in the Arctic Ocean where 1.5 millions of km2 of ice area melted during the summer of 2007 in comparison with the former 2005 summer minimum (see figure). The next article by Garric et al. is dealing with the sea ice in the Mercator-Ocean Global 1/4° system assimilating Sea Surface Temperature, Temperature and Salinity in situ profiles, and Sea Level Anomalies, using the LIM2 sea ice model (Louvain-la-Neuve Ice Model, version 2). Then comes the description of the new LIM3 sea ice model by Vancoppenolle et al. Mathiot et al. follow with a description of the sensibility of polynyas to atmospheric forcing. Girard-Ardhuin et al. are describing the sea ice concentration and drift products developed at Ifremer/CERSAT. And last but not the least is an article that gathers 5 international contributions on data assimilation of ice concentration and/or drift.

The next April 2008 newsletter papers will review the current work on global ocean forecast systems. We wish you a pleasant reading.

Contents

The integrated European project Damocles and the International Polar Year

***By Jean-Claude Gascard*[1]**

[1] Senior scientist at CNRS, LOCEAN (UPMC), 4 place Jussieu, 75252 Paris, France

The International Polar Year that began officially on March 1st, 2007, is a great opportunity for enhancing scientific research activities in Polar Regions. The European Union is participating actively to that effort with the integrated project Damocles in order to develop our capabilities for observing and modelling the Arctic Ocean and better predict its short, medium and long-term evolution. Earth Global warming, mainly due to an increase in Greenhouse Gas concentration, is more intense at the Poles than at the Equator, especially in the northern hemisphere. In the Polar Regions, the temperature increase is mainly due to the albedo positive feedback of the ice and snow that is very high (0.8) compared to the ocean albedo that is very low (0.2). Important changes were recently observed in the Arctic. First of all there was a spectacular retreat of the sea-ice cover at the end of the 2007 summer season with a loss of 1.5 million square kilometers by comparison with the previous record minimum in 2005. Secondly, we noted a very significant increase of the speed of the transpolar sea-ice drift that shortened the Tara Damocles mission by more than 8 months. Indeed the French schooner Tara voluntarily frozen in sea-ice in the northern Laptev Sea (79.53°N and 143°E) on September 3, 2006, crossed Fram Strait at about 80°N and 3°W on December 9, 2007, after 460 days instead of 2 years as initially predicted using 20 years of sea-ice drift statistics from the International Arctic Buoy Program (IABP).

A close look at the lower atmosphere by means of satellites and ground truth measurements revealed a significant warming mainly during the fall. Estimated in number of freezing degrees days during the whole freezing season extending from September to May the following year, it appears that this cumulative number has decreased by about 1000°C during the past 20 years corresponding to a loss of 1meter of ice thickness. In contrast, the melting season is characterized by a high interannual variability corresponding to +/-20cm of ice thickness variability. The sea level pressure field does not fit with any scheme such as the Arctic Oscillation and/or the North Atlantic Oscillation. Indeed it appears that the dominant scheme corresponds now to a low pressure system over Eurasia and Siberia and a high pressure system extending from Greenland to Alaska. Consequently, warm and humid air masses from the northern Pacific, driven over the Polar regions, enhanced the arctic sea-ice transpolar drift, entraining warm and fresh water masses through the Bering Strait into the Arctic Ocean. This is also increasing significantly the ocean heat flux for melting a lot of ice. All this information was confirmed by recent observations. The most surprising is that none of the actual models were able to predict that an extreme event like the 2007 summer minimum extent would happen so rapidly.

A closer look at the past 15 years could have triggered some warning. Indeed one of the peculiarities of the Arctic Ocean in contrast with the Antarctic Ocean is that it produces multiyear ice floes that we call perennial ice. This ice type resists the summer melting process and is accumulated over several winters (at least one winter) if it does not exit the Arctic Ocean in the mean time. The perennial ice is very different from the first year ice. It is usually thicker, more deformed and less salty than the young ice. Exposed to active and/or passive microwave sensors (usually airborne and/or spaceborne sensors), old ice is easily distinguishable from young ice except when sea ice is covered by melt ponds like during the summer season. Because of the global warming, the arctic perennial ice is an endangered species and it is quite important to look after its seasonal cycle and interannual variability. Over the past 15 to 20 years, we observed several anomalies all very critical for the arctic multiyear ice survival. These anomalies are mainly due to a less intense freezing season (in particular during the Fall period) producing i) less ice furthermore becoming more and more vulnerable to the summer melt and ii) also more ice to exit the Arctic Ocean through Fram Strait, the northern Barents Sea and the Canadian archipelago due to a change in wind pattern forcing. The snow and ice versus ocean positive albedo feedback is also enhancing the local warming since more heat stored in the upper ocean needs to be extracted by the atmosphere before the freezing season gets a chance to start again. In fact we observed that the onset of freezing in the Arctic was more and more delayed due to this albedo feedback.

During the 2005 summer season, characterised by the absolute record for summer sea-ice minimum extent prior to 2007, we noticed a very unusual event characterized by a quasi disappearance of all the young ice formed during the previous winter. This was partly due to an abnormal wind pattern contributing to force young ice to exit the Arctic Ocean prematurely. Consequently, no second year ice could replenish the Arctic Ocean and balance the loss of multiyear ice floes that exited the Arctic Ocean (mainly through Fram Strait) during the whole year. This is a very efficient mechanism in retarding the onset of freezing and accelerating the weakening of the arctic sea-ice pack. In addition, during the 2007 fall season, we noticed air temperatures 10°C above the mean seasonal values in the western arctic that remained an ice free ocean during most of the 2007 summer season. This winter the arctic sea-ice is starting with a strong handicap that will be difficult to compensate during the remaining part of the winter-spring season unless there would be a drastic change in the climatological situation which

seems very unlikely. There are many reasons to think that the 2008 summer will establish a new record in Arctic Sea-Ice minimum extent.

Damocles, a European integrated project coordinated by France, is one of the pilot projects of the European Union for the International Polar Year. 48 laboratories spread over 10 European countries involving also the Russian federation and the USA (the Search for Damocles project), are engaged in this project. Damocles is a sea-ice centric project dedicated to the Arctic sea-ice situation and evolution, implying an important observational program of the upper ocean, lower atmosphere, sea-ice as well as data assimilation and integration in numerical models (including Numerical Weather Prediction models). Damocles is also involved in an important effort for high tech development adapted to the Arctic harsh environment and long-term monitoring. Damocles is a four year program (2005-2009) in phase with the International Polar year (2007-2008). The first year Damocles field season (2007) coincided with an extreme retreat of the arctic sea-ice cover. This first year field season was highlighted by the transpolar drift of the French schooner Tara emulating the ground breaking Fram expedition that occurred 112 years ago. The major aspects concerning Damocles and related programs are: (1) the seasonal cycle and the interannual variability of the Arctic sea-ice (multi year, first and second year ice) and the contribution of the second year ice to replenish the Arctic Ocean with multi year ice at the end of each summer season, (2) the drastic acceleration of the transpolar drift mainly due to the sea-ice thinning (50%) observed during the past 20 years and also to the change in the atmospheric circulation and weather patterns over the Arctic with low pressure systems developing over most of Eurasia and Siberia in contrast with high pressure systems extending from Greenland to Alaska, (3) the significant warming of the lower atmosphere in particular during the Fall season in the western Arctic delaying the onset of freezing, (4) the increase of the melting season, (5) the increase of heat fluxes advected by ocean currents of Atlantic and Pacific origins, and (6) the increase of heat fluxes advected by the atmospheric circulation (storms) due to a weakening of the polar vortex. In July 2007, we observed air temperatures above +10°C between 800m and 1500m altitude near the North Pole during the Tara Damocles mission. 2008 will be an interesting and critical year to observe and to better understand the evolution of the Arctic climate system in the context of a profound transformation of the Arctic Ocean having strong potential impacts on Arctic ecosystems and human populations.

Preliminary assessment of sea ice in the global ¼° Mercator Ocean forecasting system

By Gilles Garric[1], Nathalie Verbrugge[1], Sylvain Bouillon[2] and Martin Vancoppenolle[2]

[1] Mercator Ocean, 8-10 rue Hermes, Parc technologique du canal, 31520 Ramonville st Agne
[2] Institut d'Astronomie et de Géophysique G. Lemaître, Université Catholique de Louvain, Louvain-la-Neuve, Belgium

Introduction

This note gives us the opportunity to assess the sea ice in the global operational Mercator-Ocean system. Section 2 provides a full description of the sea ice component as well as a brief review of the forecasting system. We then give an evaluation of the sea ice extent from April to September 2007 in section 3. In section 4, we analyse an interannual experiment led with the same model in a forced run (without data assimilation). We present how the sea ice model is able to reproduce recent interannual variability, and especially the Arctic sea ice coverage decline. Recent work done to improve the sea ice representation at ¼° resolution is also presented in this section. Finally, prospects are briefly discussed in section 5.

Treatment of sea ice in the global ocean ¼° Mercator-Ocean forecasting system

From April 4th until October 2007, the target MERSEA (Marine EnviRonment and Security for the European Area, http://www.mersea.eu.org) ¼° global forecasting system (hereafter Global V2), implemented by Mercator-Ocean, was delivering products operationally. Compared to the previous version of the system (Global V1 launched in October 2005), two main components, i.e. the assimilation scheme and the model configuration, have been replaced. The operational processing of atmospheric forcing fields and input data, as well as the processing of outputs, for display and distribution of the ocean analyses and forecasts remain unchanged. The reader can refer to (Drevillon *et al.*, 2006) and (Drevillon *et al.*, 2007) for a description of the system components, i.e. the oceanic model and the data assimilation scheme.

The sea ice is fully comprehensive with the implementation of the LIM2 model. A short description of the current version of this model is given here. Further details of an earlier version can be found in (Fichefet and Maqueda, 1997, 1999), in (Goosse and Fichefet, 1999) and in the CLIO users' guide (Goosse *et al.*, 2001), or in the webpage http://www.astr.ucl.ac.be/research/.

Sensible heat storage and vertical heat conduction within snow and ice are determined by a three-layer model (one layer for snow and two layers for ice) based on the (Semtner, 1976) solution. The effect of the sub grid-scale snow and ice thickness distribution is accounted for through an effective thermal conductivity, which is computed by assuming that the snow and ice thicknesses are uniformly distributed between zero and twice their mean value over the ice-covered portion of the grid cell. The storage of latent heat inside the ice resulting from the trapping of shortwave radiation within brine pockets is taken into account. The parameterization of the surface albedo is that of (Shine and Henderson-Sellers, 1985), combined with the modifications for clear and overcast conditions recommended by (Greenfell and Perovich, 1984). This albedo formulation takes into consideration the state of the surface (frozen or melting) and the thickness of the snow and ice cover. The model also allows for the presence of leads within the ice pack. Vertical and lateral growth/decay rates of the ice are obtained from prognostic energy budgets at both the bottom and surface boundaries of the snow-ice cover and in leads. The snow-ice formation process is also parameterized (Fichefet and Maqueda, 1999).

For the momentum balance, sea ice is considered as a two-dimensional continuum in dynamical interaction with atmosphere and ocean. The viscous-plastic constitutive law proposed by (Hibler, 1979) with modifications described in (Kreyscher *et al.*, 2000) is used for computing the internal ice force. The ice strength is taken as a function of the ice thickness and compactness (Hibler, 1979).

This model has been largely evaluated (Fichefet and Maqueda, 1997, 1999; Goosse and Fichefet, 1999; Timmermann *et al.*, 2005). Furthermore, LIM2 ranks among the most comprehensive large-scale thermodynamic-dynamic sea ice models existing nowadays. It has shown its ability to represent in a realistic manner the annual cycle of the sea ice growing and melting processes either in atmospheric driven configuration (Timmermann *et al.*, 2005), either in coupled atmosphere/ocean configuration (Parkinson *et al.*, 2006a, b).

Resolution-dependent parameters have been fitted to our configuration. These concern mainly: 1) the eddy diffusivity coefficient set to 150 $m^2.s^{-1}$, 2) the ice thickness of newly formed ice in the leads set to 1m in both hemispheres and 3) the drag coefficient for oceanic stress set to 1.10^{-2}. In order to prevent peculiar instabilities observed in the sea ice/ocean coupling, the oceanic velocities in the ocean/sea ice momentum flux have been crudely set to zero at the moment.

Before starting delivering ocean and sea ice forecasts operationally every week, the Global V2 has been run from the 3rd of January 2007 up to the 4th of April 2007. This numerical experiment was meant to spin up and tune the system. The initial conditions are averaged January climatological conditions from (Levitus et al., 1998) for ocean and from a previous ORCA05_LIM (0.5° horizontal resolution configuration) climatological run for sea ice (concentration, thickness and temperature). Ocean and sea ice are considered at rest at the beginning of the run. The system takes about three months to cumulate statistics that are necessary for the data assimilation process. As no data assimilation is implemented yet in the sea ice model, these three months remain very short for sea ice to reach a balanced seasonal cycle, particularly in the Arctic Basin. However, the sea ice model in the Global V2, constrained by the surrounding Global V2 Ocean which includes data assimilation towards observations, may be balanced faster at his oceanic interface. Moreover, the Global V2 is the first to our knowledge proposing sea ice variables forecasts for both Arctic and Antarctic areas. We do not present here results based on the sea ice forecasts skills as this work is not accomplished yet. All the results shown here are issued from the best estimates daily outputs, i.e. the D-14 days before the forecasts. Although we present our results for both hemispheres, this note is more dedicated to the Arctic Ocean.

Evaluation of Sea ice in the Mercator-Ocean operational system from April 2007 to September 2007

In order to have a coordinated assessment of all the MERSEA systems in the Arctic region, and in consultation with the NERSC (Nansen Environmental and Remote Sensing Center, Norway) and the UKMO (United Kingdom Meteorological Office, United Kingdom), Arctic metrics have been defined (Bertino *et al.*, 2006). Such metrics have also been proposed in the scope of the GODAE (Global Ocean Data Assimilation) intercomparison Project. We have developed sea ice diagnostics in several sub regions of the Arctic (Figure 1) which are chosen using dynamical or/and geographical considerations. All the oceanic surfaces likely to be covered by sea ice are considered. Mercator-Ocean has also defined sub regions in Antarctica (Figure 1).

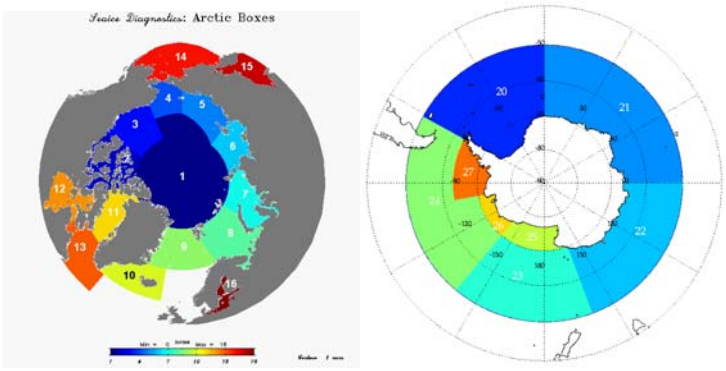

Figure 1

(Left) Arctic boxes defined in the framework of the MERSEA/GODAE projects. (Right) Antarctic boxes used in the Mercator-Ocean system.

The Global V2 has been compared to the daily CERSAT Sea Ice Concentration (SIC hereafter) satellite product (see F. Girard-Ardhuin *et al.* in this issue and (Ezraty *et al.*, 2007)), where we have kept the coastal areas values flagged by the CERSAT quality control in addition to the area covered by sea ice in the open ocean. These data processing tools have been developed for the future production of Class4 diagnostics on the Sea Ice concentration field.

Figure 2 presents monthly means from Global V2 and CERSAT SIC in April and September 2007. Even if the modeled sea ice extent is too spread in both seasons for the Northern Hemisphere, the cycle of sea ice growth and decay over 2007 is realistically captured in both hemispheres. These sea ice overestimations are largely in the error brackets of the sea ice models widely used in the scientific community (see (Parkinson *et al.*, 2006a) for example). The Global V2 SIC overestimation is however particularly true in September 2007, because of the strong melting observed during the summer 2007 which ended with a new record minimum sea ice extent ($4.12.10^6$ km2 the 14th of September) for the years of the satellite record (Comiso *et al.*, 2008). These overestimations are essentially located in the marginal ice zones: a) the North Atlantic and Pacific during the spring, b) the Beaufort, Chukchi, Laptev, Kara and Barents seas during the summer. The presence of sea ice during summer 2007 in the Global V2 in the Canadian Archipelago prevents the Northwest Passage from being free. We can note the lack of sea ice in the Global V2 along the South-Eastern coast of Greenland and in the South-Eastern area of the Labrador Sea. The sea ice is closely linked to the presence of coastal currents in these zones. The absence of the oceanic velocities in the sea ice/ocean stress may explain the non advection of sea ice in these regions.

Figure 3 presents the differences of the SIC RMS (Root Mean Square) between the Global V2 and the CERSAT dataset in two sub regions. The SIC RMS is a measure of the total spatial error of the system by sub regions. We do not present RMS for all the boxes but the conclusions made for Box 1 (the North Pole area) and 4 (Chukchi Sea) give an overview of the Arctic behaviour. Figure (3) shows: (1) A good representation on the Central North Pole box (box 1) with a constant RMS difference along the period and, also, near-zero spatial mean error on the box and with ~10-15% of error (not shown), (2) A frequent increase of the errors at the end of the period (Ice melting period). We note a strong ice melting event at the beginning of June in the observations (box 4) which is underestimated and shown too late in the model, this is also true in boxes 3 and 11 (Beaufort Sea and Queen Elisabeth Islands, not shown), (3) A general over-estimation of the SIC in the model at the end of the period. (4) A general strong RMS error of the modelled SIC. The climatological sea ice extent field used to initialize the system in January 2007 shows a too far south sea ice extent especially along the Northern Atlantic sea ice margin (Figure 4). This excess may contribute to the excess of sea ice extent in the Global V2 at the beginning of the summer.

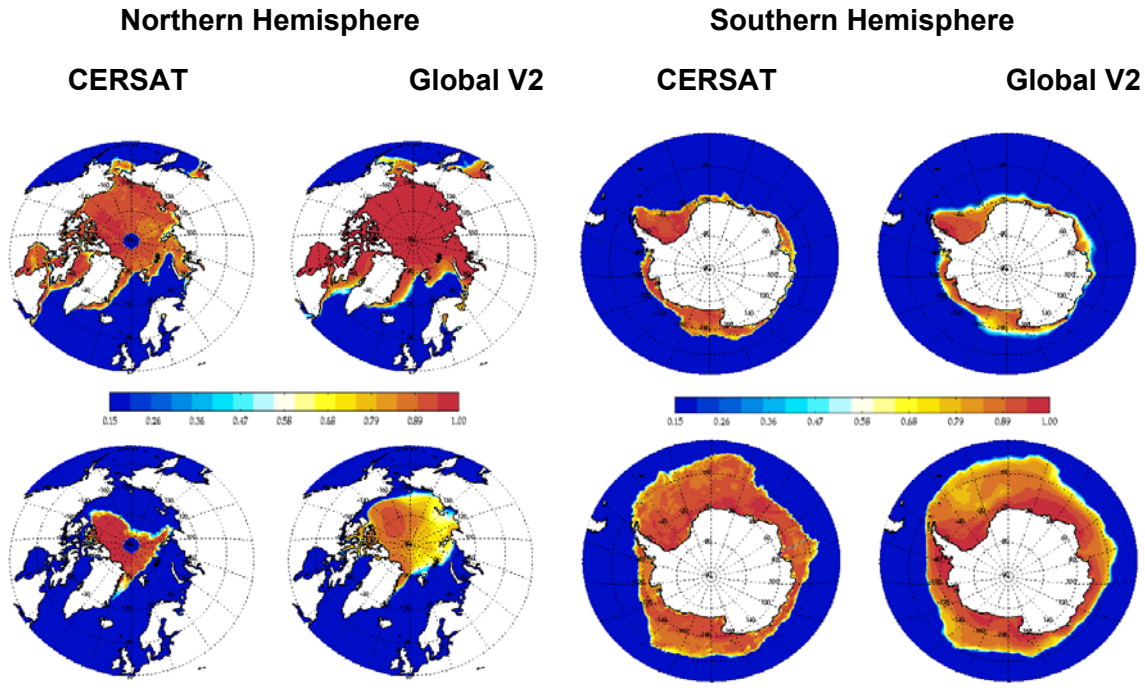

Figure 2

April (upper panels) and September (bottom panels) monthly means SIC (%) from the Mercator-Ocean Global V2 and the CERSAT in the Northern Hemisphere (left panels) and in the Southern Hemisphere (right panels). Note the missing data in the CERSAT dataset north of 87°N.

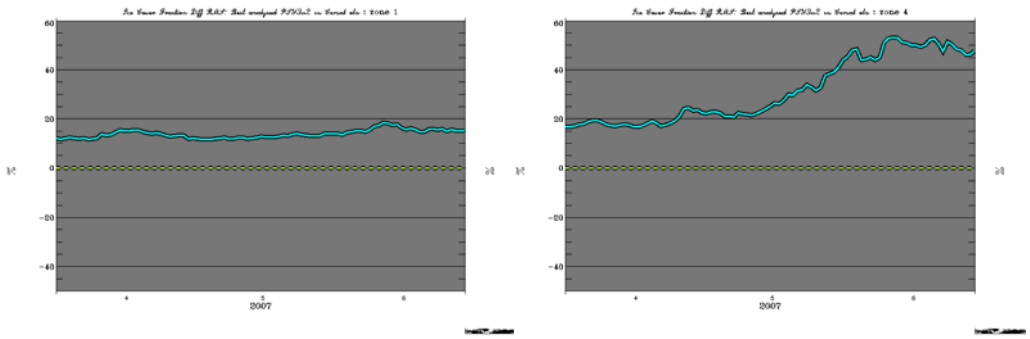

Figure 3

Global V2 versus CERSAT SIC (%) time series of the RMS difference for boxes 1 (North Pole; left) and 4 (Chukchi Sea, right panel) of the Arctic Region from April to June 2007.

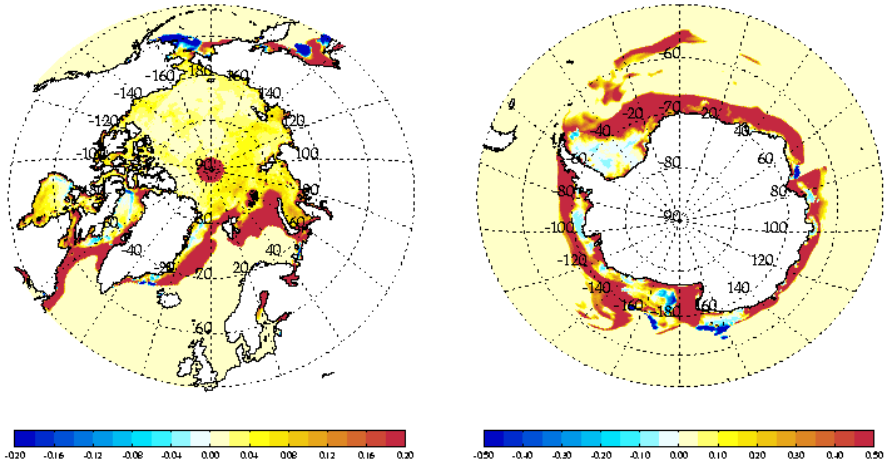

Figure 4

January monthly mean SIC differences (%) between initial conditions from the Global V2 and from CERSAT datasets in January for the Northern (left panel) and the Southern (right panel) hemispheres. 50°S is the northern limit for the Southern Hemisphere panels. Note the different colour scale between the two figures.

For boxes 1 and 4 and for two given dates at the beginning and the end of spring respectively, we have calculated probability density function (PDF hereafter) of the difference between model and CERSAT SIC (Figure 5). These two dates are representative of the absence or the delayed melting in the marginal ice zones (here the Chukchi Sea in summer) in the Global V2. A PDF peak centered on the zero value reveals a close accordance between the observations and the system. The analysis of the PDF plots shows common features with the time series analysis. Strongest biases are observed at the end of the period in the Beaufort and Chukchi Seas and in the Baffin Bay. In fact, ice melting in these regions is systematically underestimated. More generally, all the outlying regions of the central ice pack are impacted by this insufficient melting of sea ice, but in a lower extent for Siberian Sea, Laptev and Kara Seas. In Barents Sea and Greenland Basin, the ice cover is overestimated for the entire period, with little change in time. In summary in these areas, the sea ice extent limits in the Mercator-Ocean system are located too far south and east compared to CERSAT data.

The distribution of the PDF in the box 4 has a peak in high values revealing also a sea ice cover too compact in the marginal zones compared to the observations at the end of the spring. High compactness of sea ice cover is generally associated with significant sea ice thickness. This too compact discrepancy sea ice cover raises then the question of the local maximum (above 3m thick) in the sea ice thickness distribution of the Chukchi and Laptev seas used for the initial conditions in the Global V2 (Figure 6). The too thick sea ice cover prevents the strong atmospheric melting from occurring during summer 2007.

Another characteristic of the sea ice cover is the weak compactness in areas where perennial sea ice is expected, i.e. in the Central Arctic Ocean Basin (see Figure 2).

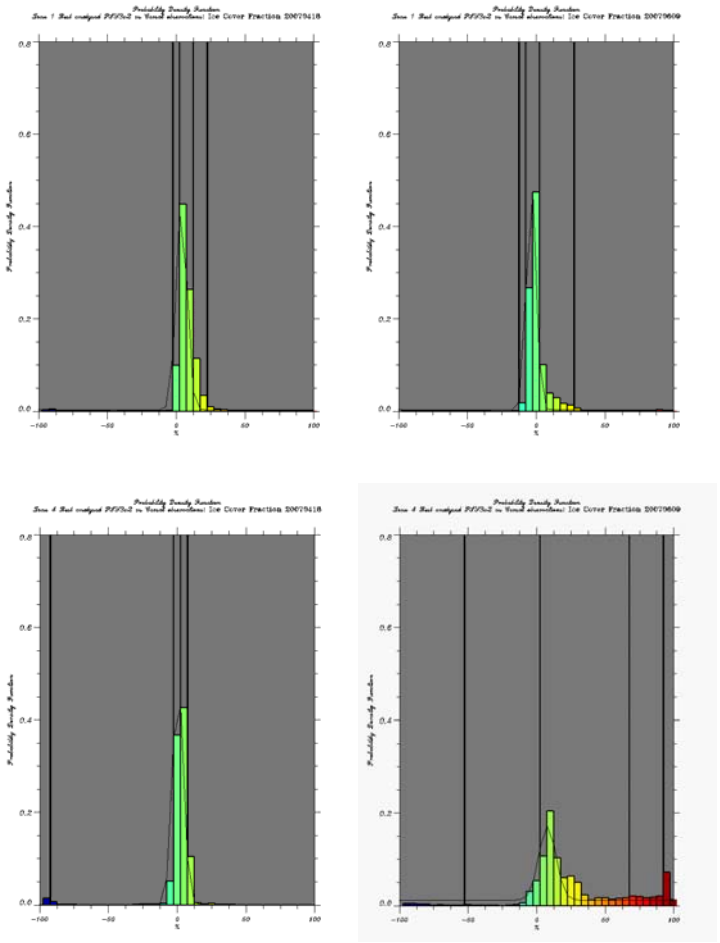

Figure 5

Probability Density Function of the difference between Mercator-Ocean Global V2 and CERSAT Sea Ice concentration (%) for box 1 (North Pole) (upper panels) and 4 (Chukchi Sea) (bottom panels) at the beginning (18th April 2007, left panels) and the end of the Spring (9th June 2007; right panels). Positive values indicate a higher SIC in the model.

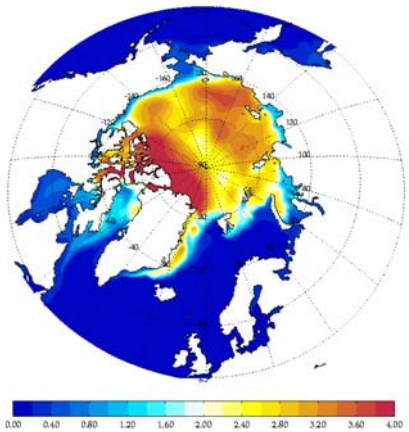

Figure 6

Sea ice concentration (%) and thickness (meter) initial conditions for the Global V2 in January 2007 for the Northern Hemisphere.

Although the synoptic patterns exhibited by the sea ice velocity in the Global V2 system follow closely those from the CERSAT datasets, the magnitude in the Global V2 remains much weaker than its observed counterpart (Figure 7). Moreover, the weaker

standard deviation of the sea ice velocity in the Global V2 compared to the CERSAT reveals less variability in the Global V2. Similarly, the analysis of the SIC signal variance for the Arctic area (not shown) shows less variability in the Mercator-Ocean system. Obvious in the Central pack, the strongest differences are located in the Baffin Bay and Beaufort, Chukchi, Siberian, Laptev, Kara and Barents Seas. The variance average on the entire domain for the Sea ice concentration is 463 ($\%^2$) for CERSAT observations, 148 ($\%^2$) for Mercator-Ocean system and 272 ($\%^2$) for the difference. The variance of the difference is lesser than the observed signal variance on the period analysed.

This lack of short-term variability may come from various reasons: (1) the potential source of oceanic variability through the momentum flux between ocean and sea ice is missing totally (2) the high compactness of the sea ice cover in the marginal zones may prevent meso-scales flows to develop freely.

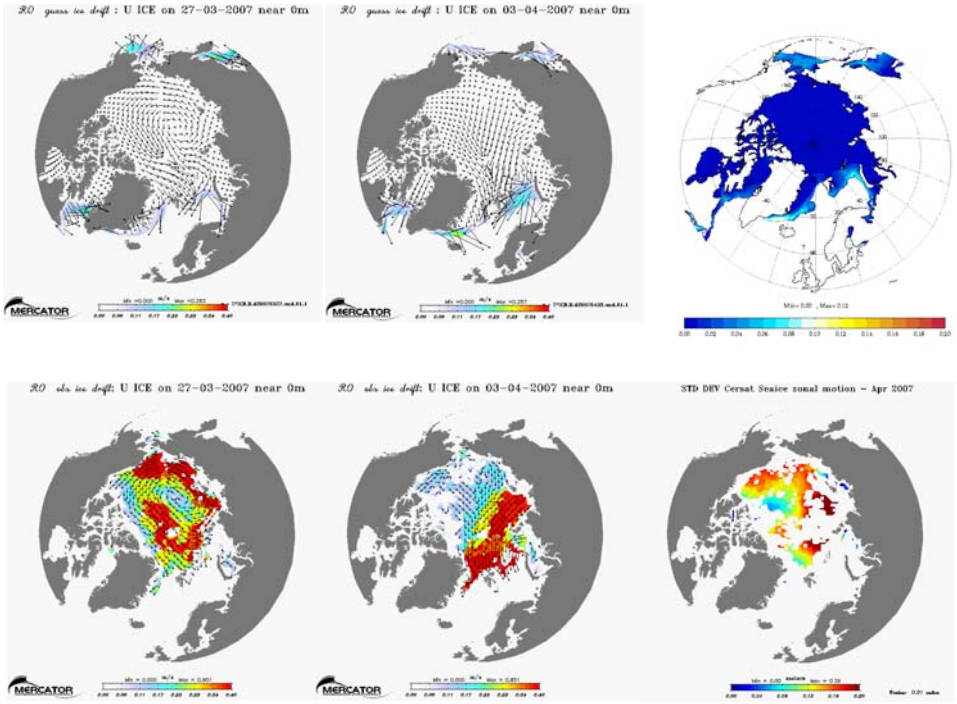

Figure 7

X-sea ice velocity component ($m.s^{-1}$) with superimposed sea ice velocity vectors on the 27th of March (Global V2: upper left; CERSAT: bottom left) and the 3rd of April 2007 (Global V2: middle upper; middle bottom). Mean April 2007 standard deviation ($m^2.s^{-2}$) of the X-sea ice velocity component for the Global V2 (upper right) and for CERSAT (bottom right).

The Southern Ocean

The Antarctic sea ice front modelled by the Global V2 is remarkably well represented compared to the observations (Figure 2) and to major climate models (Parkinson *et al.*, 2006a). However, unrealistic features are the followings: (1) The sea ice extent in initials conditions is too spread towards the northern limits (Figure 4) and this characteristic remains relatively true all along the year 2007 (Figure 2); (2) the Antarctic sea ice cover has a weak compactness inside the pack, in the open ocean; (3) the coastal sea ice remains however too thick. This last characteristic may come from thick initial ice conditions and errors in the representation of the air momentum flux, and particularly the representation of the katabatic winds which are supposed to push away the sea ice from the continent; (4) the short-term variability of the dynamics exhibited by the Antarctic sea ice cover has not been analysed carefully as no CERSAT observations for the Southern Ocean was available.

The seasonal cycle and the recent trends

In this part, we analyse an interannual experiment led with LIM2 in a forced run (without data assimilation) performed over the 2001-2007 period.. We present how LIM2 is able to reproduce both the annual cycle and recent interannual variability, and especially the Arctic sea ice coverage decline. Recent works made in collaboration with UCL and done to improve the sea ice representation at ¼° resolution is also presented in this section.

We have performed an interannual experiment using the model without any data assimilation. This experiment, tagged ORCA025_LIM-T09, driven by the daily 1998-2007 atmospheric ECMWF analysis uses exactly the same model as the one described in section 2. This experiment starts the 4th of April 1998 with prescribed conditions from another experiment, tagged ORCA025_LIM-T08. The latter experiment, forced at the surface by the ECMWF reanalysis project ERA40 dataset (Uppala, 2001) over the 1993-2001 period, started at rest from the 1st January 1992 with temperature and salinity derived from the (Levitus *et al.*, 1998) data set for the middle and low latitudes. For high latitudes, we chose the PHC2.1 climatology (Steele *et al.*, 2001) for temperature and salinity and the same ORCA05_LIM (0.5° horizontal resolution configuration) climatological run for sea ice initial conditions.

Figure 8 presents the sea ice extent annual cycle of the experiment ORCA025_LIM-T09 between January 2001 and September 2007. Compared to observations, this experiment overestimates systematically the sea ice extent, either in winter or in summer and in both Arctic and Antarctic areas. This is particularly true during the abrupt summer 2007 reduction. With no data assimilation of sea ice variables in the Global V2, the sea ice in the Global V2 reproduces the overestimation found in the ORCA025_LIM-T09 experiment during summer 2007. This may underline the limited impact of the water masses assimilation surrounding the sea ice cover on the Arctic sea ice lifecycle itself. Similar conclusions may be pointed out for the austral sea ice extent for which the Global V2 may relatively degrade the representation of the sea ice front. This last result was not obvious in the first instance as the assimilated water masses in the Southern Ocean was supposed to better constrain the Antarctica sea ice front.

We have then looked at how the model is able to reproduce the drastic reduction of the summer sea ice cover in the Arctic Ocean during the last recent decade. We have first compared the relevance of the CERSAT dataset and compare them with those of the NSIDC (National Snow and Ice Data Center, Boulder, Colorado). Over the period 1996-2007 analysed in (Comiso *et al.*, 2008), the trend issued from the CERSAT dataset (-107 639 km^2/year or -10.5 %/decade)) is inside the error brackets presented by the NSDIC satellite dataset (Table 1). Although this negative trend has tremendously accelerated over the last decade (2001-2007) in the CERSAT dataset (-17.6 %/decade), the trend issued from the ORCA025_LIM-T09 underestimates this rapid decline (-13.3 %/decade). Moreover, although the trend in the Southern Hemisphere remains not clear or even exhibits a stationary behaviour in the CERSAT datasets, the experiment ORCA025_LIM-T09 shows a clear unrealistic and important positive trend over the years 2001-2007.

We have then developed another configuration with the same model but with a geographical domain limited to the mid and high Northern latitudes [45°N-90°N]. This lighter configuration, which is the third of the global domain in terms of computing and spaces resources, enables us to perform various sensitivities interannual experiments over the 2001-2007 period. We present here a unique experiment, hereafter tagged ARCTIC4-T07, which presents the following differences with the model used in the ORCA025_LIM-T09 experiment: 1) the ice thickness of newly formed ice in the leads is now set to 0.6m, 2) a new snowfall profile in which the solid precipitations occurs only below the 3°C isotherm instead of the 8°C isotherm in the previous profile, 3) the C-grid elastic-viscous-plastic (EVP) rheology (Bouillon *et al.*, 2008) replaces the viscous-plastic formulation, 4) the momentum flux between sea ice and ocean is re-calculated at each oceanic time step, it is fully comprehensive (non null oceanic components) with, however, a damping coefficient set to $e^{[-|Uice - Uoce| / U^*)]}$ where U_{ice} is the sea ice velocity and U_{oce} the oceanic one and U*=0.1 $m.s^{-1}$; 5) the sea ice eddy diffusivity coefficient is now 100 $m^2.s^{-1}$; 6) the creep limit for viscosity is set to 1.10^{-9} instead of 1.10^{-8}, 7) the ice strength parameter (P*) is set to 7500 $N.m^{-2}$ instead of 15000 $N.m^{-2}$. This experiment started the 1st of January 2001 with prescribed initial conditions from (Levitus *et al.*, 1998) for water masses and the same ORCA05_LIM (0.5° horizontal resolution configuration) climatological run for sea ice initial conditions.

In terms of mean state, the seasonal cycle reproduced by the ARCTIC4-T07 experiment exhibits a better seasonal cycle with a major improvement of the simulation during summer (Figure 8) conjointly with better melting processes in the Beaufort and East Siberian seas (Figure 9). With -173 924 km^2/year (or -14.7 %/decade) (Table 1), the ARCTIC4-T07 long-term trend over the years 2001-2007 is now getting nearer the observed ones. Again, the correlation between monthly mean anomalies of sea ice extent over the years 2001-2007 between the ARCTIC4-T07 experiment and CERSAT data reaches 0.77, value to be compared with a correlation of 0.58 obtained with the ORCA025_LIM-T09 experiment. Further investigations are going on to study the short-term variability in this simulation.

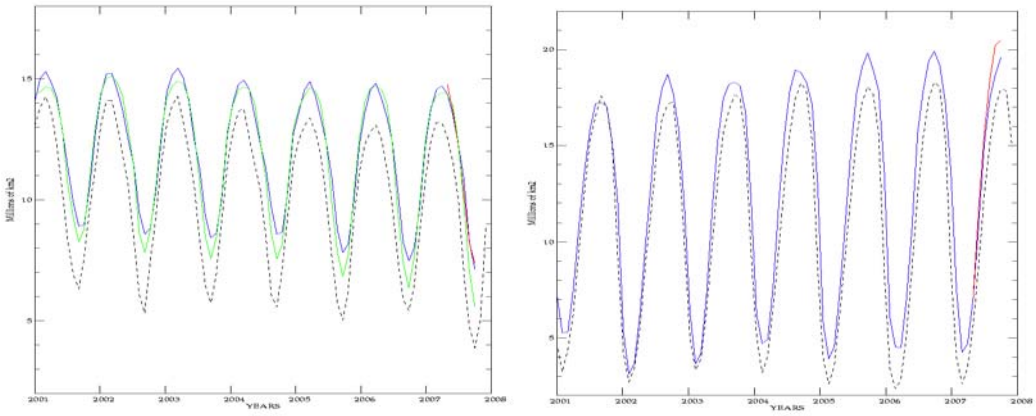

Figure 8

Arctic (left panel) and Antarctic (right panel) monthly sea ice extent time series for the ORCA025_LIM-T09 experiment (blue), the Global V2 system (red), the ARCTIC4-T07 experiment (green) and the CERSAT dataset (dashed black).

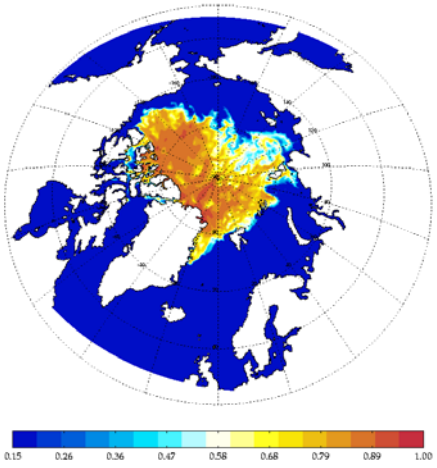

Figure 9

SIC (%) September 2007 mean in the ARCTIC4-T07 experiment.

Sea ice extend trend in km^2/yr (%/decade)		NSIDC	CERSAT	ORCA025_LIM	ARCTIC4
1996-2007	North. Hem.	-114 195 ± 88 263 (-10.1 ± 0.73)	-107 639 (–10.5)		
	South. Hem.		+852 (+0.08)		
2001-2007	North. Hem.		**-175827 (-17.6)**	**-159388 (-13.3)**	**-173924 (-14.7)**
	South. Hem.		-10378.6 (-0.9)	+293300 (+23.4)	

Table 1

Sea ice extent trend (in km^2/yr and in %/decade in bracket) from January 1996 to September 2007 and from January 2001 to September 2007 from 12-month running sea ice extent anomalies of the NSIDC (National Snow and Ice Data Center, Boulder, Colorado) dataset (Comiso *et al.*, 2008), of the CERSAT dataset (Ezraty *et al.*, 2007), of the two interannual experiment led with the Mercator-Ocean global ¼° (ORCA025_LIM) and the Mercator-Ocean ¼° Arctic configuration (ARCTIC4). Non applicable data are grey shaded cells.

Future updates

The Global V2 reproduces the sea ice cover as the majority of sea ice models used widely by the scientific community and presents similar discrepancies. However, the recent and rapid decline of the Arctic sea ice cover highlights these biases. This work has underlined the need to start the Global V2 system with better initial conditions for the sea ice cover. The recent changes proposed by the R&D Mercator-Ocean team improved substantially the large-scale representation of sea ice. Before being implemented in the new release of the Global V2, these changes need to be tested in a global sense with the ORCA025_LIM configuration. In any case, if a monitoring of the rapid Arctic sea ice decline needs to be carried out, these changes are necessary. These changes will also be tested in the new eddy-resolving (1/12°) version of the Mercator-Ocean global model.

The Mercator-Ocean system over-estimates the sea ice concentration but under-estimates its variability. The need for improving the short term variability in the sea ice pack passes also certainly by the application of an assimilation scheme. Plans to implement the SEEK filter onto the Mercator-Ocean sea ice model are under investigations (this issue).

The R&D Mercator-Ocean team plans also to implement the new model LIM3 (Vancoppenolle *et al*, this issue) in the global ¼° configuration. Thanks to its multilayer halo-thermodynamic representation together with the use of several thickness categories, Vancoppenolle et al. shows that this model better resolves the thinning of sea ice in the marginal ice zones and improves largely the sea ice thickness distribution.

Acknowledgments

The authors would like to thank gratefully Profs. T. Fichefet and H. Goosse from the G. Lemaître Institute (Univ. Catholique de Louvain-la-Neuve, Belgium) for fruitful discussions.

References

Bertino, L., K.A. Lisaeter, G. Garric, J. Stark, L. Crosnier, and F. Hernandez, Definition of Class 1-4 metrics for the Arctic, *Deliverable D5.4.5, MERSEA Project*, *MERSEA-WP05-NERSC-TECN-0017-02A*, 2006.

Bouillon, S., T. Fichefet, and M.A.M. Maqueda, The Elastic-Viscous-Plastic sea ice model on different grid types, in *in preparation*, 2008.

Comiso, J.C., C.L. Parkinson, R. Gersten, and L. Stock, Accelerated decline in the Arctic sea ice cover, *Geophys. Res. Lett.*, *35(L01703)*, doi:10.1029/2007GL031972, 2008.

Drevillon, M., L. Crosnier, N. Ferry, E. Greiner, M. Benkiran, R. Bourdalle-Badie, C. Bricaud, E. Durand, Y. Drillet, G. Garric, O.L. Galloudec, J.M. Lellouche, , F. Messal, L. Nouel, L. Parent, C.E. Testut, and B. Tranchant, The new 1/4° Mercator-Ocean global multivariate analysis and forecasting system: Tropical oceans outlook, *Mercator Newsletter*, *26*, 2007.

Drevillon, M., Y. Drillet, G. Garric, J.-M. Lellouche, E. Remy, C. Derval, R. Bourdalle-Badie, B. Tranchant, M. Laborie, N. Ferry, E. DUrand, O.L. Galloudec}, P. Bahurel, E. Greiner, S. Guinehut, M. Benkiran, N. Verbrugee, E. Dombrowsky, C.-E. Testut, L. Nouel, and F. Messal, *The GODAE/Mercator global ocean forecasting system: results, applications and prospects.*, World Maritime Technology Conference, London 6-10 March, 2006.

Ezraty, R., F. Girard-Ardhuin, J.F. Piolle, L. Kaleschke, and G. Heygster, *Arctic and Antarctic sea ice concentraiton and Arctic sea ice drift estimated from Special Sensor Microwave data*, CERSAT, 2007.

Fichefet, T., and M.A.M. Maqueda, Sensitivity of a global sea ice model to the treatment of ice thermodynamics and dynamics, *J. Geophys. Res.*, *102-C6*, 12,609-12,646, 1997.

Fichefet, T., and M.A.M. Maqueda, Modelling the influence of snow accumulation and snow-ice formation on the seasonal cycle of the Antarctic sea ice cover, *Clim. Dyn.*, *15*, 251-268, 1999.

Goosse, H., J.-M. Campin, E. Deleersnijder, T. Fichefet, P.-P. Mathieu, M.A.M. Maqueda, and B. Tartinville, *Description of the CLIO model version 3.0*, Institut d'Astronomie et de Geophysique Georges Lemaitre, Catholic University of Louvain (Belgium), 2001.

Goosse, H., and T. Fichefet, Importance of ice-ocean interactions for the global ocean circulation: a model study, *J. Geophys. Res.*, *104*, 23,337-23,355, 1999.

Greenfell, T.C., and D.K. Perovich, Spectral albedos of sea ice and incident solar irradiance in the Southern Beaufort Sea, *JGRO*, *89*, 3573-3580, 1984.

Hibler, W.D.I., A dynamic thermodynamic sea ice model, *J. Phys. Oceanogr.*, *9*, 815-846, 1979.

Kreyscher, M., M. Harder, P. Lemke, and G.M. Flato, Results of the Sea Ice Model Intercomparison Project : Evaluation of sea ice rheology schemes for use in climate simulaiotns, *J. Geophys. Res.*, *105*, 11,299-11,320, 2000.

Levitus, S., T.P. Boyer, M.E. Conkright, T. OBrian, J.I. Antonov, C. Stephens, L. Stathopolos, D. Johnson, and R. Gelfeld, *World Ocean Database 1998 - NOAA Atlas NESDID18*, National Oceanographic Data Center, Silver Spring, MD., 1998.

Parkinson, C.L., K.Y. Vinnikov, and D.J. Cavalieri, Correction to "Evaluation of the simulation of the annual cycle of Arctic and Antarctic sea ice coverages by 11 major global climate models", *J. Geophys. Res.*, *111(C12009)*, doi:10.1029/2006JC003949, 2006a.

Parkinson, C.L., K.Y. Vinnikov, and D.J. Cavalieri, Evaluation of the simulation of the annual cycle of Arctic and Antarctic sea ice coverages by 11 major global climate models, *J. Geophys. Res.*, *111(C07012)*, doi:10.1029/2005JC003408, 2006b.

Semtner, A.J., A model for the thermodynamic growth of sea ice in numerical investigations of climate, *J. Phys. Oceanogr.*, *6*, 379-389, 1976.

Shine, K.P., and A. Henderson-Sellers, The sensitivity of a thermodynamic sea ice model to changes in surface albedo parameterization, *J. Geophys. Res.*, *90(D1)*, 2243-2250, 1985.

Steele, M., R. Morley, and W. Ermold, PHC: A global ocean hydrography with a high quality Arctic Ocean., *Journal of Climate*, *14*, 2079-2087, 2001.

Timmermann, R., H. Goosse, G. Madec, T. Fichefet, C. Ethe, and V. Duliere, On the representation of high latitude processes in the ORCA-LIM global coupled sea ice-ocean model, *Ocean Modelling*, *8*, 175-201, 2005.

Uppala, S., ECMWF Reanalysis, 1957-2001, ERA-40 - Proceedings of workshop Re-analysis, 5-9 november, ECMWF, Reading, 2001.

LIM3, an advanced sea-ice model for climate simulation and operational oceanography

By Martin Vancoppenolle[1], Thierry Fichefet[1], Hugues Goosse[1], Sylvain Bouillon[1], Chris König Beatty[1] and Miguel Angel Morales Maqueda[2]

[1] Institut d'Astronomie et de Géophysique G. Lemaître, Université Catholique de Louvain, Louvain-la-Neuve, Belgium
[2] Proudman Oceanographic Laboratory, 6 Brownlow Street, Liverpool L3 5DA, UK

In this contribution, we briefly present the version 3 of the Louvain-la-Neuve Ice Model (LIM). The results of two 1970-2007 hindcasts performed with the ocean modelling system NEMO (Nucleus for European Modelling of the Ocean) – one using LIM2 and the other using LIM3 – are compared to available observations of ice concentration, thickness and mixed layer depth. LIM3 is found to significantly improve the simulation of sea ice characteristics compared to the earlier LIM2 version, making it a more appropriate and accurate tool not only in ice-ocean and climate simulations but also presumably for operational oceanography.

Introduction

Sea ice refers to all ice found at sea which has originated from the freezing of seawater. Sea ice, which covers 7 % of the World Ocean, is an important actor and a sensitive indicator of climate change, as witnessed by the spectacular sea ice historical minimum on September 16th, 2007, which shattered all previous records by more than one million square kilometers (NSIDC, 2007). In addition, salt and freshwater releases associated to the growth and melt of sea ice have a significant impact on the World Ocean circulation.

The Louvain-la-Neuve sea ice model (LIM) has been coupled to OPA (Ocean Parallélisé) almost 10 years ago, leading to significant successes in ice-ocean and climate simulations. Meanwhile, the development of LIM kept going on, leading to LIM3, a C-grid, dynamic-thermodynamic sea-ice model including the representation of the subgrid scale variations of ice thickness, enthalpy, salinity and age, which we describe in more detail in the next section. Then, the results of two 1970-2007 hindcasts performed with NEMO – one using LIM2 and the other using LIM3 – are compared to available observations of ice concentration, thickness and mixed layer depth.

Model description

LIM was originally a dynamic-thermodynamic sea ice model developed by Fichefet and Morales Maqueda (1997). LIM1 was subsequently coupled to the OPA model (Timmermann et al., 2005) and rewritten by Christian Ethé and Gurvan Madec at the LOCEAN laboratory, resulting in LIM2, the present sea ice component used in the reference version of the NEMO system. The newly developed LIM3 is based on this previous work and is included into the NEMO system.

LIM3 includes three major new developments (see Table 1 and Vancoppenolle et al., 2008). First, the C-grid elastic-viscous-plastic (EVP) rheology (Bouillon et al., 2008) replaces the classical former viscous-plastic (VP) formulation of Hibler (1979). Because it allows to drastically reducing the numerical viscous flow limit, using EVP gives a better solution of the ice momentum equation. The C-grid allows the dynamical coupling to OPA (also in C-grid) in a much more natural way. EVP is explicit, which allows easier parallelization. Second, in order to account for unresolved variations in ice thickness, several thickness categories have been included into the model. Ice volume is redistributed among categories due to thermodynamic (growth and melt) and dynamic (opening, rafting and ridging) processes. Finally, a multi-layer halo-thermodynamic module (Vancoppenolle et al., 2007) replaces the former Semtner (1976) 3-layer model. This includes an explicit representation of brine entrapment and drainage, as well as the brine impact on sea ice growth and decay. LIM3 includes also several other features (e.g., age of sea ice, frazil ice formation in leads and polynyas) which are not detailed here.

Model component	LIM2	LIM3
Thermodynamics	Semtner 3-layer	Multilayer halo-thermodynamic
Dynamics	VP, B-grid	EVP, C-grid
Ice Thickness Distribution	2 levels (ice + open water). No redistribution.	6 levels (5 for ice + 1 for open water). Redistribution by opening, rafting, ridging, and ice growth/melt.

Table 1

Comparison of model components in LIM2 and LIM3

Model variables include the ice velocity vector (computed by the dynamical module), the ice area, volume, enthalpy, salt content and age content, as well as snow volume and enthalpy (computed by the ice thermodynamics and redistribution modules). In LIM3, the ice is represented as a series of minimum M=5 ice thickness categories. This means that all sea ice variables (except velocity) have a specific value for each of the thickness categories. In addition, in each thickness category, a series of N=5 vertical ice layers are used to resolve the heat diffusion equation. This number can decrease to 2 without deteriorating the results. The increase in CPU of the NEMO system using LIM3 is around 30 % compared to LIM2.

In the next section, we describe the results of a 1970-2007 hindcast simulation performed with NEMO, using alternatively LIM2 and LIM3, with default parameters[1], in the ORCA2 2°x 2° configuration, forced by the NCEP-NCAR surface air temperatures and winds and various meteorological climatologies. The years 1970-1978 are considered as model spinup. Though the model is global, we mostly focus the discussion on the Northern Hemisphere. For more information, notably on the Southern Hemisphere, we invite the reader to refer to Vancoppenolle et al. (2008) which will describe extensively the results of NEMO-LIM3.

Results

Ice state

The sea ice physical state as simulated by LIM3 is summarized in figure 1. Significantly different ice packs are found in the Northern and Southern Hemispheres. Arctic ice is on average older, thicker, and less saline and has a deeper snow cover and a lower brine volume than its Antarctic counterpart.

[1] We want to compare LIM2 and LIM3, each of them with its “best” set of parameters, in order to illustrate the transition from LIM2 to LIM3. The main parameters’ values in LIM2 are, for the ice strength P^*=10000 N.m^{-1}, for the thickness of new ice h^0=0.5m, and for the melting bare ice albedo α_{su}=0.5. In LIM3, the default values of the main parameters are different: P^*=40000 N.m^{-1}, h^0=0.1m and α_{su}=0.53. These values are closer to observations.

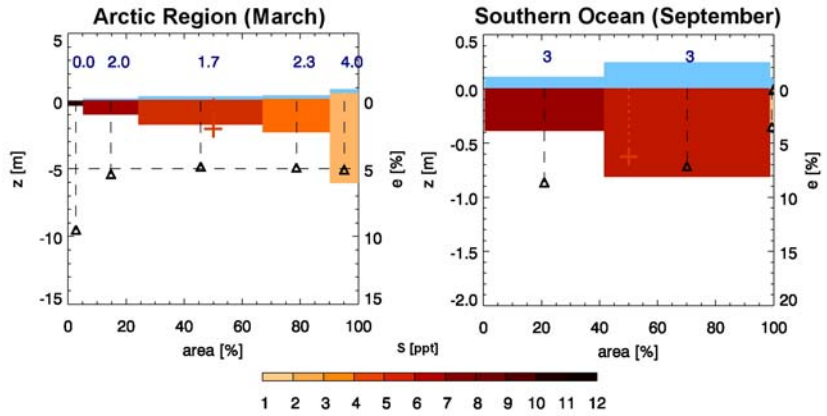

Figure 1

Average winter sea ice physical state (1979-2006) for the Arctic (left) and the Antarctic (right). The ice concentration in each of the ice thickness categories is represented horizontally. The ice thickness (negative values) and snow depth (positive values) are shown vertically (m, left axis). Note the difference in scale in the two figures. The colors refer to the ice salinity (‰) in each category, the light blue corresponding to snow (fresh, S=0‰). The black triangles indicate the relative brine volume e (computed from temperature and salinity, %, right axis). The numbers on top refer to ice age (years in the Arctic, months in the Antarctic). The crosses indicate mean ice thickness. Note that in the SH, only the first two thickness categories are not empty.

The simulated sources and sinks of ice mass also differ from one hemisphere to the other. In the Arctic, bottom congelation domines in winter, whereas surface and bottom melt contribute equivalently in summer. In the Antarctic, in winter, bottom congelation, new ice formation in open water and snow ice formation contribute in similar amounts, while bottom melt largely domines in summer. This agrees with information inferred from in situ observations of ice and snow thicknesses and textural analysis of ice cores taken in situ.

Mean state

The sea ice mass balance is well characterized by the evolution of ice coverage and volume. Ice coverage is described by ice concentration (defined as the relative areal ice coverage in a given region). Ice concentration has been observed from space from 1979 on by passive microwave sensors onboard sattelites, which provides a good basis for model validation. The difference between simulated and observed Arctic sea ice extent averaged over 1979-2006 is -0.51 (0.71)×10^6 km² with LIM3 (LIM2). In winter, both models simulate very well the geographical distribution of ice concentration. In summer (see figure 2), LIM2 overestimates the ice coverage in the seasonal ice regions, in particular along the east coast of Greenland and along the Siberian shelf. In contrast, the LIM3 simulation is much more realistic. In LIM3, the ice-albedo feedback is governed by the behaviour of thin ice and can be characterized as follows. In early summer, thin ice in the marginal ice zones disappears quickly, which significantly reduces the ice concentration compared to LIM2 and promotes higher absorption of shortwave radiation in the ocean. This enhances the basal oceanic heat flux and hence bottom melt, leading to a decrease in ice thickness. Yet the LIM3 simulation is not perfect. Laptev and Beaufort Seas as well as Baffin Bay and Foxe Basin should be more frequently ice-free, and the ice concentration is underestimated in the Atlantic sector of the Arctic Ocean (i.e., between North Pole, Spitzbergen and Severnaya Zemlya).

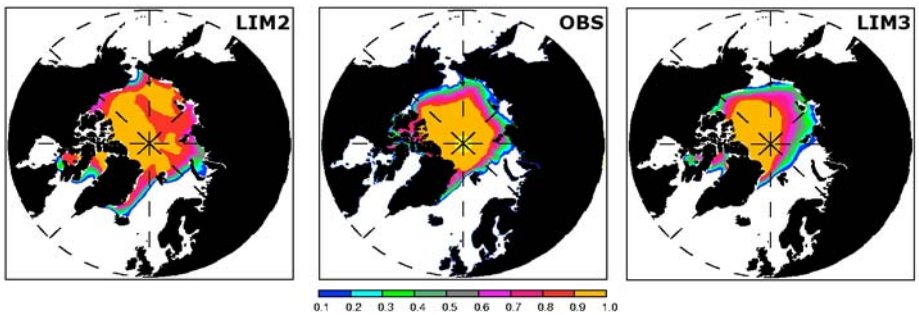

Figure 2

Simulated September geographical distribution of ice concentration in the Arctic, simulated by LIM2 (left), as derived from passive microwave observations (Comiso, 2007, center), and simulated by LIM3 (right).

Ice volume is well described in terms of ice thickness. Comparison to data from upward-looking sonars (ULS) onboard submarines (see figure 3) reveal a mean 1976-2000 LIM3 (LIM2) – data difference of -0.55 ± 1.04 m (1.88 ± 0.97 m). The improvement is due to a combination of the improved ice dynamics, of the more realistic ice-albedo feedback, of the inclusion of thickness redistribution through rafting and ridging and of the time-varying ice salinity. Significant ice thickness biases remain in LIM3. Ice is too thick in the Beaufort Gyre and too thin in the Atlantic sector of the Arctic Ocean. Comparison with several other models showed that this pattern is typical of multicategory ice models and has been suggested to be due to underestimated shear strength. Ongoing work is directed towards solving this problem.

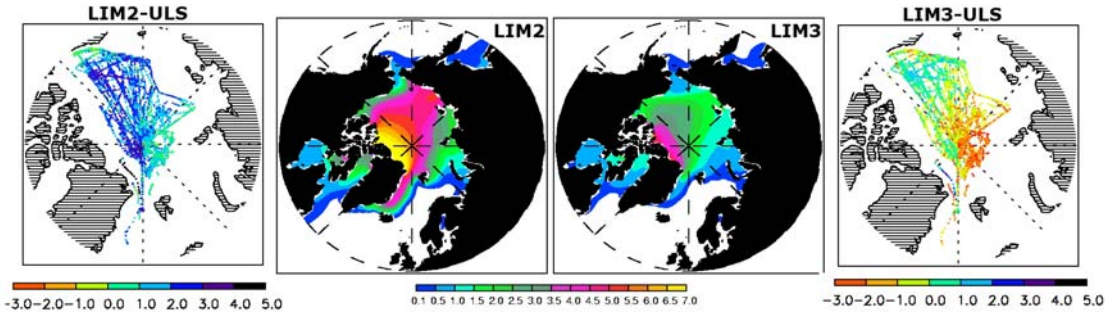

Figure 3

Geographical distribution of January Arctic ice thickness (m). From left to right: difference LIM2 – ULS data, LIM2, LIM3 and difference LIM3 – ULS data. ULS data come from NSIDC (2006).

In the Southern Ocean, the simulations are reasonably good and quite comparable. The 1979-2006 average difference between the annual mean simulated and observed global hemispheric areas is -1.20×10^6 km^2 (-1.12×10^6 km^2) with LIM3 (LIM2). The winter ice extent is well simulated, but in summer the ice disappears excessively. The geographical distribution of ice thickness is well represented, though the ice is slightly too thin in both models.

Variability

Associated with the better mean seasonal cycle, the simulation of interannual variability is also improved. In the Arctic (see figure 4, left panel), the correlation between the simulated and observed monthly mean anomalies of ice area is 0.52 in LIM2 and 0.74 in LIM3. LIM3's better representation of the ice-albedo feedback makes it more efficient to simulate the September minimum of extent, the interannual variations and the long-term trend. In addition, the spatial distribution of anomalies is also much better captured with LIM3, as illustrated by the simulation of the recent 2007 minimum of extent (see figure 4), which reached a record value of 4.28×10^6 km^2 (NSIDC, 2007). LIM3 simulates a pattern close to observations and slightly underestimates the summer 2007 ice extent (3.66×10^6 km^2). LIM2 does not manage to melt enough ice and significantly overestimates the ice extent (5.85×10^6 km^2). In the Southern Ocean, LIM2 and LIM3 models yield a similar correlation between the simulated and observed monthly mean anomalies of ice area (0.65). There is no significant long-term trend.

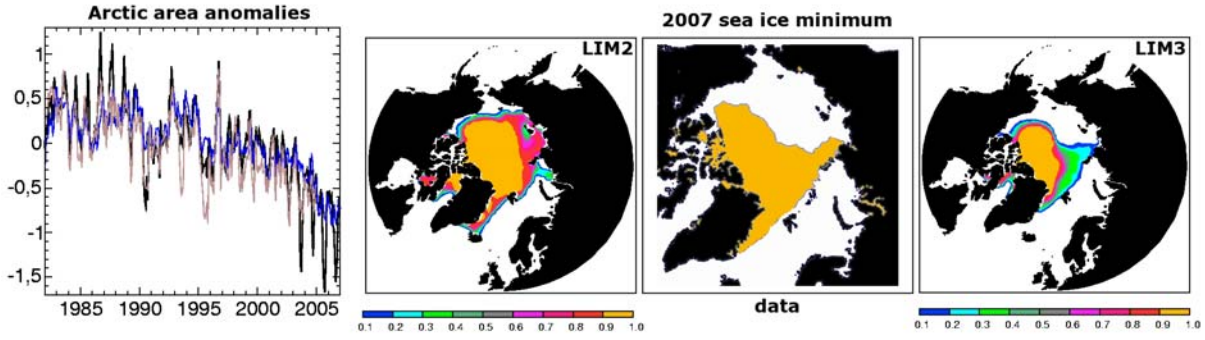

Figure 4

(left) Monthly mean anomalies (i.e., differences of monthly means from the mean 1979-2006 seasonal cycle) of sea ice area (10^6 km^2) in the Northern Hemisphere as simulated by LIM3 (black), by LIM2 (blue) and as derived from passive microwave observations (brown). (Right) The maps show, from left to right, first, the September 2007 distribution of ice concentration in the Arctic as simulated by LIM2; second, the September 2007 ice covered-area taken from NSIDC website (www.nsidc.org); and finally, simulation with LIM3.

Obviously, the sensitivities of LIM2 and LIM3 to a change in external forcing are different. This is also true for a change in internal parameters. For example, for a diminution of the albedo of melting ice from 0.53 to 0.50, the response of LIM2 is stronger. In the Arctic basin, the difference in thickness due to such a change in albedo is between -0.5 and -0.2 m with LIM2 (-0.3 and -0.1 m with LIM3).

Impact on the ocean

Briefly, we show that the response of the ocean to the change in sea ice model is important. This is particularly the case in the North Atlantic (see figure 5), where the role of sea ice inflow domines the buoyancy forcing. Compared to LIM2, LIM3 has a more realistic, smaller ice volume export through Fram Strait and an associated reduced freshwater transport to the North Atlantic. In turn, the frequency of deep convection increases in LIM3 compared to LIM2, which leads to a more realistic distribution of convection sites, in particular in the Labrador Sea.

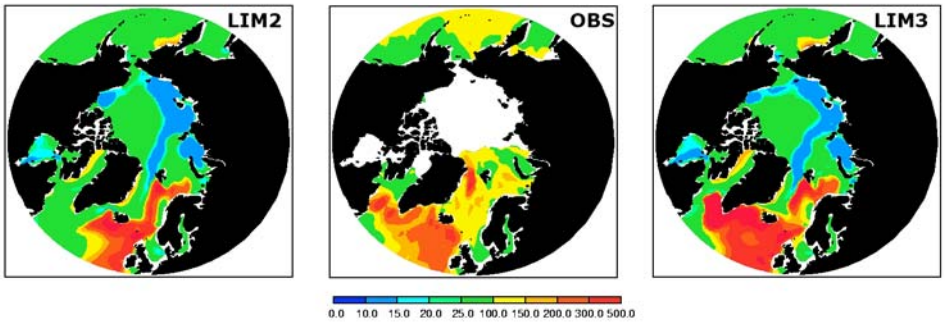

Figure 5

Average seasonal maximum (1979-2006) mixed layer depth as simulated by LIM2 (left), as derived from observations based on a 0.2°C temperature criterion (de Boyer Montégut et al., 2004) and as simulated by LIM3 (right) with the corresponding density criterion ($\Delta\rho$=0.03 kg.m^{-3}).

Conclusion and perspectives

In this letter, we presented the new LIM3 sea ice model and reviewed the results of a 1970-2007 hindcast simulation performed with NEMO using LIM2 / LIM3. The results show that NEMO-LIM3 produces mean sea ice coverage and thickness fields that compare significantly better to available observations. In addition, variability and trends in ice coverage, as well as patterns of anomalies are also better captured. This suggests that the inclusion of LIM3 would affect and probably improve the results of climate projections in coupled GCMs. Finally, the improved sea ice field also results in a better distribution of the convection sites in the North Atlantic. In conclusion, LIM3 is certainly a more accurate tool for ice-ocean and climate simulations as well as for operational oceanography. Further development, calibration and use of NEMO-LIM will continue during the next few years in Louvain-la-Neuve.

Acknowledgments

We thank G. Madec and the NEMO team for confidence and support. R. Timmermann, V. Dulière, C. M. Bitz and J. Haapala are also gratefully acknowledged for their human and scientific contribution to LIM3. The authors also acknowledge NCEP and NSIDC for providing data used in this work. This research was supported by the Belgian Federal Science Policy office, Program on Global Change and Sustainable Development, and is carried within the scope of the project “A Second-Generation of the Ocean System” funded by the Communauté Française de Belgique (ARC 04/09-316).

References

Bouillon, S., T. Fichefet, and M.A. Morales Maqueda, 2008. The Elastic-Viscous-Plastic sea ice model on different grid types, in preparation.

Comiso, J.C., 1999, updated 2007. Bootstrap sea ice concentrations from NIMBUS-7 SMMR and DMSP SSM/I, 1979-2006. National Snow and Ice Data Center, Boulder, Colorado, USA. Digital Media.

de Boyer Montégut, C., G. Madec, A. S. Fischer, A. Lazar and D. Iudicone, 2004. Mixed layer depth over the global ocean: An examination of profile data and a profile-based climatology. Journal of Geophysical Research, 109, C12003, doi:10.1029/2004JC002378.

Fichefet, T., and M. A. Morales Maqueda, 1997. Sensitivity of a global sea ice model to the treatment of ice thermodynamics and dynamics. Journal of Geophysical Research, 102, 12,609 – 12,646.

Hibler, W. D., 1979. A dynamic thermodynamic sea ice model. Journal of Physical Oceanography, 9, 815 – 846.

National Snow and Ice Data Center (NSIDC), 1998, update 2006. Submarine upward looking sonar ice draft profile data and statistics. Boulder, Colorado, USA.

National Snow and Ice Data Center (NSIDC), 2007. Arctic Sea Ice Shatters All Previous Record Lows. Online press release, Oct 1, 2007 (www.nsidc.org/news/press).

Semtner, A.J., Jr, 1976. A model for the thermodynamic growth of sea ice in numerical investigations of climate. Journal of Physical Oceanography, 6, 379 – 389.

Timmermann, R., H. Goosse, G. Madec, T. Fichefet C. Ethé and V. Dulière, 2005. On the representation of high-latitude processes in the ORCA-LIM global coupled se ice-ocean model. Ocean Modelling, 8, 175-201.

Vancoppenolle, M., C. M. Bitz and T. Fichefet, 2007. Summer landfast sea ice desalination at Point Barrow, Alaska: Model and observations. Journal of Geophysical Research, 112, CO4022, doi:10.1029/2006JC003493.

Vancoppenolle, M., T. Fichefet, H. Goosse, S. Bouillon and M. A. Morales Maqueda, 2008. Simulating the mass balance and salinity of Arctic and Antarctic sea ice. 1. Description and validation of the ice-ocean model NEMO-LIM3, submitted.

Sensitivity of a model of the Ross Ice shelf Polynya to different atmospheric forcing sets

By Pierre Mathiot[1], Nicolas Jourdain[2], Bernard Barnier[1] and Hubert Gallée[2]

[1]LEGI Grenoble, Domaine Universitaire BP 53 38041 Grenoble Cedex 9 France
[2]LGGE, Grenoble, Domaine Universitaire BP 96 38041 Grenoble Cedex 9 France

Introduction

Polynyas are openings within the sea ice cover. Often driven by continental winds, their area varies over a wide range (from 10 to 10^5 km^2). They play an important role both in atmospheric and oceanic systems. The atmospheric effect is a warming of the lower air layers which affects the mesoscale atmospheric dynamics. The oceanic effect is an intense cooling of the surface waters, and a brine rejection associated to the formation of new sea ice. Ocean vertical mixing and convection are consequently increased, and dense water formed will later influence the properties of intermediate and deep waters in both the Southern Ocean and the Arctic Ocean (Maqueda et al. 2004).

Because the opening of most polynyas is a direct consequence of the wind effect on sea-ice, and because polynyas have a very strong influence on air-sea exchanges, the representation of their properties in operational and climate ocean models is certainly very sensitive to the atmospheric forcing used. This sensitivity is examined here in the context of a regional ocean model of the Ross Sea, based on the NEMO numerical code (Madec, 2007). The sensitivity of the Ross Ice Shelf Polynya (RISP) to two different sets of atmospheric variables is investigated. The regional ocean model and its open boundary forcing are presented in section 2. The two different sets of atmospheric variables and fluxes used to drive the model are described in section 3. One relies on the ERA40 reanalysis (Simmons and Gibson, 2000), and the other is issued from a regional downscaling of ERA40 with the Regional Atmospheric Model (MAR). Section 4 compares the properties of the RISP as simulated by these two forcing sets.

Ross Sea regional model

The regional ocean/sea ice model of the Ross Sea used in this study is the ocean/sea ice component of the TANGO coupled atmosphere/ocean/sea-ice regional model (Jourdain, 2007). TANGO is jointly developed by LGGE (Grenoble France) and LEGI (Grenoble France). Its atmospheric component is the MAR (see section 3.2). The ocean/sea-ice component is an original set-up of NEMO on the same grid as MAR (oblic strereographic grid), at 20 km resolution. In NEMO, the sea ice model is the second generation of model developped at Louvain la neuve (LIM2) by Fichefet and Maqueda (1997). The thermodynamic of LIM2 is based on a tree layers model (2 layers of ice and one layer of snow) and the dynamic part is based on the viscous plastic law. OASIS3 (Valcke et al., 2004) is used for the coupling. The model domain common to both the ocean and atmospheric models is shown in Figure 1. Although the domain extends to the South Pole, there are no ocean points at latitudes higher than 78°S (Figure 2). In other words, the part of the ocean that goes under the Ross Ice Shelf (area in light grey in Figure 2) is not considered.

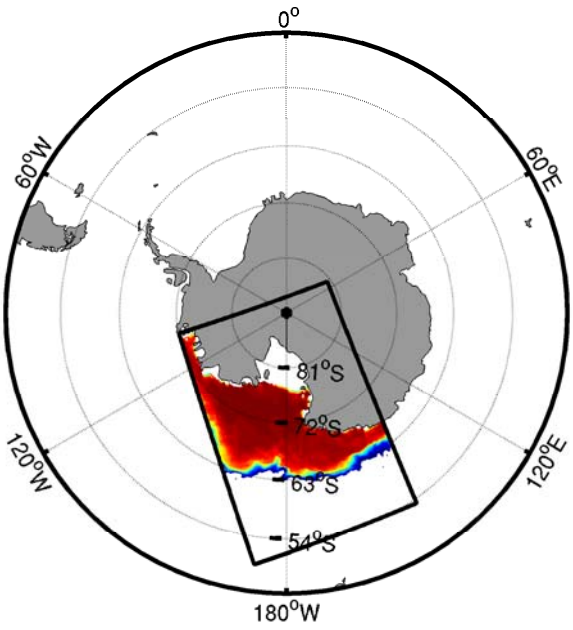

Figure 1

Black rectangle: Ross Sea model area. This domain is shared by the Ross Sea ocean model and the regional atmospheric model MAR. Coloured area shows a snapshop of the ice concentration in a simulation of the Ross Sea ocean model forced with the atmospheric variables provided by a MAR run where surface and lateral forcing were from ERA40 .The colour scale (from 0 to 1) is the same as in Fig. 2, and varies from dark red for high concentration above 0.9 to dark blue for low concentration under 0.1

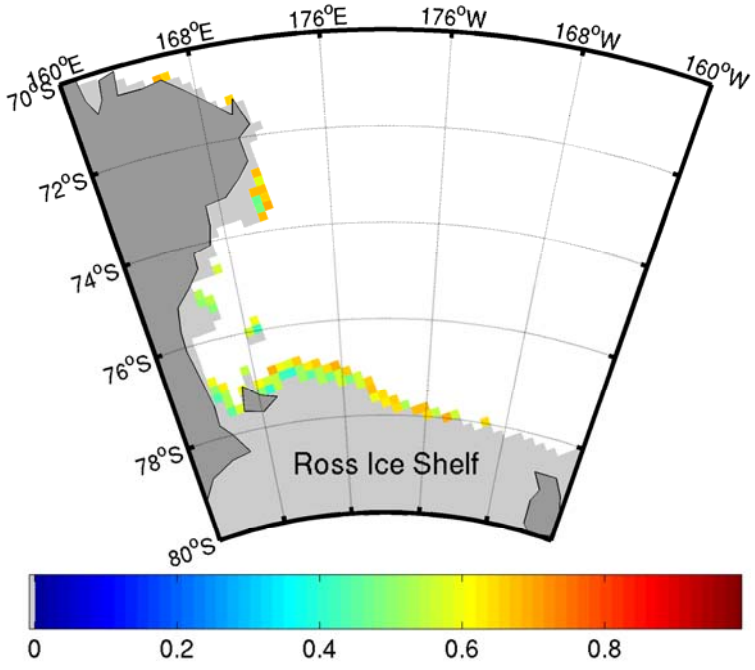

Figure 2

Sea-ice concentration in coastal polynyas on July 18, 1992, in the simulation driven by the MAR forcing. Coloured points indicate areas matching the “coastal polynya criterion“ (see text). The RISP is the long polynya stretching from 162°E to 168°W along the southern limit of the ocean model (i.e. the edge of Ross Ice Shelf). In this figure, light grey areas show the ice shelves, and dark grey areas show continental surface.

The basic set-up of the Ross Sea ocean model (numerical schemes and parameterisations) is that used in the global DRAKKAR ORCA025-G70 experiment (Drakkar Group, 2007), a 47 year long experiment (1958-2004) driven with the DFS3 atmospheric forcing (see section 3.1). The latter experiment is also used to provide the ocean and sea-ice fields at the open boundaries of the regional model.

In the present study, the Ross Sea ocean model is used alone in a forced mode (i.e. not coupled to the MAR atmospheric model). Initial conditions are the ocean and sea-ice conditions of January 1st, 1991 extracted from the ORCA025-G70 experiment. The model is spun-up for one year with DFS3 forcing for 1991. All experiments discussed in the following start January 1st, 1992, and cover the full 1992 year.

Surface conditions of the two simulations

Two different forcing sets representing year 1992 are used to drive the model, and their respective impact on the dynamics of Polynya are compared. This first is the Drakkar Forcing Set No3 (DFS3) used to drive the ORCA025-G70 experiment. The second is provided by a regional downscaling of year 1992 of ERA40 by the atmospheric MAR model.

Experiment driven by DFS3

DFS3 combines elements of the CORE forcing data set of Large and Yeager (2004) with atmospheric state variables of ERA40 reanalysis. As described in details in Brodeau et al. (2007), the atmospheric forcing variables of DFS3 are i) from CORE: precipitation (rain and snow), downward shortwave and longwave radiations, ii) and from ERA40: wind, air humidity and air temperature. DFS3 provides monthly precipitation, daily radiation fluxes and at 6 hourly turbulent variables (Table 1). Forcing fields are interpolated from their original resolution of about 1° onto the finer model grid using the SOSIE interpolation software (Brodeau, 2007).

Note that a correction of the strength of the katabatic winds around Antarctica is applied to DFS3 winds (Mathiot et al. 2007), based on a comparison of ERA40 with previous results of regional scale atmospheric simulations carried out with MAR. This correction significantly increases the strength of the continental winds at the coast, to correct for a drastic underestimation of the katabatic winds in ERA40.

DFS3 covers the period 1958 to 2004. Year 1992 is used to continue this run and to produce a reference experiment of the Ross Sea ocean model (referred to as the "DFS3 run" hereafter). The solution of this DSF3 run was compared to the solution of the ORCA025-G70 experiment in year 1992 in the Ross Sea region by Jourdain (2007), who found that both solutions are very similar, indicating a good behaviour of the open boundaries.

Experiment driven by MAR

The second forcing set was built from simulations carried out by Jourdain (2007) with the MAR model. MAR is a regional mesoscale atmospheric model based on 3-dimensional primitive equations in sigma coordinates (Gallée and Shayes, 1994).

Four hydrometeors are represented in the hydrologic cycle, with autoconversion, but also nucleation and sedimentation of crystals. The ice sheet is assumed to be entirely covered with snow, and a snow model allows snow metamorphism. The surface energy fluxes depend on the metamorphism.

The radiative scheme takes into account clouds with their optical thickness. The turbulent fluxes in the surface boundary layer are from implicit schemes based on Monin-Obukov theory. Blown snow is also represented in the turbulent scheme (Gallee, 2001), so it plays a role on the hydrologic cycle and the atmosphere stability. The orographic roughness length is deduced from the variance of the topography. This length has been tuned with automatic weather stations (AWS) so that valleys in the Transantarctic Mountains are represented as well as possible with regard to the resolution. This is a key point in order to get a good representation of katabatic winds.

The configuration of MAR used here covers the same domain as the Ross Sea ocean model shown in Figure 1. The horizontal grid resolution used here is 40 km and the first vertical level is about 10 m. MAR has been coupled to the Ross Sea ocean model by Jourdain (2007). Here, MAR is used in a forced mode, and is integrated for 1 year (1992) with the surface boundary conditions (sea ice and ocean) and lateral conditions taken from year 1992 of ERA40. Surface variables from that experiment are used to define an atmospheric forcing for year 1992 for the Ross Sea ocean model. The same time sampling as for DFS3 is used and variables are interpolated on the ocean model grid. We refer to this forcing as the "MAR forcing" hereafter.

The MAR forcing is used to drive the Ross Sea ocean model. This experiment is referred to as the "MAR run" and is compared to the DFS3 run in section 4.

Comparison of the two forcing sets

The MAR forcing is compared to DFS3 in the Ross Sea domain in Table 1. MAR produces a colder (by 2°C) and dryer air at the surface. But the greatest impact of a dryer atmosphere in MAR is seen on the amount of snow and precipitation (3 to 5 times smaller in MAR) and in the radiation fluxes (an increase of 40 Wm^{-2} in the shortwave downward radiation, is nearly balanced by a decrease of 50 Wm^{-2} in the longwave downward. The low precipitation in MAR is attributed to the non-prescription of clouds and their water content at the open boundaries of the regional model.

	Frequency	*Origin*	*Mean value*	*Origin*	*Mean Value*
T10 *(°C)*	6h	ERA40	270.12	MAR	268.84
Q10 *(Kg/kg)*	6h	ERA40	2.96×10^{-3}	MAR	2.13×10^{-3}
|U10| *(m/s^1)*	6h	ERA40	8.68	MAR	8.75
Lw *(W/m^2)*	24h	CORE	259.62	MAR	210.21
Sw *(W/m^2)*	24h	CORE	102.75	MAR	140.44
Precip *(mm/s)*	1 month	CORE adjusted	2.28×10^{-5}	MAR	4.32×10^{-6}
Snow *(mm/s)*	1 month	CORE adjusted	9.35×10^{-6}	MAR	2.74×10^{-6}

Table 1

Domain averaged mean 1992 value of the surface fluxes and atmospheric variables entering the forcing of the Ross Sea ocean model for ERA40 and MAR.

Polynya properties

This section concentrates on the properties of the RISP in the MAR run and in the DFS3 run. Coastal polynyas such as the RISP are mainly driven by winds. They exhibit low ice fraction and large rates of sea ice production. The area which defines a coastal polynya is defined here according the criterion of Marsland et al. (2004).

- ice fraction lower than 70%
- ice production greater than 1 m per month
- ocean depth shallower than 1200 m

This criterion allows discriminating coastal polynyas from ice edge and open ocean polynyas. An example on the coastal polynyas detected on 18 July 1992 in the MAR run is shown in Figure 2. The RISP is the long polynya stretching along the Ross Ice Shelf at the southern limit on the domain. Note that sea-ice concentration gets down to nearly 40% in some locations, suggesting the possible occurrence of very strong air-sea exchanges of heat.

In the following, the comparison between MAR and DFS3 runs is made from daily means, and only for the area that defines the RISP. This area varies from day to day, and area averaged values presented in this study take these variations into account. Note that the RISP is not defined in January and December since most of the sea ice is melted in austral summer in our experiments.

Area, ice production, heat flux

Fluxes produced by MAR and DFS3 runs over the RISP have a very comparable time variability: the correlation of the two daily time series is about 0.61 for the wind stress and 0.53 for the net heat flux. Time-mean area-averaged properties of the RISP are summarised in Table 2. The heat loss is greater by 63 Wm^{-2} and shows a much greater standard deviation in MAR. As shown in Figure 3, the net heat loss often exceeds 400 Wm^{-2} in MAR, and values ranging from 90 Wm^{-2} to 700 Wm^{-2} are found during the year. In DFS3, daily values of the heat flux are concentrated in a narrower range between 150 Wm^{-2} and 400 Wm^{-2}, values above 400 Wm^{-2} being rarely reached. The wind stress is in average 10% stronger in DFS3 (thanks to the rescaling applied as described in section 3.1), but large values (> 0.2 Nm^{-2}) are more frequent and maximums higher in MAR. Theses discrepancies in the local forcing have a strong impact on the RISP sea ice production rate (Figure 3). The volume of ice formed in the polynya (Table 2) is in average greater in MAR (100 km^3/year) than in DFS3 (70 km^3/year). Figure 3 illustrates an interesting feature of the impact of the atmospheric forcing on ice formation, which is robust in both runs: For small winds (stress

below 0.2 Nm^{-2}), strength of the wind, amplitude of the heat loss and volume of sea ice formed appear to be correlated (stronger winds corresponding to greater heat loss and more ice). This correlation does not seem to hold at higher wind speed. For stress above 0.2 Nm^{-2}, the influence of the heat exchanges is greatly diminished and the volume of new ice formed is more directly driven by the strength of the wind. In DFS3, no obvious correlation between the three variables is shown.

	MAR		DFS3	
	Mean	Std	Mean	Std
Wind stress (N/m^2)	0.09	0.10	0.11	0.12
Heat fluxes (W/m^2) Turbulent Radiation	-325 -243 -82	95	-262 -204 -58	55
Polynya area (km^2)	8848	5624	10487	6302
Total ice produced (km^3)	100 km^3		70 km^3	
Mixed layer overturning (May-Nov) (Sv)	0.45	0.36	0.37	0.30

Table 2

Mean value and standard deviation of area averaged properties of the Ross Ice Shelf Polynya in MAR and DFS3 simulations.

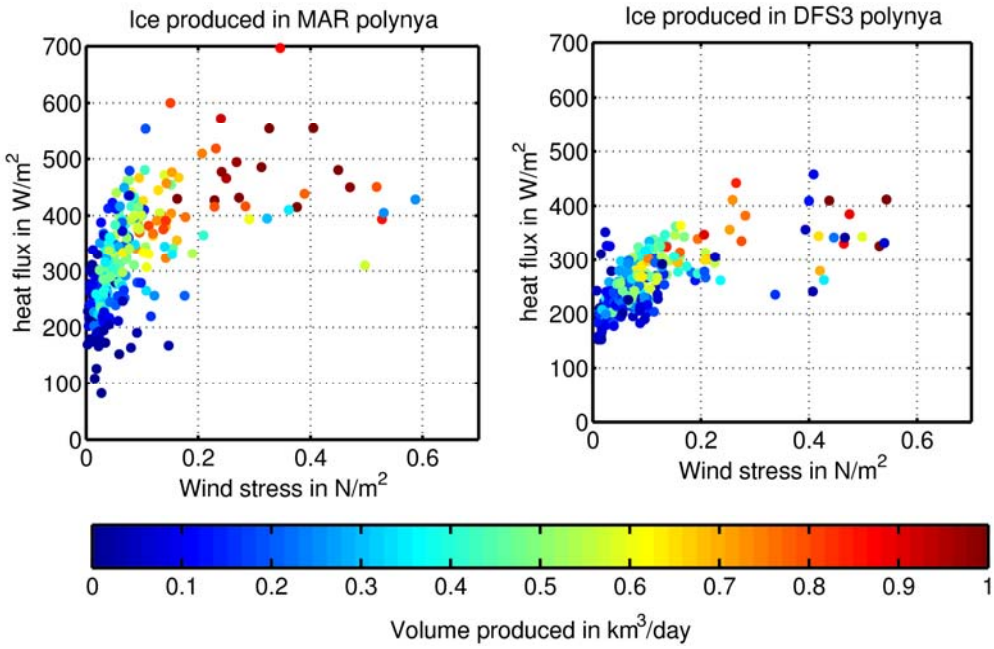

Figure 3

Volume of Ice (km3/day) produced in the MAR run (left) and in the DFS3 run (right) for every day of year 1992, as a function of the area averaged heat flux and wind stress. Each dot corresponds to a day of 1992, and its colour represents, in km^3, the volume of ice formed that day.

If the polynya simulated in the MAR run shows, in annual mean, the greatest volume of ice produced, it also represents a smaller area (8848 km^2 against 10487 km^2 in DFS3), which may seems a contradiction since Figure 4 shows that the daily ice production is strongly related to the polynya area. However, this figure also shows that for comparable polynya areas, MAR often produces more ice than DFS3, likely due to its colder atmosphere. Figure 4 also shows that the MAR run presents a much greater spread, indicating a much greater variability in ice production for a given polynya area. MAR also shows a much greater number of days of high (> 0.6 km^3) ice production, but DFS3 shows a greater number of days of high extent (> 20 000 km^2). Therefore, we conclude that the RISP simulated by MAR is significantly more productive than the one simulated by DFS3, its smaller extent suggesting difficulty to export the excess of newly formed sea-ice in MAR (+30km^3 per year, Table 2).

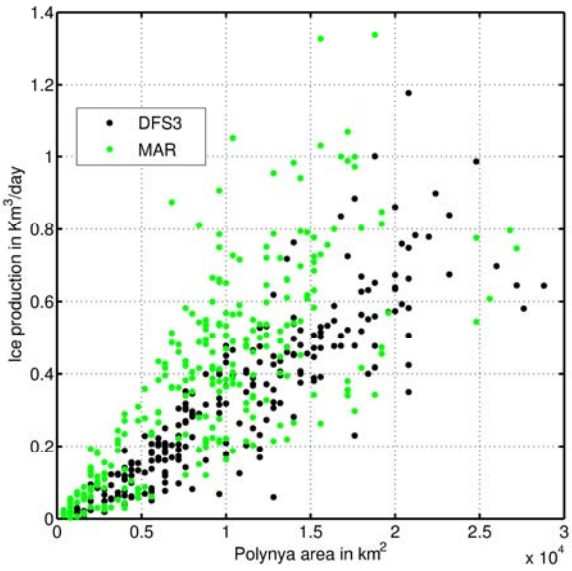

Figure 4

Total sea ice production in polynya in km^3/day against polynya area in km^2 for DFS3 (black) and MAR (green) for each day of the one year simulation.

If the polynya simulated in the MAR run shows, in annual mean, the greatest volume of ice produced, it also represents a smaller area (8848 km^2 against 10487 km^2 in DFS3), which may seems a contradiction since Figure 4 shows that the daily ice production is strongly related to the polynya area. However, this figure also shows that for comparable polynya areas, MAR often produces more ice than DFS3, likely due to its colder atmosphere. Figure 4 also shows that the MAR run presents a much greater spread, indicating a much greater variability in ice production for a given polynya area. MAR also shows a much greater number of days of high (> 0.6 km^3) ice production, but DFS3 shows a greater number of days of high extent (> 20 000 km^2). Therefore, we conclude that the RISP simulated by MAR is significantly more productive than the one simulated by DFS3, its smaller extent suggesting difficulty to export the excess of newly formed sea-ice in MAR (+30km^3 per year, Table 2).

Comparison with the few available observations is difficult and may not be reliable since the criterion used to define polynyas varies between studies. Using satellite observations, Tamura et al. (2007) estimates the ice production in the RISP to 300 km^3/year, three times the MAR estimate (detection criterion based on an ice production greater than 4m per year). In a review study, Maqueda (2004) gives an averaged polynya area of about 25 000 km^2 (more than twice the value obtained in DSF3), and a maximum extent of 50 000 km^2 (28 800 km^2 in DFS3). In this latter study, detection criterion is based on a brightness temperature T_b lower than 190 K. These results suggest that the model polynya underestimates both the ice production and the ice area. The reason is not yet identified. It seems that the export of newly formed sea ice is insufficient in both simulations (MAR and DFS3). This could be a flaw of sea ice model, but also the result of inaccuracies in the reanalysed winds simulated by ERA40 and MAR (Jourdain, 2007) in this region or the simulated circulation at the scale of the basin.

Tamura et al. (2007) estimates the average sea ice thickness in the polynya to 10 cm, when it is 40 cm in MAR and DFS3 runs. This value in the model is strongly dependent of the "accretion parameter" with set the minimum thickness of newly formed sea-ice, which is set to 30 cm in the model. This parameter certainly needs to be changed to improve the simulation of polynyas in NEMO.

Shelf water production in polynya

This section shows the impact of polynyas on the production of dense shelf waters. During sea ice production, salt is rejected and the salinity of surface waters increases. This leads to convection in the polynya. Surface waters sink, push the deeper shelf water outside the polynya area, and are replaced by new fresher surface waters. This process creates what we called here a convectively forced overturning. We expect this process to be of different strength in the MAR and the DFS3 runs, considering the great difference in ice production between the two runs.

The annual cycle of this overturning and of the mixed layer depth (*mld*) is shown for the two runs in Figure 5. In the MAR run, the mixed layer depth increases rapidly to 400 m between month 4 and 7 and then remains steady until a slow restratification begins at the end of month 10 (October). Note that the ocean restratification occurs mainly during the months of December and January, when the polynya no longer exists (this is why the restratification does not appear clearly in Figure 5 which present what occurs in the polynya). In DFS3, the deepening of the *mld* is slower, and the maximum (about 350 m) is not reached

before month 10. Note that the variation of the *mld* are subject to large high frequency variations in both simulations, their amplitude being greater in MAR. A very interesting feature revealed in Figure 5 is that the *mld* is unambiguously the depth where the flow crossing the borders of the polynya reverses: from May to November waters enter/exit the polynya above/below the mixed layer. The *mld* is thus the depth separating the upper and lower branches of the polynya overturning. The mean strength of the overturning (May to November mean) is 0.45 Sv in MAR, and 0.37 Sv in DFS3, but instantaneous values can be significantly greater (Table 2).

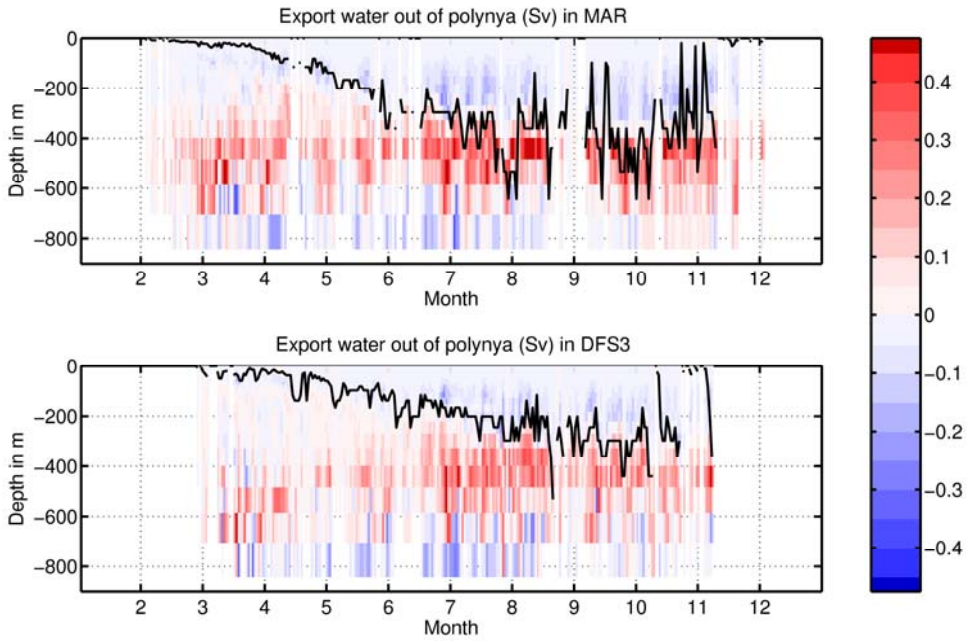

Figure 5

Daily time series of the inflow (blue) and outflow (red) volume transport in Sv in the water column defined by the Ross Ice Shelf Polynya. The black line is the area averaged mixed layer depth (in meter) in the RISP.

The properties of the mixed layer are shown in Figure 6. As expected, the mixed layer is systematically saltier (+0.15) in the MAR run (except for a short period in summer) in relation with the greater production of sea-ice. The MAR mixed layer temperature is warmer (+0.03°C) from the beginning of the year until August and colder (-0.02°C) from August to November. Since density is strongly driven by salinity in cold water, the density follows the salinity and the mixed layer waters are systematically denser (by 0.1 to 0.2) in MAR.

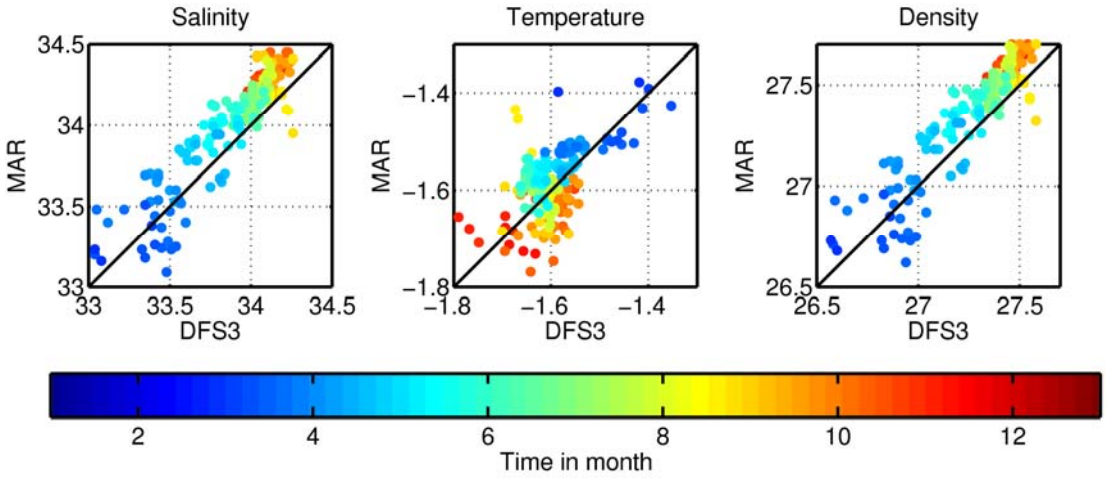

Figure 6

Scatter plot of mixed layer properties (from left to right: Temperature (°C), Salinity(psu), Potential density(kg/m^3)) between DFS3 and MAR runs over the year of simulation. Each point represents the value of a property at a given day, the colour indicating the progression of the time.

Therefore, the MAR run produces significantly saltier and denser shelf waters than DFS3. In long model runs (decades or more), this would have an impact on the amount and properties of the high salinity shelf waters and their contribution to the formation of the Antarctic Bottom Waters (AABW). The importance of the local forcing around Antarctica for the global ocean circulation is therefore stressed out by these model results.

Conclusion

We have shown that the Ross Ice Shelf Polynya is strongly influenced by the atmospheric forcing fields, and that two different estimates of the forcing, which a priori are both representative of the air-sea exchanges in the region, produce different properties of the polynya and of the dense water formed on the shelf. The MAR forcing, which is a downscaling of ERA40 with a regional atmospheric model produces a colder and dryer atmosphere and more extremes in the variability of the atmospheric forcing. Compare to the DFS3 forcing strongly based on ERA40, MAR produces a polynya of smaller extent, but much more productive in terms of ice production and formation of high salinity shelf waters. However, comparison with available observations indicates that the NEMO based model still underestimates several important polynya properties such as the extent and ice production, and overestimates the ice thickness in the polynya. The behaviour of the sea ice model itself certainly contributes to these flaws, and its sensitivity to a wide range of parameter values will have to be explored.

A next step is to simulate coastal polynyas all around Antarctica and to study the different paths taken by the high salinity waters they produce. The present work already confirmed that shelf waters produced in the Ross Sea travel around Wilkes Land Coast. The development of the coupled ocean/Ice/Atmosphere model initiated by Jourdain (2007) will be continued. However, the realism of this model will be limited by the absence of ice shelf cavities in the ocean model. This will have to be introduced in NEMO in a near future. In the short term, a parameterisation of the effect of the ice shelves on the temperature and salinity of the Antarctic shelf waters is being implemented to reach a greater realism and to confront model results with the observations of Rintoul (1998, 2007). The extension of the present work to the whole Antarctica will be carried out with the southern ocean model developed by the Drakkar consortium at 1/2° (PERIANT05) and 1/4° (PERIANT025).

References

Brodeau L., B. Barnier, T. Penduff, A.-M. Treguier and S. Gulev, 2007: An ERA40 based atmospheric forcing for global ocean circulation models. In preparation for *Ocean Modelling*.

Brodeau L., 2007: Contribution à l'amélioration de la fonction de forçage des modèles de circulation générale océanique, PhD Thesis, Université Joseph Fourier.

Drakkar Group, 2007: Barnier B., Brodeau L., Le Sommer J., Molines J.-M, Penduff T., Theetten S., Treguier A.-M., Madec G., Biastoch A., Böning C., Dengg J., Gulev S., Bourdallé Badie R., Chanut J., Garric G., ALderson S., Coward A., de Cuevas B., Haines K., Smith G., Drijfhout S., Hazeleger W., Severijns C., KNMI, Myers P: Eddy permitting ocean circulation hindcasts of past decades. *CLIVAR Exchanges*, No 42 (vol 12 No3), 8-10.

Fichefet T. and M.A. Morales Maqueda, 1997: Sensitivity of a global sea ice model to the treatment of ice thermodynamics and dynamics, *Journal of Geophysical Research*, Vol. 102, N° C6, pp 12.609-12.646.

Gallée, H., G. Guyomarc'h, and E. Brun, 2001: Impact of snow drift on the antarctic ice sheet surface mass balance: Possible sensitivity to snow-surface properties, *Boundary-Layer Meteorology* , 99 , 1–19.

Gallée H. and G. Shayes, 1994: Development of a three dimensional meso-scale primitive equations model, katabatic winds simulation in the area of Terra Nova Bay, *Ant. Mon. Weather Rev*., 122, 671-685.

Jourdain, N., 2007. Simulations climatiques couplées Atmosphère Océan Glace de mer en Antarctique. PhD Thesis, Université Joseph Fourier.

Large W.G. and S. G. Yeager, 2004: Diurnal to decadal global forcing for ocean and sea-ice models: The data sets and flux climatologies. *Technical Report TN-460+STR*, NCAR, 105pp

Madec, G., 2007: the NEMO ocean engine, Note du Pôle de Modélisation de L'IPSL.

Maqueda M.A., A.J. Willmot and N.R.T. Biggs: 2004. Polynya Dynamics : A Review of Observations and Modelling. *Review of geophysics*, 42

Marsland, S;J., N.L. Bindoff, G.D. Williams, W.F. Budd: 2004. Modeling water mass formation in the Mertz Glacier Polynya and Adélie Depression, East Antarctica, *Journal of Geophysical Research*, Vol 109, N° C11.

Mathiot P., B. Barnier, H. Gallée, J.M. Molines and T. Penduff, 2007: Correction of katabatic winds in ERA40 and its effect on polynya and shelf water in Antarctica. *Geophysical Research Abstracts,* vol.9, 02795.

Rintoul, S.R: 1998. On the origin and influence af Adèlie Land Bottom Water. Ocean, Ice, and Atmosphere: Interactions at the Antarctic Continental Margin, *Antarctic Research Series,* Volume 75, Pages 151-171

Rintoul, S.R.: 2007. Rapid freshening of Antarctica Bottom Water formed in the Indian and Pacific oceans. *Geophysical Research Letters*, 34, L06606

Simmons, A. J., et J. K. Gibson: 2000, The era-40 pro ject plan, ERA-40 project report series , 1 , 63 pp,. 43

Tamura, T., K.I. Ohshima, S. Nihashi: 2007, Mapping of thin sea ice and ice production in the Southern Ocean and Okhotsk Sea. IUGG JGS005, July 9, Perugia.

Valke S., A. Caubel, R. Vogelsang, D. Declat, 2004: OASIS3, Ocean Atmosphere Sea Ice Soil, User's guide. Report TR/CMGC/04/48, CERFACS, Toulouse, France, 73 pp.

Arctic and Antarctic sea ice concentration and sea ice drift satellite products at Ifremer/CERSAT

By Fanny Girard-Ardhuin[1] , Robert Ezraty[1] and Denis Croizé-Fillon[2]

[1] Ifremer, DOPS/LOS, BP 70, 29280 Plouzané, France
[2] Ifremer, CERSAT, BP 70, 29280 Plouzané, France

Introduction

Sea ice cover and motion have major impacts on heat fluxes between ocean and atmosphere in polar areas. Moreover, the Arctic ice growth and melt impact the fresh water flux which then has an important role in the thermohaline circulation of European seas (Aagaard et al., 1985). This is why sea ice observations are required at global scale in order to better understand the role of sea ice in ocean circulation or climate change.

This paper presents the sea ice concentration and sea ice drift datasets from satellite, available at Ifremer via the Centre d'Exploitation et de Recherche SATellitaire (CERSAT). Ifremer/CERSAT datasets are unique: the data are systematically produced daily (only during the winter for the drift), at polar scale, since 1992 (a time series longer than 15 years exists). Moreover, we show that merging independent drift fields inferred from independent sensors on different satellites improves the reliability of each of the final merged drift field. It has been proven that the Ifremer/CERSAT sea ice drift dataset is suited for assimilation in models. Section 2 presents the sea ice concentration data, section 3 the sea ice drift data. Conclusions and perspectives follow in section 4

First, we present our sea ice concentration product in Arctic and Antarctic oceans (section 2). Since the 1970's, passive microwave radiometers as the Special Sensor Microwave Imager(s) (SSM/I) have been commonly used to estimate sea ice concentration from the daily brightness temperature data. The final resolution is a 25 km x 25 km pixel for the lower frequencies and a 12.5 km x 12.5 km resolution for the 85.5 GHz channels. We focus here on the 12.5 km resolution sea ice concentration dataset produced at Ifremer/CERSAT which starts in 1992. The methods used to infer sea ice concentration are described, and the improvements implemented at Ifremer/CERSAT are presented. Then the description of Ifremer/CERSAT concentration dataset follows.

Second, we present our sea ice drift products (section 3). The sea ice drifts shown here concern only the Arctic ocean where it has been extensively validated with in situ data, which is not the case for the Antarctic ocean. Nevertheless, some test for Antarctic drift data exist but they need to be improved and then validated for systematic production.

Since 1979, buoys are moored in Arctic ice, each year, in the framework of the International Arctic Buoy Program (IABP). They provide continuous local measurements (pressure, air temperature, ice drift) at very high spatial and temporal resolutions but at a very coarse spatial distribution, providing a short term view of the velocity field (Colony and Thorndike, 1984). Since the 1990's, sea ice drift can be estimated from satellite data, daily and with global coverage of the polar ocean. Given the sensor spatial resolution and the magnitude of the expected drifts, the signature of the feature to be tracked must persist for several days. The ice motion is thus estimated at the scale of large ice floes, whereas a buoy measures the drift of a single ice floe. Data from high spatial resolution satellite sensors have also been used for sea ice drift estimate in feasibility studies, for example with Advanced Very High Resolution Radiometer (AVHRR, Emery et al., 1991) and Synthetic Aperture Radar (Kwok et al., 1990). These demonstrations are limited to local or regional studies. Here, we focus on sea ice drift at large scale (or polar scale). These estimates are inferred from passive (radiometers) and active microwave sensors (scatterometers). The methods used to infer sea ice drift are described, then the specific processing performed at Ifremer/CERSAT is presented. The two final Ifremer/CERSAT products are the Merged drift product which results from the optimal combination of SSM/I drift data with QuikSCAT drift data, and a higher grid resolution product estimated from data of the Advanced Microwave Scanning Radiometer Earth observing system (AMSR-E).

Conclusions and perspectives on the use of the Ifremer/CERSAT sea ice concentration and drifts datasets are presented in section 4.

Arctic & Antarctic sea ice concentration maps

This section presents the sea ice concentration data, with the methods used to infer the data (section 2.1) and the Ifremer/CERSAT dataset (section 2.2).

Methods

Among various algorithms, sea ice concentration is usually estimated either from the NASA team algorithm (Cavalieri et al., 1992) or from the Bootstrap algorithm (Comiso et al., 1997). Both algorithms use the low frequency channels of the SSM/I, yielding the 25 km x 25 km resolution of the sea ice concentration maps as distributed by the National Snow and Ice Data Center (NSIDC, Boulder, Colorado, data available at http://nsidc.org/).

The need for higher resolution sea ice concentration data to monitor the marginal ice zones, polynia and leads opening has required the development of new algorithms relying on the 85.5 GHz channel brightness temperature data. Among these algorithms, the Artist Sea Ice (ASI) algorithm developed at the University of Bremen (Germany) provides reliable results (Kaleshke et al., 2001). This algorithm combines the Svendsen algorithm (Svendsen et al., 1987) and the NASA team algorithm (Cavalieri et al., 1992) used as background information.

Note that no matter which algorithm is used, it is not possible during the summer period to distinguish open water area from melt ponds, which induce concentration artefacts.

In order to produce the Ifremer/CERSAT sea ice concentration maps and dataset at a resolution of 12.5 km x 12.5 km, the ASI algorithm is applied to the whole 85.5 GHz brightness temperatures dataset (1992-present) of the SSM/I. At this frequency the sensor resolution matches the map resolution. In order to discard artefacts at low latitudes, a monthly climatological sea ice mask is applied. A “neutral area”, defined as a three pixel-wide band along the coast lines is flagged, because there, the concentration estimates are quantitatively not reliable. This is due to land contamination effect within the footprint of the sensor. Finally, a correction has been applied to dismiss some of the remaining unrealistic concentration values in this area, mainly in the estuaries.

Ifremer/CERSAT sea ice concentration dataset

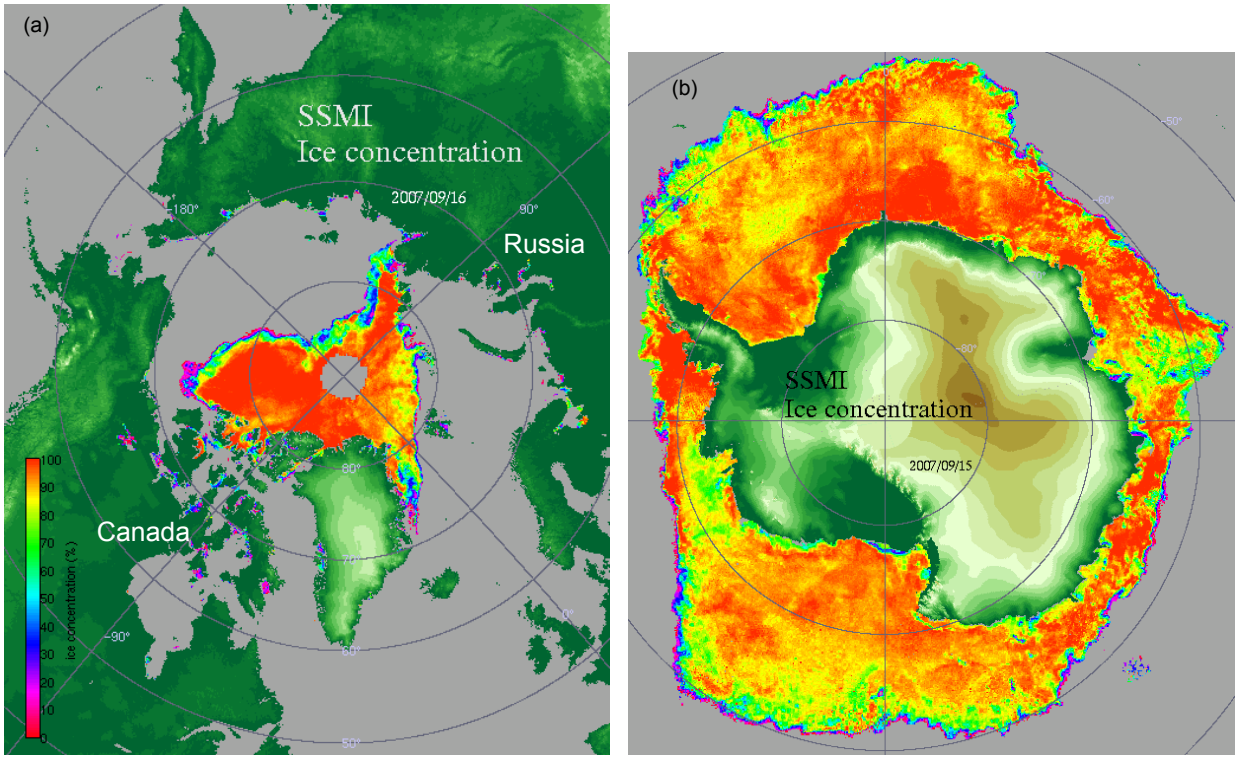

Figure 1

Daily sea ice concentration maps in mid-September 2007 in Arctic (a) at its minimum record area to date and Antarctic (b) from SSM/I radiometer data. Grid spacing is 12.5 km. Concentration is in percentage.

Arctic and Antarctic sea ice concentration data and maps at 12.5 km resolution are available daily (see examples in figure 1). Monthly data and a 15-year long climatology (1992-2006) are also available (Ezraty et al., 2007a). These maps are produced systematically because they are used as a background for the sea ice drift estimations presented hereafter. Sea ice concentration data, maps and documentation are available on the CERSAT anonymous FTP site at Ifremer: ftp://ftp.ifremer.fr/ifremer/cersat/products/gridded/psi-concentration/

Data are provided in polar stereographic projection with the projection plane intersecting the earth at 70° latitude so that little or no distortion occurs in the ice zone. The near-polar orbit of the satellite and the sensor geometry induce a data gap near the Pole (circle of 254 km radius), which appears on Arctic maps but not on Antarctic maps where the data gap is located over the continent.

Arctic sea ice drift field products

Sea ice drift fields at global scale exist since the beginning of the Arctic monitoring with the low frequency channels of the SSM/I radiometer sensor. Methods used to infer drift are presented in section 3.1. Sea ice drifts can be inferred as long as the pixel resolution of the sensor is adapted to the drift values. This is why sea ice drifts measurements concern mainly Arctic area, in Antarctic area, drifts have larger values and are thus more difficult to deduce. We present here the Ifremer/CERSAT systematically processed sea ice drifts in the Arctic.

Sea ice drifts deduced from radiometers have a reasonable accuracy but are limited by data gaps and low data density at the beginning and the end of the cold period. This can be improved using scatterometer data to built a merged product (section 3.2). Recently, AMSR-E radiometer provides a higher grid resolution because of its enhanced ground resolution. The drift dataset inferred is presented in section 3.3. More information about Ifremer/CERSAT drift datasets are in section 3.4.

Methods and results

In this section, methods to infer sea ice drifts are presented. Moreover, the results of the comparison with in situ buoys measurements are summarized.

Passive microwave radiometers data like SSM/I brightness temperature data have been also widely used to estimate Arctic sea ice drift. High frequencies data are very sensitive to atmospheric effects (moisture and liquid water). In order to determine sea ice drift from successive brightness temperature maps, stable radiation of the sea ice cover and negligible influence of the atmospheric conditions are needed. This implies sea ice drift estimations at periods of low water vapour during winter, from October to April (Martin and Augstein, 2000, Ezraty et al., 2007b).

All techniques assume that the structures tracked have spatial dimensions larger than the pixel resolution. For the pixel resolution available, single ice floes cannot be detected. Several methods have been tested to determine sea ice displacements: algorithms are based on tracking common features in pairs of sequential satellite maps.

One technique which is the most widely used is the Maximum Cross Correlation (MCC), as it was used successfully with AVHRR data for example (Emery et al., 1991; Ninnis et al., 1986). This method only enables detection of translation displacement (Kamachi, 1989; Ninnis et al., 1986). A correlation is estimated between two arrays of brightness temperature: one at a given day and another one lagged in time. In particular, Ezraty et al. (2007b) apply this process to the Laplacian field of brightness temperature in order to enhance the structures to be tracked. This is the technique used for the present Ifremer/CERSAT products. The correlation is computed at each position in order to obtain a correlation coefficient array. The location of the maximum correlation is the location of the maximum similarity between the two original images. The displacement can thus be inferred. Details can also be found in Martin and Augstein (2000), Emery et al. (1997), or Kwok et al. (1998). In order to remove outliers, a minimum coefficient correlation is imposed. A comparison with the wind pattern is often applied (ECMWF model for Ezraty et al., 2007b, NCEP re-analyses for Kwok et al., 1998) since mean sea ice drift is strongly linked with the geostrophic wind (Thorndike and Colony, 1982).

Another technique to enhance the feature to be tracked is the wavelet analysis, which is similar to the Fourier transform, both in time and in space. It is applied on various spatial scales in order to separate ice features. A two-dimensional Gaussian wavelet (also called Mexican hat wavelet) can be used for ice feature detection (Liu and Cavalieri, 1998; Liu et al., 1999). It turns out that this wavelet technique is very similar to the Laplacian field enhancement as used for the Ifremer/CERSAT product. For the latter product, the statistical independence between adjacent drift vectors is achieved by properly matching the grid size of the drift field with the size of the pattern to be tracked (Ezraty et al., 2007b).

Sea ice drifts from SSM/I have been validated with buoys. Some results are summarized in Table 1. The displacements (in km) are usually converted into ice speed (in cm s^{-1}) in order to improperly compare the quality of the drift magnitude estimated at different day-lags or at various pixel size. Nevertheless, this introduces a non linear effect in the ratio. Moreover, the constant half-pixel minimum displacement embedded in the original measurement is then erroneously accounted for.

std speed difference (cm s^{-1})	std direction difference (°)	day-lag (nb of days)	sensor	reference
6		1	SSM/I	Emery et al., 1997
2.6 → 2.9	18 → 25.9	1	SSM/I	Liu and Cavalieri, 1998
4.28 → 4.52 2.58 *→ 2.89 *	46.5 → 50.4 30.6 *→ 32.8 *	3	SSM/I	Kwok et al., 1998
2.96	34.4	4	SSM/I	Liu et al., 1999
2.27 *	35.5 *	4	SSM/I	Zhao et al., 2002

Table 1

Results of the comparison between satellite drift vectors and buoys drifts for several experiments: standard deviation (std) for sea ice drift difference and for direction difference, number of day-lag, satellite sensor, and reference. * indicates that the drift magnitudes less than one pixel are excluded.

These results show that with SSM/I, sea ice drifts can be retrieved with good accuracy. Note that with a pixel resolution of 12.5 km, for 1 day-lag, the minimum displacement that can be detected is 6.25 km which corresponds to a velocity of 7 cm s^{-1}, whereas the mean buoys velocity are about 7 cm s^{-1}. Then the day-lag value to be used for a 12.5 km resolution pixel must be larger: 3 day-lag corresponds to a minimum velocity of 4.8 cm s^{-1}. The 3-day lag is commonly used.

The day-lag must be chosen accordingly to the magnitude of the expected drift (small drift – large lag; large drift – short lag). That's why the Ifremer/CERSAT products (presented in section 3.2) used 3 day-lag and 6 day-lag to infer large and small drifts (Ezraty et al., 2007a, 2007b). A 2 day-lag is also used with the 6 km resolution pixel product of AMSR-E Ifremer/CERSAT product (Ezraty et al., 2007c, see section 3.3).

Merging sea ice drift fields

We present here the advantages brought by the combination of several independent drift fields as performed at Ifremer.

Ifremer/CERSAT sea ice drift maps from SSM/I are based on the two channels of the sensor (horizontal and vertical polarizations, 'H' and 'V'). From each channel, a drift map is inferred. This results in two independent drift fields. Merging the two fields gives a drift product which is more reliable than the one inferred from a single channel.

Since 1999, SeaWinds/QuikSCAT scatterometer provides one day averaged backscatter maps at a pixel resolution of 12.5 km. These maps can be also used to estimate sea ice drift fields with the Lagrangian enhancement and MCC techniques described earlier. Due to satellite geometry and near-polar orbit, the data gap near the North Pole is smaller than that of the SSM/I (circle of 40 km radius). Ezraty et al. (2007b) combine the 'H' SSM/I, the 'V' SSM/I and the QuikSCAT sea ice drift products by optimally merging the three, leading to the "Merged" product.

The theoretical uncertainty due to the grid size can be estimated. For a square pixel of dimension D, the variance for each component is $D^2/12$. For the Merged product, this theoretical uncertainty due to quantification effect corresponds to a constant standard deviation of 3.6 km. This pixel size impact is an absolute constant error: its relative importance decreases as the magnitude of the drift increases.

std speed difference (cm s^{-1})	std direction difference (°)	day-lag (nb of days)	sensor	reference
2.91 2.90 *	39.2 29.6 *	3	SSM/I combined with QuikSCAT	Ezraty et al., 2007b (Ifremer/CERSAT product)
1.72 1.76 *	29.6 24.3 *	6	SSM/ I combined with QuikSCAT	Ezraty et al., 2007b (Ifremer/CERSAT product)

Table 2

Results of the comparison between Ifremer/CERSAT Merged drift vectors and buoys drifts during five winters: standard deviation for sea ice drift difference and for direction difference, number of day-lag, satellite sensor, and reference. * indicates that the drift magnitudes less than one pixel are excluded.

The Merged product has been validated using IABP buoys during five winters (see Table 2): the standard deviation of the difference at 3 day-lag is 2.91 cm s^{-1}, comparable with previous results quoted above for 3 and 4 day-lags (Table 1). Using 6 day-lag is even more adequate for small drifts with a standard deviation of the difference of 1.72 cm s^{-1}. Consequently, the angular data have a better resolution. The angle difference sharply decreases (to values lower than 45°) for drifts higher than 40 km. This was also noticed by Liu et al. (1999). Standard deviations decrease when small drifts (displacement lower than the pixel size) are excluded, in particular for drift direction.

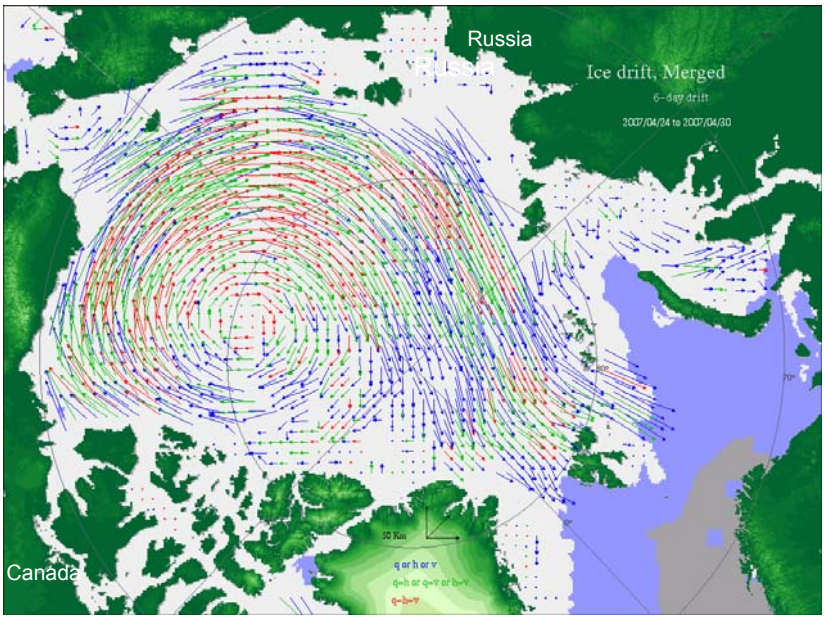

Figure 2

"Merged" Arctic sea ice drift from SSM/I radiometer drift field (2 channels) and SeaWinds/QuikSCAT scatterometer drift field at 6 day-lag on April 24th-30th, 2007. Grid spacing is 62.5 km. Drift vectors less than one pixel are marked with a cross. In red: identical drift vector for the three products, in green: identical drift vector for two products, in blue: selection or validation of a single drift vector.

Figure 2 presents an example of merged sea ice drift product at 6 day lag in April 2007 where the Beaufort gyre is visible and the transpolar drift towards Fram strait is clearly marked. The optimal combination of the three independent drift fields provides better confidence in the final resulting field than for the individual ones since each drift is inferred from independent measurement. First, the data gap at the North Pole is reduced to the smallest one (40 km large). Second, the number of valid drift vectors is increased by 12 to 15%. In particular for early fall and early spring, more than 80% of data density is reached

whereas radiometer provides hardly 60% or even less at the beginning and at the end of the winter period (see Figure 3). Third, the sea ice merged drift field enables discrimination of remaining vectors outliers of the individual products.

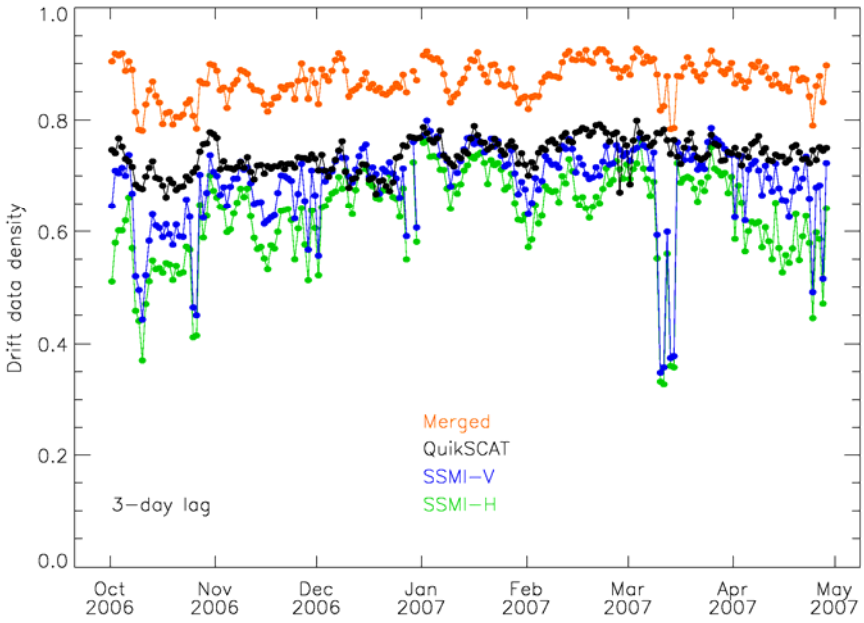

Figure 3

Times series of drift data density for the 2006-2007 winter for SSM/I at horizontal (in green) and vertical (in blue) polarizations, QuikSCAT (in black) and Merged (in red) drifts at 3 day-lag. Low data density for SSM/I in March is due to missing brightness temperature data.

Higher resolution ice drift fields

In this section, the Ifremer/CERSAT higher resolution drift product from AMSR-E radiometer data is described.

Since 2002, AMSR-E radiometer data with two polarizations at 89.0 GHz frequency provides brightness temperature maps with a pixel resolution of 6.25 km, particularly suited to detect small drifts. Similarly to SSM/I brightness temperature maps, drifts can be inferred with the Lagrangian enhancement and the MCC techniques (Ezraty et al., 2007c), keeping the same ratio between the size features to be tracked and the grid size which insures statistical independency of adjacent drift estimates.

Figure 4 presents an AMSR-E drift map for 6 day-lag with a grid spacing of 31.25 km. This map shows the same pattern as Figure 2 for the same period; but thanks to the pixel size of the AMSR-E, the grid resolution of the drift field is increased by a factor of four compared with that of the merged product. Yet with AMSR-E, there are also more patches of missing data and a wider data gap near the North Pole. Nevertheless, the angular resolution is largely improved providing a smoother drift field, than with the merged drift field (see Figure 2).

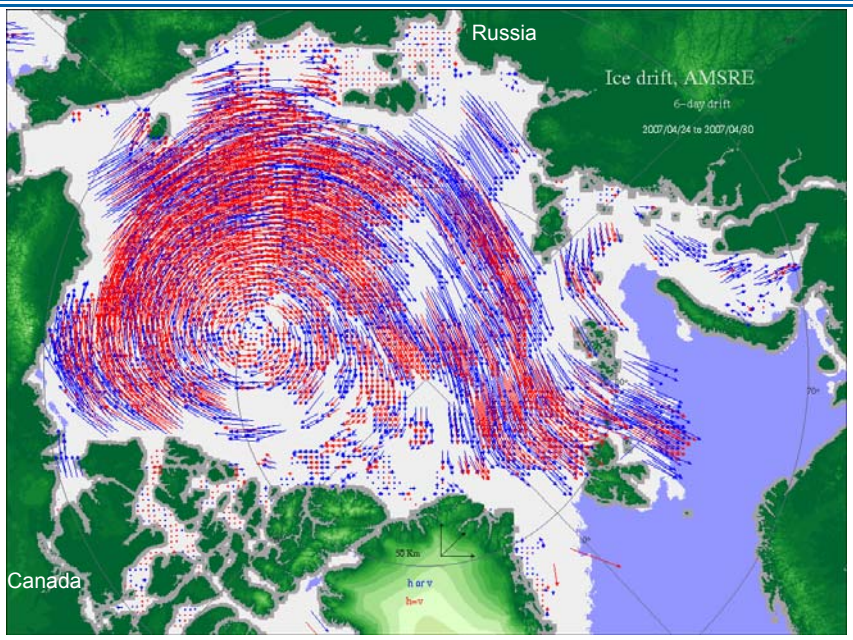

Figure 4

Arctic sea ice drift from AMSR-E radiometer data at 6 day-lag on April 24th-30th, 2007. Grid spacing is 31.25 km. Drift vectors less than one pixel are marked with a cross. In red: identical drift for horizontal and vertical polarizations, in blue: selection or validation of a single polarization.

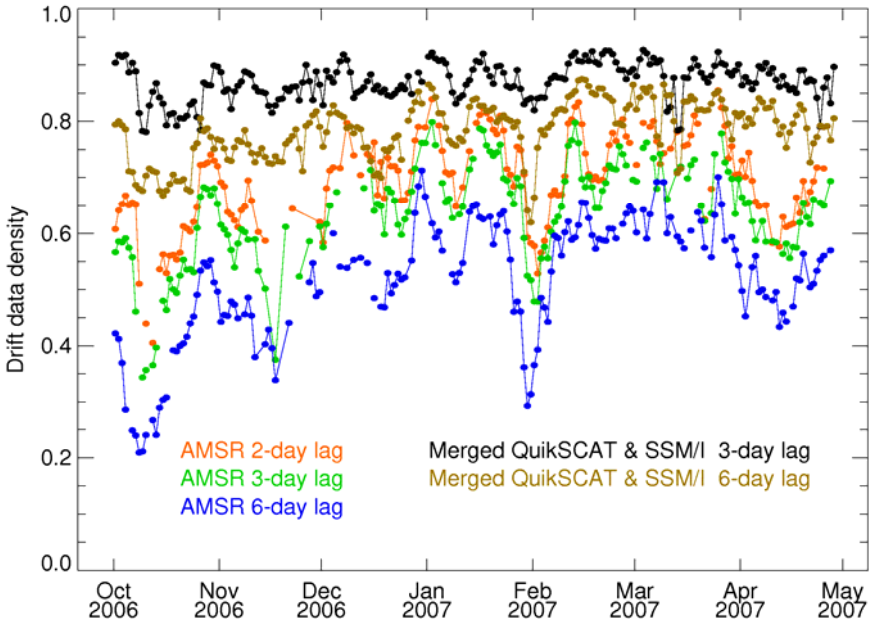

Figure 5

Times series of drift data density for the 2006-2007 winter for AMSR-E and Merged drifts at 2, 3 and 6 day-lags. Low data density for AMSR-E in November and January are due to missing brightness temperature data.

AMSR-E drifts are in good agreement with IABP buoys with a standard deviation decreasing to 2.60 cm s^{-1} at 3 day-lag and 1.59 cm s^{-1} at 6 day-lag. Figure 5 shows drift data density for several day-lags for winter 2006-2007 for AMSR-E and Merged drifts. Most of the time, AMSR-E provides 50 to 80% data density from December to March. This decreases sharply for early fall and early spring down to 20 to 50% whereas the Merged product has a data density higher than 80% for the period December-March and higher than 60% for early fall and early spring. This product is thus more suited for regional study than the merged product, which is adapted to global study.

Ifremer/CERSAT sea ice drift datasets

Three and 6 day-lags Merged Arctic sea ice drift fields dataset are available every day during winter (October until April) since 1992, using SSM/I horizontal and vertical polarizations data and with QuikSCAT data since 1999. The grid resolution is 62.5 km (Ezraty et al., 2007b). Monthly Merged drifts are also computed. At present, a 15 year long winter time series of Merged ice drifts is available.

AMSR-E Arctic sea ice drift dataset covers the period 2002-present, and drifts are available at 2, 3 and 6 day-lags with a 31.25 km grid resolution (Ezraty et al, 2007c).

Data are presented in polar stereographic projection, with the projection plane intersecting the earth at 70°N latitude so that little or no distortion occurs in the ice zone. Sea ice drift data, maps and documentation are available on the CERSAT anonymous FTP site at Ifremer: ftp://ftp.ifremer.fr/ifremer/cersat/products/gridded/psi-drift

Conclusions and perspectives

Satellites provide a unique monitoring capability of sea ice dynamics. Sea ice maps from satellite data have the advantage to cover the whole polar areas every day. This allows better coverage than that of buoys data, which have a precise daily timing, better spatial resolution but a very coarse spatial distribution.

Passive microwave measurements provide sea ice concentration datasets for both poles. The 12.5 km resolution-Ifremer/CERSAT sea ice concentration dataset is available all year long, since 1992. It is noteworthy to pin-point that the pixel size of the concentration map produced here (grid size of the concentration product) matches the ground resolution of the sensor. A 15 year long climatology is also available.

Sea ice drifts inferred only from radiometers have a reasonable accuracy but are limited by data gaps and low data density at the beginning and the end of the cold period. The main limitation is the angular resolution for small drifts: for slow motion areas, ice vector have a larger uncertainty. Recently, AMSR-E radiometer provides a better vector accuracy because of its enhanced ground resolution. Thus the time lag can be reduced to two days. The optimal merging of three independent fields of drift data (two SSM/I and one QuikSCAT) at the same resolution improves the data density and the usable time period over winter. It also enables the discrimination of the vector outliers remaining in the individual products. Noise level is dominated by the sensor ground resolution and pixel size.

Ifremer/CERSAT hosts a unique database of 15 years winter time series of sea ice drift. This dataset is available for oceanic and climate modelling. The time series will continue for Arctic long term monitoring using the new MetOp/ASCAT operational scatterometers, planned to be operated for the next 20 years. In order to ease the use of these datasets by modelers, interpolated fields filling the remaining gaps of the Merged drift fields will be available in 2008.

Satellite inferred sea ice drifts can be used to estimate the sea ice flux (Martin and Augstein, 2000; Spreen et al., 2006) and to improve large scale sea ice models by data assimilation. Radiometers drift fields have been assimilated in models, sometimes with other data (buoys for example) or with Optimal Interpolation (Zhang et al., 2003) to fill in the map. The UK MetOffice FOAM model shows better realistic results for sea ice motion when the systematically processed Ifremer/CERSAT Merged drift product at 3 day-lag are assimilated (Girard-Ardhuin et al., 2006; see also Stark et al., this issue). These drifts will also be used for assimilation in the Mercator-Ocean operational system in 2008 (see Garric et al., this issue).

References

Aagaard, K., J. H. Swift, and E. C. Carmack, 1985: Thermohaline circulation in the Arctic Mediterranean seas. *J. Geophys. Res.*, vol. 90 (C3), 4833-4846.

Cavalieri, D. J., 1992: Sea ice algorithm. *NASA Sea ice validation program for the Defense Meteorological Satellite Program Special Microwave Imager: Final report, 95 pp., NASA technical memorandum 104559, NASA, Washington, DC.*

Colony, R., and S. Thorndike, 1984: An estimate of the mean field of Arctic sea ice motion. *J. Geophys. Res.*, vol. 89 (C6), 10623-10629.

Comiso, J. C., D. Cavalieri, C. Parkinson, and P. Gloersen, 1997: Passive microwave algorithms for sea ice concentrations. *Rem. Sensing of Env.*, vol. 60, 357-384.

Emery, W. J., C. W. Fowler, J. Hawkins, and R. H. Preller, 1991: Fram strait satellite image-derived ice motions. *J. Geophys. Res.*, vol. 96 (C3), 4751-4768.

Emery, W. J., C. W. Fowler, and J. A. Maslanik, 1997: Satellite-derived maps of Arctic and Antarctic sea ice motion: 1988 to 1994. *Geophys. Res. Lett.*, vol. 24 (8), 897-900.

Ezraty, R., F. Girard-Ardhuin, J. F. Piollé, L. Kaleschke, and G. Heygster, 2007a: Arctic and Antarctic sea ice concentration and Artic sea ice drift estimated from Special Sensor Microwave data, User's manual, version 2.1, February 2007.

Ezraty, R., F. Girard-Ardhuin, and J. F. Piollé, 2007b: Sea ice drift in the central Arctic combining QuikSCAT and SSM/I sea ice drift data, User's manual, version 2.0, February 2007.

Ezraty, R., F. Girard-Ardhuin and D. Croizé-Fillon, 2007c: Sea-ice drift in the central Arctic using the 89 GHz brightness temperatures of the Advanced Microwave Scanning Radiometer, User's manual, version 2.0, February 2007.

Girard-Ardhuin, F., R. Ezraty, and J. Stark, 2006: Improving ocean models with sea ice remote sensing data. *3rd annual MERSEA meeting, London, United Kingdom. 6-7 March 2006*.

Kaleschke, L., C. Lüpkes, T. Vihma, J. Haarpainter, A. Bochert, J. Hartmann, and G. Heygster, 2001: SSM/I sea ice remote sensing for mesoscale ocean-atmosphere interaction analysis. *Canadian J. of Remote Sensing*, vol. 27 (5), 526-537.

Kamachi, M., 1989: Advective surface velocities derived from sequential images for rotational flow field: limitations and applications of Maximum Cross Correlation method with rotational registration. *J. Geophys. Res.*, vol. 94 (C12), 18227-18233.

Kwok, R., J.C. Curlander, R. McConnell, and S. S. Pang, 1990: An ice motion tracking system at the Alaska SAR Facility. *IEEE. J. Ocean. Eng.*, vol. 15 (1), 44-54.

Kwok, R., A. Schweiger, D. A. Rothrock, S. Pang, and C. Kottmeier, 1998: Sea ice motion from satellite passive microwave imagery assessed with ERS SAR and buoy motions. *J. Geophys. Res.*, vol. 103 (C4), 8191-8214.

Liu, A. K. and D. J. Cavalieri, 1998: On sea ice drift from the wavelet analysis of the Defense Meteorological Satellite Program (DMSP) Special Sensor Microwave Imager (SSM/I) data. *Int. J. Rem. Sens.*, vol. 19 (7), 1415-1423.

Liu, A. K., Y. Zhao and S. Y. Wu, 1999: Arctic sea ice drift from wavelet analysis of NSCAT and special sensor microwave imager data. *J. Geophys. Res.*, vol. 104 (C5), 11529-11538.

Martin, T., and E. Augstein, 2000: Large-scale drift of Arctic sea ice retrieved from passive microwave satellite data. *J. Geophys. Res.*, vol. 105 (C4), 8775-8788.

Ninnis, R. M., W. J. Emery, and M. J. Collins, 1986: Automated extraction of pack ice motion from Advanced Very High Resolution Radiometer imagery. *J. Geophys. Res.*, vol. 91 (C9), 10725-10734.

Spreen, G., S. Kern, D. Stammer, R. Forsberg, and J. Haarpaintner, 2006: Satellite-based estimates of sea ice volume flux through Fram strait. *Annals of Glaciology*, vol. 44, 321-328.

Svendsen, E., C. Mätzler, and T. C. Grenfell, 1987: A model for retrieving total sea ice concentration from a spaceborne dual-polarized passive microwave instrument operating near 90 GHz. *Int. J. of Remote Sensing*, vol. 8 (10), 1479-1487.

Thorndike, A. S., and R. Colony, 1982: Sea ice motion in response to geostrophic winds. *J. Geophys. Res.*, vol. 87, 5845-5852.

Zhang, J., D. R. Thomas, D. A. Rothrock, R. W. Lindsay, and Y. Yu, 2003: Assimilation of ice motion observations and comparisons with submarine ice thickness data. *J. Geophys. Res.*, vol. 108 (C6), 3170, doi:10.1029/2001JC001041.

Zhao, Y., A. K. Liu and D. G. Long, 2002: Validation of sea ice motion from QuikSCAT with those from SSM/I and buoy. *IEEE Trans. On Geosc. and Rem. Sens.,* vol. 40 (6), 1241-1246.

Sea ice concentration, ice drift and/or ice thickness data assimilation: a review of the work done in Norway, UK, France, Belgium and Canada

Introduction

After describing in details in the previous article the available data sets of Sea Ice concentration and drift (Ardhuin et al., this issue), the present article describes how these observations are used in numerical models with data assimilation. Indeed, this article gathers 5 different contributions about data assimilation of Sea Ice variables. We review the work done in Norway, UK, France, Belgium and Canada. The present article is split into the several sections below dealing with the Sea ice concentration and drift data assimilation. Note that Sea ice thickness data assimilation has been tested in Norway:

- In Norway, by Laurent Bertino and Knut Lisaeter, Mohn Sverdrup Center, Bergen, Norway.
- In the UK, by John Stark and Adrian Hines, Met Office, Exeter, UK.
- In France, by Gilles Garric and Jerome Pernin, Charles-Emmanuel Testut, Eric Greiner from Mercator-Ocean (Toulouse, France) and Fanny Girard-Ardhuin, Denis Croize-Fillon from Ifremer/CERSAT, DOPS/LOS, BP 70, 29280 Plouzané, France.
- In Belgium, by Valérie Dulière and Thierry Fichefet, Institut d'astronomie et de géophysique G. Lemaître, UCL, Louvain-la-Neuve, Belgium.
- In Canada, by Alain Caya, Mark Buehner and Tom Carrieres, Meteorological Research Division, Environment Canada and Ice and Marine Services/Environment Canada, Canada.
- Conclusions are given by Eric Greiner, from CLS/Mercator-Ocean (Toulouse, France).

Sea ice concentration, sea ice drift and thickness data assimilation in Norway: Assimilation and real-time forecasting with the TOPAZ system

By Laurent Bertino[1] and Knut Lisaeter[1]

[1] Mohn Sverdrup Center, Nansen Environmental and Remote Sensing Center, Thormoehlensgate 47, N-5006 Bergen, Norway

Introduction

At present day, 25% of the remaining natural gas reserves are expected on the Arctic Shelves. The Arctic Ocean also holds important stocks of valuable fish species, whose recruitment is sensitive to ocean conditions. There is therefore an increasing demand for accurate monitoring of ocean and sea-ice conditions in the Arctic to support public authorities and commercial activities. In parallel, the interest in the Arctic has increased as the global climate has proven sensitive to the Arctic climate, and as the sea-ice has retreated spectacularly in the recent years.

Data assimilation of Sea ice concentration and drift into the TOPAZ system

The TOPAZ system developed at the Mohn-Sverdrup Center provides forecasts of ocean currents and sea-ice conditions, with a focus on the Arctic. The HYCOM model (Bleck 2002) has been implemented in the North Atlantic and Arctic Oceans – with a horizontal resolution of 11 km to 12 km across the Arctic – and is coupled to the Elastic Viscous Plastic sea-ice model (Hunke and Dukowicz 1997). The data assimilation technique used is the Ensemble Kalman Filter (EnKF; Evensen 2006). The EnKF is set up with model errors assumed in atmospheric temperature and wind velocity to increase the model spread as the ensemble is integrated forward in time. The definition of the model errors is crucial in the EnKF to avoid ensemble bias (Lisæter *et al.* 2007). TOPAZ runs an ensemble of 100 members in near-real-time mode, assimilates ocean variables, but also sea-ice concentrations from SSM/I and merged sea-ice drift products from Ifremer (cf Girard-Ardhuin et al, this issue).

a) b)

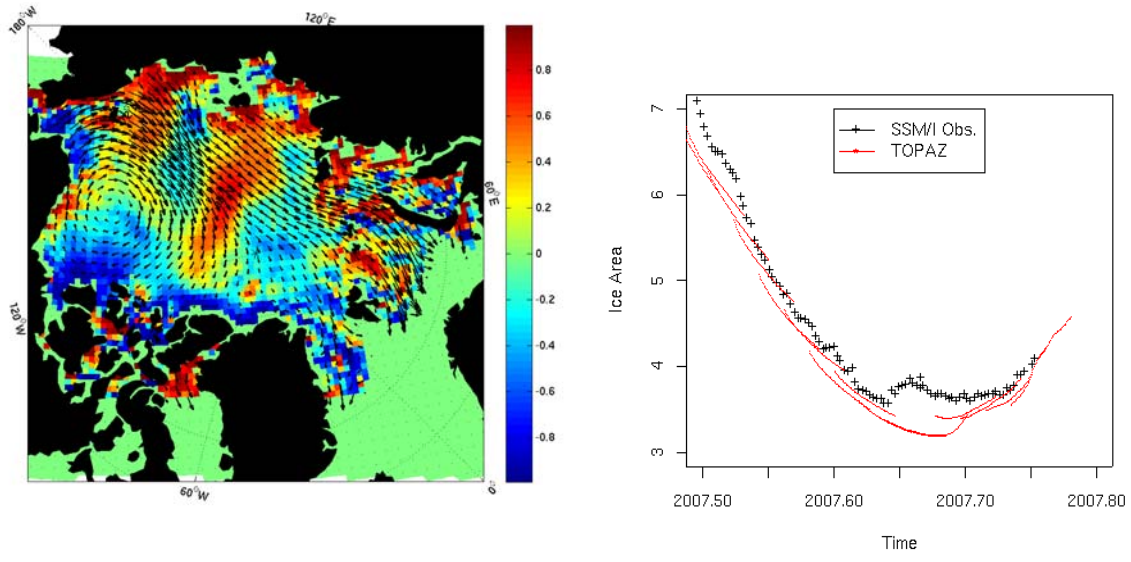

Figure 1

a) Correlation (colour background) between the y-component of the ice drift and the ice thickness, the arrows indicate average drift of the ensemble b) Arctic ice area from observations and from successive TOPAZ cycles (7 days analysis and 10 days forecasts). The time axis is fraction of a year, whereas the vertical axis has units of million square kilometers.

The ice-ocean coupling presents challenging features for the purpose of data assimilation. Firstly the system is quickly variable: the movements of the ice edge are rapid on a daily basis. The sea-ice is an insulating medium controlling the fluxes of heat and momentum into the ocean, whereas the melting or freezing of ice controls the ocean surface salinity. As a consequence the correlations between variables in the ice-ocean model system change following the location of the ice edge, and depending on the processes locally active, thus justifying a dynamical data assimilation approach (Kalman filter type). Figure 1a shows an example of correlation between the Y-component of the sea-ice drift and the thickness of the sea-ice, showing that the correlation takes different sign in areas of convergence or divergence of the ice.

The correlation shows how ice thickness reacts to changes in the ice motion – as such it is a complex plot and can be difficult to interpret; some details can be more easily explained however. For instance, north of Greenland and the Canadian Arctic Archipelago a positive ice y-component drift anomaly (which would have a upward direction on the plot) leads to a decrease of ice thickness as there is a divergence of sea-ice in that region. This leads to the predominantly negative correlation in that region. A similar mechanism leads to correlation of opposite sign along the coast of Siberia.

The coupled ice-ocean processes are everything but linear: the variables considered exhibit non-Gaussian distributions and their multivariate relationships are non-linear (Lisæter et al. 2003). A typical example is the behavior of sea surface temperature when sea-ice is present/absent. If ice is present the surface temperature is close to the freezing point while ice concentration is positive. If ice is absent the surface temperature can be above the freezing point whereas ice concentration is nearly zero. This can give a nearly step like appearance of the ensemble scatter plot of SST versus ice concentration in a given location of the model grid. This and similar behavior motivates the application of advanced data assimilation techniques, valid for strongly non-linear systems, like the Ensemble Kalman Filter. The method is valid for assimilation of different ice data types and is multivariate even though the Gaussian assumption remains limiting at times.

The Ensemble Kalman Filter uses an ensemble of model states to estimate the model error statistics. The EnKF can be seen as a version of the Kalman Filter, where the covariance matrix is replaced by the sample covariance matrix – which is the covariance matrix calculated from N estimates of the model state, where N is the number of ensemble members. The fundamental equations for the time evolution of error statistics are the Fokker-Planck equations, which describe the evolution of the probability density function (pdf) of the model. This set of equations, however, is impractical to solve for high-dimensional systems. An alternative approach for solving the equations is to sample the pdf N times, and integrate these samples (model states) forward in time using the model equations. This Monte Carlo technique is at the basis of the EnKF, and considerably reduces the computational burden compared to the Fokker-Planck equations. It should be noted, however, that the EnKF still requires a large number of ensemble members N, typically O(100), and is more costly than many other assimilation techniques. On the other hand the forward integration of one model state is completely independent from other model states, and therefore ideally suited for parallel computing.

The TOPAZ model system, as mentioned, provides weekly forecasts of sea-ice conditions in the Arctic. In 2007 the summertime sea-ice extent reached a minimum for the time period of passive microwave measurements of the sea-ice cover. How did the model perform during the historical sea-ice minimum of the summer 2007? Figure 1b shows time series of Arctic sea-ice area over successive forecasts, along with observed sea-ice extent from passive microwave sensors. It shows the forecast is accurate; the forecast tendency is to delay slightly both the melting and the freeze-up time. Surprisingly, the tendency was the opposite in 2006 although the system parameterization was the same. Simplified model parameterizations as well as the uncertainty of the atmospheric forcing in Arctic regions may cause these interannual variations in model performance.

Sea ice thickness data assimilation

In addition to the assimilation of ice drift and ice concentration, assimilation of synthetic sea-ice thickness data has been tested in anticipation of the launch of CryoSat in 2009 (Lisæter *et al.* 2007). This sensor will lead to a more complete picture of the sea-ice conditions in the Arctic – giving sea-ice thickness estimates from freeboard measurements of the sea-ice. Even though the uncertainty of individual measurements is large, the assimilation of this data set can still have a significant impact on the model description of the sea-ice cover. In Lisæter *et al.* 2007, a synthetic dataset with similar measurement characteristics that is expected from the CryoSat sensor was assimilated into a coupled ice-ocean model with the EnKF. The study clearly showed how the assimilation improved the ice thickness field in the model (relative to the synthetic data), indicating that this will be a useful dataset for assimilation purposes.

Perspectives

The TOPAZ system is being continuously improved and some of the anticipated future improvements of the TOPAZ system include the developments of a sea-ice rheology specific for the Marginal Ice Zone and data assimilation methods that can handle non-Gaussian distributions (Bertino *et al.* 2003).

TOPAZ is the Arctic component of the MERSEA integrated system and has been running three successive prototypes in forecast mode since January 2003. The authors acknowledge partial funding from the MERSEA integrated project and a grant of CPU time from the Norwegian supercomputing committee (NOTUR).

Sea ice concentration and drift data assimilation in the UK

By John Stark[1] and Adrian Hines[1]

[1] Met Office, FitzRoy Road, Exeter, Devon, EX1 3PB, UK

Investigations into Sea Ice Data Assimilation using FOAM

The technique of data assimilation is the combination of observation and model data to produce an analysis combining the information from both sources. In order to combine observations and models, the strengths and weaknesses of each must be accurately specified, in terms of biases, errors and error correlations. Some recent experiments with the FOAM model are presented showing that sea ice data assimilation can give quantitative improvements to the sea ice analysis.

The Met Office operational Forecasting Ocean Assimilation Model (FOAM, Martin et al, 2007) is a nested suite of ocean models which are run daily, producing an analysis and forecast of the global ocean out to 5 days. The sea ice assimilation scheme currently uses ice concentration fields from NCEP which are assimilated using a simple nudging scheme. Several experiments using a modified version of the FOAM suite have been performed to assimilate ice concentration and ice motion data (Stark et al. 2005), and these are described briefly below. This work was funded by the European Space Agency (ESA) under ESA/ ESTEC Contract No.17334/03/NL/FF

Within these experiments, FOAM was upgraded to include the CICE (Hunke & Lipscomb, 2004) sea ice model with 5 ice thickness categories and Elastic-Viscous-Plastic (Hunke and Dukowicz, 1997) sea ice rheology. A sea ice concentration and velocity assimilation scheme was developed and tested, and is described below. The experiments cover the period from September 1999 to December 2000.

Ice Concentration Assimilation

Ice concentration data was produced from SSM/I swath data using the Artist Sea Ice (ASI) algorithm (Kaleschke et al. 2001; Girard-Ardhuin et al., this issue). These data were assimilated using an optimal interpolation (OI) procedure similar to SST (Martin et al 2007). The increments were nudged in incrementally during the 24h cycle, with compensating changes to the surface ocean salinity to balance total salt. In order to minimise changes to the ice volume and latent heat, the assimilation increments were made to the thinnest model ice layer only.

Ice Velocity Assimilation

Sea ice has very little inertia compared to the stresses acting on it. Any changes to the modelled sea ice velocity made by the assimilation are only effective for a few hours, since the sea ice can easily return to the model equilibrium state. This means that without compensating changes to the external fields, very little forecast improvement can be made to sea ice motion through assimilation. In our experiments with FOAM we therefore introduced an extra stress term, $\boldsymbol{\tau}^{\mathrm{i}}$ into the sea ice momentum equation:

$$m\frac{\partial \mathbf{u}}{\partial t} = a\boldsymbol{\tau}^{\mathrm{a}} + a\boldsymbol{\tau}^{\mathrm{w}} - \hat{k}\times mf\mathbf{u} + \nabla\cdot\sigma + a\boldsymbol{\tau}^{\mathrm{i}} \quad . \qquad (1)$$

where m is the combined mass of ice and snow per unit grid box area, $\boldsymbol{\tau}^{\mathrm{a}}$ and $\boldsymbol{\tau}^{\mathrm{w}}$ are the grid box mean wind and ocean stresses, $\mathbf{u}$ is the ice velocity, a is the ice fractional area, f is the Coriolis parameter, and $\nabla\cdot\sigma$ represents the internal forces exerted by the ice. Forcing due to the slope of the sea surface is neglected.

The 3-day drift observations are converted to mean velocities, and an OI analysis of the difference between these and the modelled mean velocities (analysis increments) is computed.

The stress term, $\boldsymbol{\tau}^{\mathrm{i}}$ is computed using a free drift approximation to the ice momentum equation above. The ice stress increment required to obtain a new equilibrium state, at velocity u + ui is given by

$$a\boldsymbol{\tau}^{\mathrm{i}} = a\boldsymbol{\tau}^{\mathrm{w}}\left(\mathbf{u}+\mathbf{u}^{\mathrm{i}}\right) - a\boldsymbol{\tau}^{\mathrm{w}}\left(\mathbf{u}\right) + \hat{k}\times mf\mathbf{u}^{\mathrm{i}} \qquad (2)$$

where $\boldsymbol{\tau}^{w}(\mathbf{u})$ gives the ice-ocean stress at ice velocity $\mathbf{u}$. Here, the wind stress and internal ice stresses are assumed to be independent of ice velocity.

Sea ice motion data were assimilated from Ifremer/CERSAT (Ezraty et al., 2007, see also Girard-Ardhuin et al., this issue) in the Arctic and NSIDC (Fowler, 2003) in both the Arctic and Antarctic Oceans. In order to improve the forecast performance, and reduce the impact of model biases, a portion of the addition stress was persisted into the model forecast.

In order to make use of the ice velocity data using the assimilation scheme presented above, a re-run must be performed each day to cover the full period of the observation. For a 3-day observation (created using images spaced 3 days apart) this means that the previous 4 days must be re-run to get a new analysis. This requires substantial additional computational resources.

Results of sea ice assimilation experiments

The ice concentration assimilation is able to constrain the model close to the observations, reducing some of the model biases, as shown in Figure 2. Ice velocity assimilation is able to improve drift hindcasts of International Arctic Buoy (IABP, Rigor, 2002) motion as shown in Figure 3. The improvement is much smaller during summer, when there is no Ifremer/CERSAT ice motion data, since the melt alters the surface characteristics, making motion difficult to detect. Comparison with independent RGPS (Lindsay and Stern, 2003) ice motion data shows that the assimilation improves the model ice velocity throughout the winter, reducing RMS errors by approximately 50% (Figure 4). Due to the limited number of Antarctic drifting buoy data in the study period, we were not able to quantitatively assess the modelled velocity in the Southern Hemisphere.

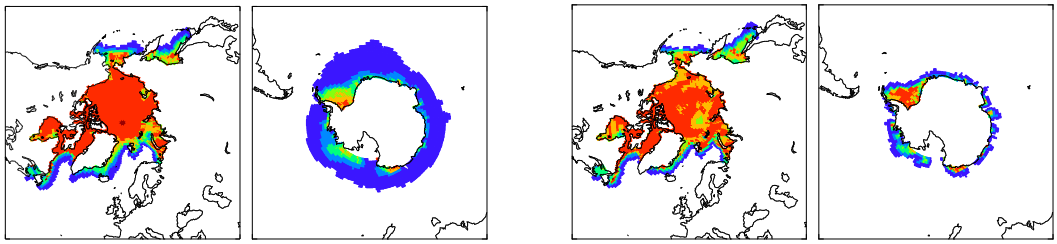

a) No Assimilation

b) Ice Concentration and velocity assimilation.

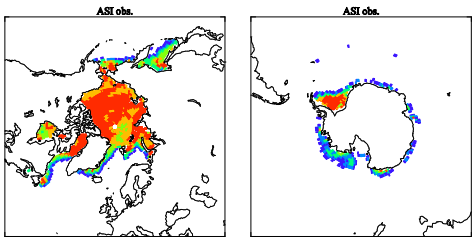

c) Gridded ice concentration observations using the ASI algorithm

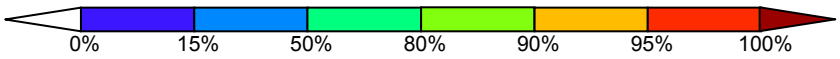

Ice Concentration.

Figure 2

Simulated (top) and observed (bottom) sea ice concentration fields for 1 March 2000. The ice concentration assimilation results in modelled fields that match the observations much better than the free running model, but this comparison is not against independent data.

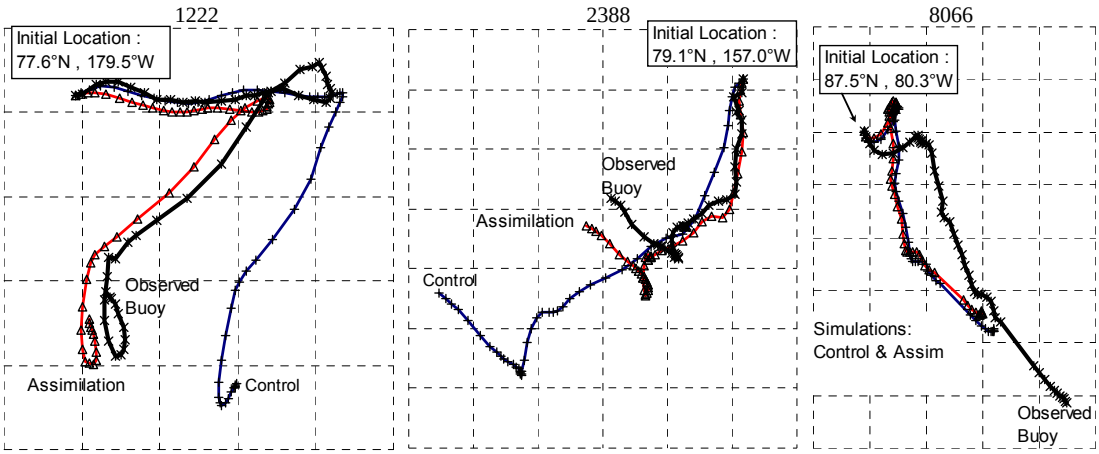

a)Buoy 1222, October 1999. b) Buoy 2388, February 2000. c) Buoy 8066, June 2000.

Figure 3

Observed (black) compared to simulated buoy drifts with and without assimilation (red and blue respectively) for three IABP buoys. 28 days of simulated drift are shown in each case. The assimilation greatly improves the simulated motion during the winter, but has less impact during the summer when there are very few satellite motion vectors to assimilate. The grid lines are spaced at intervals of 20km in polar-stereographic projection.

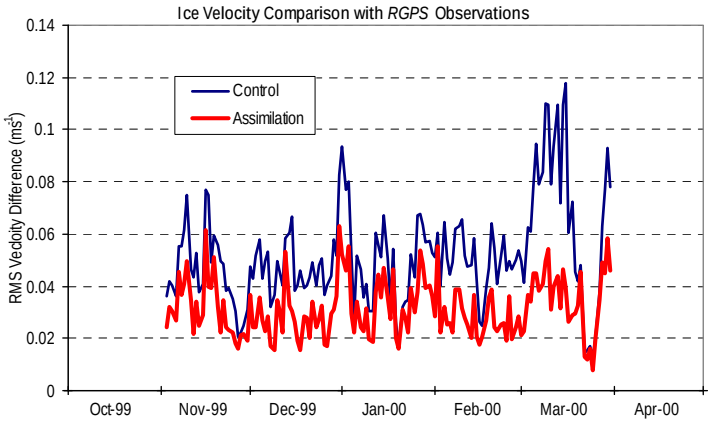

Figure 4

Comparison of simulated ice velocity compared to RGPS observations for the FOAM experiments without assimilation (Control in blue) and with sea ice concentration and velocity assimilation (Assimilation in red). The RMS errors are improved by approximately 2cm/s throughout most of the test period.

Operational Implementation

The ice concentration assimilation scheme above is currently being implemented in the FOAM system, as part of on-going improvements and transition of the system to the NEMO / CICE model. Due to the additional resource requirements of the ice velocity assimilation scheme, this is not being implemented in the operational model for the time being.

Sea ice concentration and drift data assimilation in France: Investigations on implementing the SEEK method for Sea Ice data assimilation into the Mercator operational System

By Gilles Garric[1], Jérôme Pernin[1], Charles-Emmanuel Testut[1], Eric Greiner[1], Fanny Girard-Ardhuin[2], Denis Croize-Fillon[2]

[1] Mercator-Ocean, 8-10 rue Hermès, 31520 Ramonville St Agne, France
[2] Ifremer/CERSAT, DOPS/LOS, BP 70, 29280 Plouzané, France

Introduction

The April 2007 update of the Mercator-Ocean global ¼° operational system includes a new assimilation platform using the SEEK (Singular Evolutive Extended Kalman) filter, together with improved ocean model component Analyses concern only oceanic quantities. At high latitudes, the system is not constrained by any assimilation tool. The present work evaluates the ability to implement the SEEK filter into the sea ice component of the global system. This is a preliminary work done in order to estimate the feasibility of assimilating Sea ice concentration and drift data in the Mercator-Ocean global system.

We use outputs from an interannual hindcast experiment performed with the ocean model described in section 4.2 in order to build time series anomalies as input for the assimilation tool. The latter is described in section 4.4. Similar time series anomalies are constructed with observations, which are briefly described in section 4.3, in order to compare with the statistical modelled results.

The eddy-permitting NEMO-based hindcast experiment

The experiment shown in the present study uses the eddy permitting ¼° global Mercator model based on the primitive equations ocean circulation model NEMO (Nucleus for European Models of the Ocean). It includes the latest version of OPA version 9.0 (Madec *et al.* 1998), coupled to the thermodynamic-dynamic sea ice model LIM2 (Louvain sea Ice Model 2) (Fichefet and Maqueda 1997). The horizontal resolution based on an ORCA-type grid (Madec and Imbard 1996) is about 10 km in the Arctic. The reader can refer to Barnier et al. (2006) for a detailed description of the physics of this model. The sea ice is fully comprehensive with the implementation of the LIM2 model. This model handles most of the processes linked to the sea ice lifecycle, with sea ice concentration, sea ice/snow thickness, sea ice drift and sea ice thermal content prognosed by the 3-layers model and viscous-plastic formulation.

Daily surface atmospheric conditions are given by the ECMWF (European Centre for Medium Range Weather Forecast) reanalysis project ERA40 (Uppala 2001). The experiment starts at rest on 1st January 1992 with prescribed conditions for temperature and salinity derived from Levitus et al. (1998) climatology for the middle and low latitudes. For high latitudes, we chose the PHC2.1 climatology (Steele *et al.* 2001). The year 1992 has been integrated three times before launching the interannual experiment over the 1993-2001 period.

The observations

The observations used in this study are the satellite data produced by the Ifremer/CERSAT (see Girard-Ardhuin et al., this issue, for more details). Briefly, they consist of daily sea ice concentration at the 12.5km resolution as well as 3-days mean sea ice drift at 62.5km resolution.

The assimilation scheme: the Mercator-Ocean approach

The SEEK filter is a Reduced-Order Extended Kalman Filter, in which the error statistics are expressed in terms of a three-dimensional, multivariate sub-space [Pham et al., 1998]. This error subspace is initialized with an ensemble of error modes parameterised by temporal anomalies built from the 1993-2001 experiment described in the previous section. With a 3-days mean sampling for the experiment, these anomalies are built thanks to a Hanning window of length 40 days in order to correctly represent the standard 7-days analysis cycle chosen in all the Mercator operational systems. Moreover, in order to prevent the data from exerting a spurious influence at remote distances through large-scale signatures in the error modes, a local analysis scheme using influence bubble has been adopted: It enforces to zero the error covariances between distant variables which are believed to be uncorrelated in the real ocean. The spatial properties of the local background errors used in SEEK filter could be then illustrated by calculating the representer functions (*r*) defined by:

$$r(X_1, X_2, z_0, z) = \frac{\sigma_2}{\sigma_1} c(X_1, X_2, z_0, z)$$

where *c* is the correlation coefficient, σ_1 (resp. σ_2) is the variance of the X_1 (resp. X_2) quantity and z_0 is the reference point. Physically, the representer r is the response of the variable X_2 through the regional assimilation of the variable X_1 at the z_0 geographical point.

We have limited the study to the auto-correlation and auto-representer for variables which may be directly assimilated, i.e. sea ice concentration and drift. We also focus our results during the winter (January-March) to limit the error and to avoid temporal discrepancies of the observed satellite data and over the Arctic region, as the CERSAT Antarctic satellite database was not available by the time of this study. The observed error modes are also calculated with a Hanning window of length 40 days.

Discussion

Figure 5 shows partial results for two reference points which may present different sea ice properties. The first one is localized in the marginal ice zone in the Fram Strait at the end of the Transpolar Drift Stream. The second one is found inside the ice pack.

First, we look into the feasibility of assimilating Sea ice concentration data, using the first reference point. As expected, the auto-correlation for the sea ice concentration presents a Dirac-type shape response for both the experiment and the observations, even if the response in the observations is more pronounced and exhibits a downstream pattern from the Fram Strait. In the figures, the representer field represent the large scale response of the variable X_2 (here the sea ice concentration) to the assimilation of the variable X_1 (here again the sea ice concentration) with an amplitude of 1, here 100% of concentration. Same conclusions can be drawn with similar patterns associated to the response for the representer. The higher amplitude of the response present at the sea ice edge for the representer reveals the high variability of these areas. Nevertheless, they are uncorrelated with the reference point. However, the higher variability found downstream the reference point in the observed representer is also present in the modelled sea ice cover but with unrealistic signals at the edge. Similar patterns found in both correlation and representer fields suggest that sea ice concentration could be assimilated.

Second, we look into the feasibility of assimilating Sea ice drift data, using the second reference point. We obtain roughly similar results for the X-component of the sea ice velocity (Figure 6) with the reference point situated in the pack. Similar patterns found in both correlation and representer fields allow us to consider favourably assimilation of this variable with the SEEK filter. We obtain similar results with the Y-component of the sea ice velocity. The response is however smoother in the experiment than in the observed field, suggesting a potential supply of variability with the assimilation of such quantities. The high amplitude of the response in the marginal ice zones reveals again artificial correlation with areas of high variability.

Conclusions made above are also valid for similar calculations performed for reference points located in different areas.

Our next step is to perform a short reanalysis over a winter time period with assimilation of sea ice concentration and velocity in a NEMO ¼° Arctic configuration. This sea ice assimilation scheme is supposed to be implemented in the global ¼° operational system and in the future Mercator reanalysis system in order to get proper sea ice reanalysis products for the recent past decades. We also plan to apply the same methodology of work for the Antarctic sea ice cover.

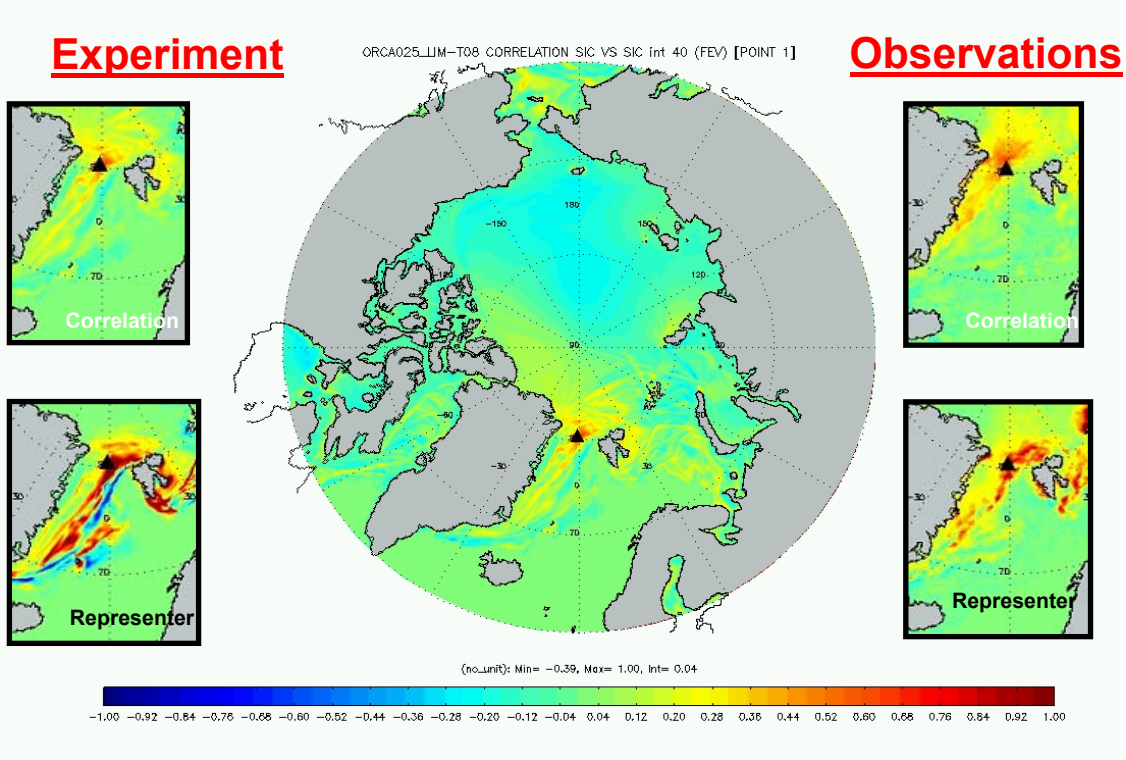

Figure 5

Auto-correlation coefficient and auto-representer for sea ice concentration in the experiment (left panels) and observations (right panels). The sign ▲ is the reference point for both correlation and representer

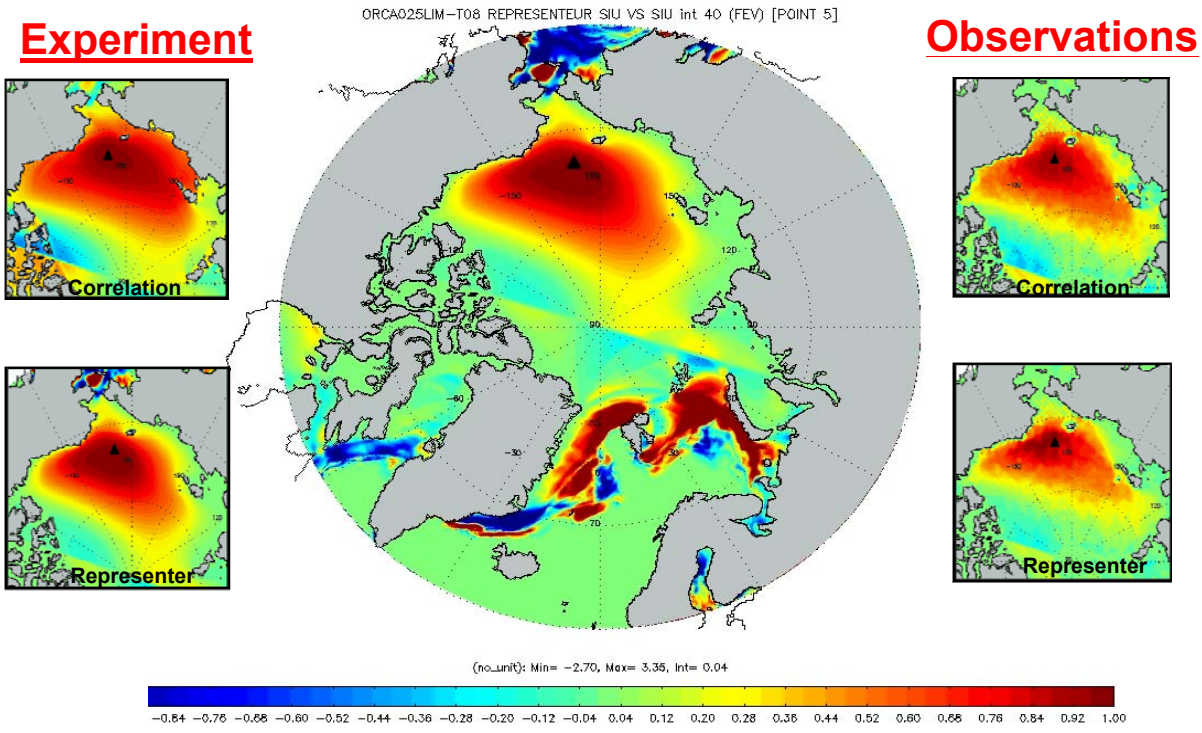

Figure 6

Same as Figure 5 but for the X component of the sea ice velocity

Sea ice concentration and drift data assimilation in Belgium

By Valérie Dulière[1] and Thierry Fichefet[1]

[1]Institut d'astronomie et de géophysique G. Lemaître, UCL, Louvain-la-Neuve, Belgium

The sea ice data assimilation method and model used

This work follows up a study in which twin experiments (i.e. experiments in which the data to be assimilated are model outputs) have been conducted with a simplified toy model of the Artic sea ice pack [Dulière and Fichefet, 2007]. During this first study, we made a thorough analysis of the impact of data assimilation on the model behaviour. In the present work, we test the robustness of the conclusions drawn in the previous work by performing a couple of twin experiments with NEMO-LIM2. We assess to which extent those conclusions are applicable in a realistic framework.

The NEMO-LIM2 model

The NEMO-LIM2 model is a primitive equation ocean general circulation model coupled to LIM2, the second version of the Louvain-la-Neuve sea ice model. A full model description can be found in Dulière [2007] (see also Vancoppenolle et al., this issue).

In comparison to the sea ice toy model used in Dulière and Fichefet [2007], the NEMO-LIM2 model includes more complex sea ice thermodynamics and dynamics, a snow layer, feedbacks between ocean and sea ice, etc. NEMO-LIM2 is thus more realistic but also more expensive in CPU time.

The data assimilation method

At each time step, a scheme derived from optimal interpolation is used to assimilate ice concentration and velocity data into the model according to:

$$A_{ass} = A + k_A\left(A_{obs} - A\right)$$

$$\dot{u}_{ass} = \dot{u} + k_u\left(\dot{u}_{obs} - \dot{u}\right)$$

where A and $\dot{u}$ are the sea ice concentration and velocity. The subscripts ass and obs stand for assimilated and observed data. k_A and k_u are the weights for ice concentration and velocity data assimilation, respectively, and are usually determined through a least squares minimization of the error variance of the assimilated value compared to a statistical true value [Meier et al., 2000; Lindsay and Zhang, 2006]. However, the present experimental design, as described in the following section, provides one "observation" per model grid cell with zero error. The weight should then be set to one, and "observed data" would directly be inserted into the model. Yet, a weight equal to 1 does actually improve one of the assimilated sea ice variable but not systematically the other ones [Duliere and Fichefet, 2007]. Therefore, in this study, we rather choose the weights on a physical basis in order to take into account the interactions between the different sea ice variables to improve the global sea ice state.

This assimilation technique is fairly simple. Yet, it was found to be very useful in underlining a number of problems posed by the assimilation of ice concentration and/or velocity data into large-scale sea ice models [Dulière and Fichefet, 2007].

Experimental set up

The rather poor knowledge of both modelling and observational errors [Weaver et al., 2000] enhances the difficulty in assessing in details the impact of data assimilation on the global performance of a large-scale sea ice model. To overcome this problem, we build an idealized "observational" dataset with the model. Then the model is perturbed through its forcing or its initial conditions and this "observational" dataset is assimilated into the model. These kinds of experiments are called twin experiments.

The NEMO-LIM2 model is perturbed in a way that the perturbations remain consistent with model and forcing uncertainties. Therefore, perturbations are applied either to the model wind or air temperature forcing or to the model initial conditions. Usually, twin experiments are carried out in a forecasting perspective, and thus the model is perturbed by changing initial conditions. Here, as the purpose is rather oriented toward reanalysis, we also find it appropriate to alter the thermal and dynamical forcing.

For more detail on the experimental set up, see Dulière [2007].

Results

In this section, we briefly discuss some of the main results obtained with the experimental set up described above. For more details, the reader is referred to Dulière [2007].

First, the results show the importance of choosing an appropriate model to assimilate sea ice concentration and velocity data. The model should rather include smooth dynamics than discontinuous ones, like e.g. the free drift type dynamics combined with the Kreyscher et al. [2000] correction.

Second, several technical aspects of assimilating sea ice concentration and velocity data into large-scale sea ice models have been investigated. We have demonstrated that assimilating sea ice concentration data can easily lead to a deterioration of the model performance. This is mostly explained by the strong link between ice concentration and ice thickness: ***Vi=hi Ai S***, Where ***Vi, hi*** and ***Ai*** are the volume, thickness and concentration of the sea ice, respectively. S is the surface of the grid cell and is constant in time. According to this equation, either the ice thickness or volume should be changed where the data assimilation scheme corrects the ice concentration. As presented on the left panel of Figure 7, assimilating sea ice concentration data imposing ice volume conservation, fails to improve the model estimation of ice thickness (Figure 7). Indeed, for the smooth model dynamics, the best way to estimate the sea ice state through ice concentration data assimilation is to add or remove an ice block of thickness equal to that of the pre-existing ice to better fit the observed ice concentration. The fact that this additional ice block is snow covered or not and that its temperature equals either the temperature of the pre-existing ice or the seawater freezing temperature has barely no effect on the optimized sea ice distribution. The results also reveals that the additional ice block should rather not contain heat within its brine pockets, even though the impact of this on the sea ice characteristics is small. Finally, rejecting salt (freshwater) towards the ocean is not necessary when the ice block is added (removed) to better fit the sea ice concentration observations. In this process, the ice volume is not conserved. To the contrary, with dynamics similar to the toy model, one should conserve ice volume when the model error is mainly dynamic.

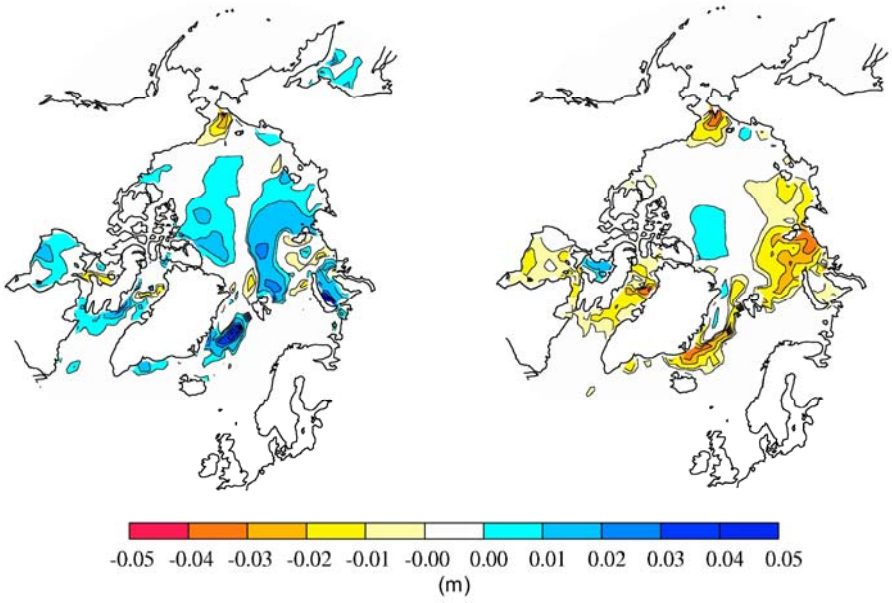

Figure 7

Geographical distributions of the 1984 annual mean ice thickness biases between experiments in which (left) the model is perturbed and sea ice concentration data are assimilated, and (right) the control experiment. For the left panel, the ice volume is conserved where ice concentration data are assimilated into the model. For the right panel, the ice volume is not conserved but the ice thickness is.

Third, the assimilation of ice velocity data was found to significantly improve the overall ice model estimation when the model dynamics are wrong. This is especially true if a large weight is used. When the model error is thermodynamic or when it comes from perturbation in initial conditions, the improvement brought by assimilation is not always as visible.

Fourth, we have also found that the assimilation of ice velocity and concentration data are complementary. Indeed, assimilating simultaneously ice velocity and concentration data into the model seems to be the best way to enhance the ability of the model to reproduce the observed features of the sea ice field. This was not obvious since sea ice is highly non-linear and ice concentration is tightly bound to ice thickness.

In all cases, we have demonstrated that the weights are playing a crucial role in the data assimilation results. An appropriate weight enhances the model performance whereas an inappropriate one can deteriorate it. Moreover, the weight can be chosen in a manner that it further improves one of the ice characteristics, but sometimes on the detriment of others. This is often the case when weights are estimated through the least-squares method. Therefore, for a global improvement of the sea ice estimate, we found that choosing the weights on a physical more than on a statistical basis is generally more appropriate.

As a summary, here are three main recommendations. First, one should assimilate sea ice velocity and concentration data simultaneously. Second, if ice concentration is modified due to the assimilation, one should conserve the ice thickness (not the ice volume). Third, one should always look into the system carefully to make sure the assimilation is done properly.

Acknowledgments

We wish to thank Gilles Garric, Hugues Goosse, Ralph Timmermann and Martin Vancoppenolle for helpful discussions about various aspects of this work. We also thank Xavier Fettweis for technical support. V.Dulière is supported by the Fonds pour la Formation à la Recherche dans l'Industrie et dans l'Agriculture. This study was carried out within the scope of the project “A Second-Generation Model of the Ocean System” funded by the Communauté Française de Belgique (Actions de Recherche Concertées, ARC 04/09-316) and the project “Contribution of the assimilation of satellite data to sea ice modelling” funded by the Université catholique de Louvain (Fonds Spécial de Recherche).

Sea ice concentration data assimilation in Canada: Three-dimensional variational data assimilation in a coupled ice-ocean model

By Alain Caya[1], Mark Buehner[1] and Tom Carrieres[2]

[1] Meteorological Research Division, Environment Canada, 2121 Trans-Canada Hwy, Dorval, Quebec, H9P 1J3, Canada
[2] Ice and Marine Services, Environment Canada, 373 Sussex Drive E-3, Ottawa, Ontario, K1A 0H3, Canada

Sea ice data assimilation method and model used

The Canadian Ice Service (CIS) manually produces daily ice charts to describe sea ice conditions in Canadian ice infested waters for clients involved in marine-related activities. Moreover, operational numerical weather prediction (NWP) in Canada is moving towards the use of coupled atmosphere-ice-ocean models to improve meteorological forecasts in maritime regions. To support both of these efforts, CIS and the Meteorological Research Division are developing a system to produce objective analyses of sea-ice conditions using multiple types of remote sensing data. To this end, data assimilation techniques similar to those developed for NWP applications are being employed. Such advanced data assimilation techniques may be helpful regarding, for example, the problem of a lack of direct measurements of the three-dimensional ocean state under sea ice by providing a means for correcting the ocean model variables given only sea ice observations.

The following provides a brief description of the data assimilation system, based on the three-dimensional variational approach (3D-Var), and includes preliminary results from assimilating CIS daily ice charts to initialize a coupled ice-ocean model configured for the Canadian east-coast region. The main focus here is on the estimation of the background-error covariances and their impact on the subsequent forecast. Other activities within the project that focus on the direct assimilation of remote sensing data in the 3D-Var (e.g. passive microwave, infrared-visible, synthetic aperture radar) are not presented here.

The assimilation method

The 3D-Var approach is employed to assimilate observations to correct the 24-h forecast (the background state) produced by the coupled ice-ocean model. The corrected model state (referred to as the analysis) is then used as the initial conditions to produce the next 24-h forecast. The data assimilation problem is cast in terms of minimizing an objective function that measures the fit of the model to the observations and to the background state. With the incremental approach (Courtier et al. 1994), the objective function J takes the following form:

$$2J(\boldsymbol{\xi}) = \boldsymbol{\xi}^{\mathrm{T}}\boldsymbol{\xi} + \left(\mathbf{y} - \mathcal{H}\left(\mathbf{x}^{\mathrm{b}}\right) - \mathbf{H}\mathbf{B}^{1/2}\boldsymbol{\xi}\right)^{\mathrm{T}}\mathbf{R}^{-1}\left(\mathbf{y} - \mathcal{H}\left(\mathbf{x}^{\mathrm{b}}\right) - \mathbf{H}\mathbf{B}^{1/2}\boldsymbol{\xi}\right) \qquad (1)$$

where $\boldsymbol{\xi}$ is the control vector, $\mathbf{y}$ is the observation vector, $\mathcal{H}$ is the (possibly nonlinear) observation operator and includes the interpolation of the background state at the observation time, $\mathbf{x}^{\mathrm{b}}$ is the background state, $\mathbf{H}$ is the tangent linear observation operator (i.e. the operator $\mathcal{H}$ linearized about $\mathbf{x}^{\mathrm{b}}$), $\mathbf{B}$ is the background-error covariance matrix, and $\mathbf{R}$ is the observation-error covariance matrix. In deriving (1), the approximation $\mathcal{H}(\mathbf{x}^{\mathrm{b}} + \Delta\mathbf{x}) \approx \mathcal{H}(\mathbf{x}^{\mathrm{b}}) + \mathbf{H}\Delta\mathbf{x}$ has been made. The analysis $\mathbf{x}^{\mathrm{a}}$ is related to the control vector by

$$\mathbf{x}^{\mathrm{a}} = \mathbf{x}^{\mathrm{b}} + \mathbf{B}^{1/2}\boldsymbol{\xi}^{\alpha} \qquad (2)$$

Where $\boldsymbol{\xi}^{\alpha}$ is the vector that minimizes (1). The minimization of (1) is performed using a quasi-Newton descent algorithm. The innovation vector ($\mathbf{y} - \mathcal{H}(\mathbf{x}^{\mathrm{b}})$) does not depend on the control vector $\boldsymbol{\xi}$ and therefore is only evaluated once at the beginning of the minimization, using the full observation operator.

In this implementation, the error covariance matrices $\mathbf{B}$ and $\mathbf{R}$ are time independent. To further simplify the problem, the observation errors are assumed uncorrelated, yielding a diagonal matrix $\mathbf{R}$ which is trivial to invert.

A coupled ice-ocean model

The model used in this study is called the Community Ice-Ocean Model (CIOM; Yao et al. 2000). It is composed of the Princeton Ocean Model (Blumberg and Mellor 1987; Mellor 1996) and a multicategory sea ice model. The model has a grid resolution of 1/5° longitude and 1/6° latitude. Prognostic ocean variables are velocity, potential temperature, salinity, and turbulence quantities on 16 sigma levels unevenly spaced in the vertical. Prognostic ice variables are velocity and ice concentration distribution with respect to 25 thickness categories, including the open water fraction category. Every component of the model is the same as in Yao et al. (2000), except for the shortwave radiation: here the clear sky solar radiation of Shine (1984) with the cloud factor of Laevastu (1960) is used. Atmospheric conditions to force the CIOM are taken from the Canadian Global Environmental Multi-scale (GEM) model (Côté et al. 1998) and refreshed every 3 hours.

Background-error covariance matrix

The background-error covariances are an essential aspect of any data assimilation system. They partially govern the level of influence the observations have on the analysis and how the information is spread spatially and to other model variables that are not directly related to the observations. One method that can estimate background-error statistics is the ensemble Kalman filter (enKf; Whitaker and Hamill 2002). In the enKf, the background-error statistics are estimated by evolving an ensemble of states, which are continuously updated using observations and statistical information regarding errors in the forcing data and the model itself. However, the enKf is computationally costly and is prone to sampling errors. The idea here is to parameterize the background-error covariance matrix and estimate its parameters using the enKf. Time averaging reduces the effect of sampling error and allows constructing a stationary background-error covariance matrix for use in the 3D-Var system, which is much less computationally expensive.

The enKf is run from December 31 2002 to April 28 2003, assimilating observations every 24 hours at 18UTC. The assimilated quantity is the total ice concentration from daily ice charts prepared by the CIS (Carrieres et al. 1996). The enKf has 48 CIOM members. To take into account uncertainties in the atmospheric forcing, 16 different atmospheric states from the ensemble prediction system run at the Meteorological Service of Canada (Houtekamer et al. 1996) are used as upper boundary conditions for the CIOM. It is noteworthy that model error is not taken into account in this enKf: only uncertainties in the initial conditions, in the atmospheric forcing and in the observations determine the estimated background-error covariances.

The background-error covariance matrix can be expressed as:

$$\mathbf{B} = \mathbf{DCD} = \mathbf{DC}^{1/2}\left(\mathbf{DC}^{1/2}\right)^{\mathbf{T}} = \mathbf{B}^{1/2}\left(\mathbf{B}^{1/2}\right)^{\mathbf{T}}, \qquad (3)$$

Where **D** is the diagonal matrix of background-error standard deviations and **C** is the correlation matrix. The correlation matrix is decomposed into vertical and horizontal correlation matrices $\mathbf{C} = \mathbf{C_v C_h}$. The horizontal correlations are modeled using a diffusion operator (Weaver and Courtier 2001). A wide variety of correlations function can be modeled using this approach. For simplicity, a Gaussian correlation function is employed here.

The vertical background-error correlation matrix $\mathbf{C_v}$ for ice concentration, ocean temperature and salinity, including multi-variate relationships, is estimated from the enKf on 32 depth levels. The error statistics are approximated to be horizontally homogeneous on depth levels, consequently the correlations and ensemble standard deviations are horizontally averaged over all grid points where sea ice is present to give more robust estimates. This results in background-error standard deviation for total ice concentration of 0.093 and a horizontal correlation length scale of 22 km.

Impact of sea ice data assimilation on short-term forecasts

Several 3D-Var data assimilation experiments were performed over the winter months of 2003. Again, the observation is the open water fraction (with open water fraction= 1 minus ice concentration) from the CIS daily ice charts, assuming an observation-error standard deviation of 0.1. The results in terms of 24-hour forecast-minus-observation (F-O) and analysis-minus-observation (A-O) of 9 experiments are presented in Table 1 and the time series for Exp. 8 and Exp. 1 are depicted in Fig. 8. Figure 9 shows how the CIS daily ice chart and the 24-h model forecast differ on April 2nd 2003. Results indicate that: 1. the use of the background-error correlation between ice concentration, ocean temperature and salinity leads to improved forecasts; 2. the best forecasts are obtained when the background-error standard deviations, estimated by time and space averaging the enKf statistics, are at least doubled and simultaneously with background-error horizontal correlation length of 20 km. It is interesting to note that a closer fit to the data (Exp. 4) does not improve the forecasts when the background-error horizontal correlations are not used.

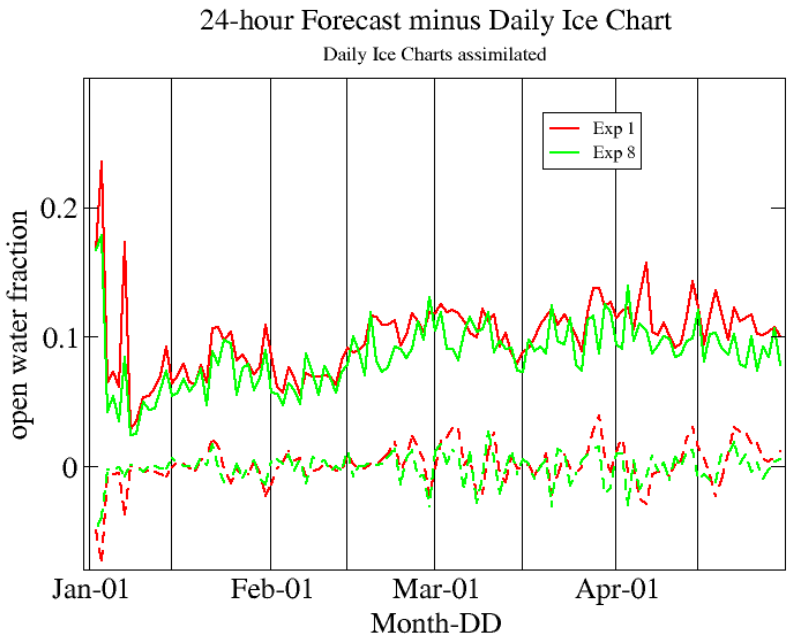

Figure 8

Statistics of the Forecast minus Observations (F-O) for 2 assimilation experiments where open water fraction from the CIS daily ice charts are assimilated. See Table 1 for the characteristics of the 2 experiments. The full lines are the F-O rms, and the dashed lines are the F-O bias.

Experiment name	Horizontal correlation length (km)	Factor multiplying the background-error standard deviations	Ocean variables update	Time-averaged rms of F-O	Time-averaged rms of A–O
Exp1	**0**	**1**	**No**	**0.0994**	**0.0611**
Exp2	**0**	**1**	**Yes**	**0.0935**	**0.0575**
Exp3	**0**	**2**	**Yes**	**0.0875**	**0.0196**
Exp4	**0**	**4**	**Yes**	**0.0875**	**0.0059**
Exp5	**10**	**1**	**Yes**	**0.0879**	**0.0381**
Exp6	**20**	**1**	**Yes**	**0.0862**	**0.0375**
Exp7	**30**	**1**	**Yes**	**0.0864**	**0.0459**
Exp8	**20**	**2**	**Yes**	**0.0856**	**0.0255**
Exp9	**20**	**4**	**Yes**	**0.0855**	**0.0176**

Table 1

Time-averaged statistics for 9 assimilation experiments where open water fraction from the CIS daily ice charts are assimilated. The horizontal correlation length is the same for all variables at all depths. The bases for the background-error standard deviations and vertical correlations are those obtained from the enKf. F-O stands for 24-h Forecast minus Observations, and A-O for Analysis minus Observations.

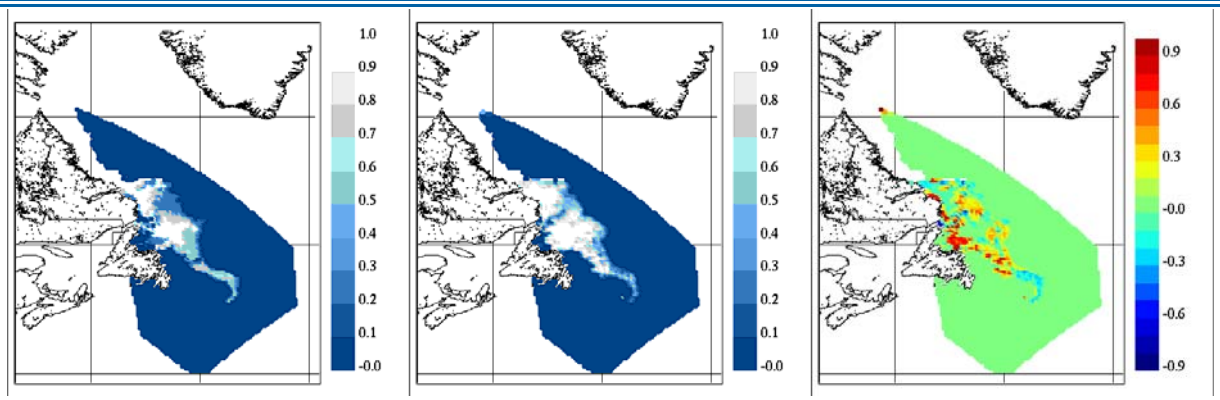

Figure 9

Ice concentration on April 2nd 2003 at 18UTC in Exp. 8. Left: observations from the CIS daily ice chart. Middle: 24-hour forecast from the CIOM. Right: Forecast-minus-observations.

Conclusion

Useful information about background-error statistics are produced by an ensemble Kalman filter and employed for 3D-Var data assimilation of sea ice concentration in a coupled ice-ocean model. The correlations between ice and ocean temperature and salinity are important and need to be taken into account for data assimilation in the coupled system. Through empirical tests, it was found that amplifying the background-error variances from the enKf lead to improved forecasts. We speculate that this may be due to the assumption of horizontally homogeneous background-error covariances.

Acknowledgments

The authors thank Dinh Hai Tran and Charles Tang for help in resolving issues related to the numerical model. The authors also acknowledge Anthony T. Weaver for help during the implementation of the diffusion operator. This work was supported by the Canadian Program of Energy Research and Development (PERD).

Conclusion

By Eric Greiner [1]

[1] CLS/Mercator-Ocean, 8-10 rue Hermès, 31520 Ramonville St Agne, France

The last decade has seen a growing interest in the Arctic and Antarctic areas for various reasons (gas and petroleum resources, fish management, shipping, climate, tourism). New opportunities have arisen from the used of satellite derived ice fraction and drift, and drifters trajectories. A step ahead should come with the availability of the satellite thickness (CryoSat, 2009). Ice models and forcing have been improved so they now give realistic simulations and ensembles, both being very beneficial for data assimilation.

Assimilating into an ice model is clearly a challenging issue. We are facing new problems. The ice thermodynamics are non linear, and the scales are small (20km). The regimes (ice formation, accumulation, melting) are quickly changing, so that the stationarity assumption is questionable. Even the Gaussian assumption is violated near the ice edge, or when the ices is almost entirely formed or melt. The choice of the control state is not even clear: model ice variables, upper underlying ocean and/or atmospheric forcing?

Those big problems are successfully tackled by separate teams, with very different approaches, from data insertion to ensemble methods. The recipe for success is a reflection before the action, aiming at adapting a known method to this new problem. In particular, assimilating both Ice concentration and drift is the main point to get a good analysis. Unobserved ice thickness can be controlled with additional constraints (climatology, conservation law or model derived cross-correlation). Finally, forecasts seem to be improved when the wind and the upper ocean are part of the control variables. The general feeling is that this challenging subject should get a nice solution in a near future.

References

Barnier, B., G. Madec and c. authors (2006). "Impact of partial steps and momentum advection schemes in a global ocean circulation model at eddy permitting resolution." Ocean Dynamics**,** doi:10.1007/s10236-006-0082-1.

Bertino, L., G. Evensen and H. Wackernagel, Sequential data assimilation methods in oceanography, *Int. Stat. Rev.*, *71* (1), 223-242. 2003.

Bleck, R., An oceanic general circulation model framed in hybrid isopycnic-Cartesian coordinates, *Ocean Modelling*, *4* (1), 55-88, 2002.

Blumberg, A. F., and G. L Mellor, 1987: A description of a three-dimensional coastal ocean circulation model. in Three-Dimensional Coastal Ocean Models, *Coastal Estuarine Sci.*, vol. 4, edited by N. S. Heaps, pp. 1-16, AGU, Washington, D. C.

Carrieres, T.; B. Greenan, S. Prinsenberg and I.K. Peterson, 1996: Comparison of Canadian ice charts with surface observations off Newfoundland, winter 1992. *Atmosphere-Ocean*, 34, 207–236.

Côté, J., S. Gravel, A. Méthot, A. Patoine, M. Roch, and A. Staniforth, 1998: The operational CMC-MRB global environmental multiscale (GEM) model. Part I: Design considerations and formulation. *Mon. Wea. Rev*., 126, 1373–1395.

Courtier, P., J.-N. Thépaut and A. Hollingsworth, 1994: A strategy for operational implementation of 4D-Var, using an incremental approach. *Quart. J. Roy. Meteor. Soc*., 120, 1367–1387.

Dulière, V. 2007. On the assimilation of ice velocity and concentration data into large-scale sea ice models. Ph.D. thesis, Université catholique de Louvain, Louvain-la-Neuve, Belgium. 143pp. http://edoc.bib.ucl.ac.be:81/

Dulière, V. and Fichefet, T. 2007. On the assimilation of ice velocity and concentration data into large-scale sea ice models, Ocean Sc., 3, 321-335.

Ezraty, R., F. Girard-Ardhuin, and J. F. Piollé, 2007: Sea ice drift in the central Arctic combining QuikSCAT and SSM/I sea ice drift data, Users manual, version 2.0, February 2007. Available at Ifremer/CERSAT: ftp://ftp.ifremer.fr/ifremer/cersat/products/gridded/psi-drift/documentation/merged.pdf

Evensen, G., Data assimilation: the Ensemble Kalman Filter. Springer. 2006.

Fichefet, T. and M. A. M. Maqueda (1997). "Sensitivity of a global sea ice model to the treatment of ice thermodynamics and dynamics." J. Geophys. Res. 102-C6: 12,609-12,646.

Fowler, C. 2003. Polar Pathfinder Daily 25 km EASE-Grid Sea Ice Motion Vectors. Boulder, CO, USA: National Snow and Ice Data Center. Digital media. (Data available from the NSIDC website, http://nsidc.org/data/nsidc-0116.html)

Houtekamer, P. L., L. Lefaivre, J. Derome, H. Ritchie, and H. L. Mitchell, 1996: A system simulation approach to ensemble prediction. *Mon. Wea. Rev*., 124, 1225–1242.

Hunke, E. and W. Lipscomb, 2004. CICE: the Los Alamos sea ice model documentation and software user's manual. Los Alamos National Laboratory.

Hunke, E. and J. Dukowicz, 1997. An elastic-viscous-plastic model for sea ice dynamics. J. Phys. Oceanogr., 27, 1849-1867.

Kaleschke, L., C. Lüpkes, T. Vihma, J. Haarpaintner, A. Bochert and G. Heygster, 2001, SSM/I Sea Ice Remote Sensing for Mesoscale Ocean-Atmosphere Interaction Analysis, Can. J. Remote Sensing, 27, 5, 526-537.

Kreyscher, M., Harder, M., Lemke, P. and Flato, G. 2000. Results of Sea Ice Model Intercomparison Project: Evaluation of sea ice rheology schemes for use in climate simulations. J. of Geophys. Res. 105(C5):11299-11320.

Laevastu, T., 1960: Factors affecting the temperature of the surface layer of the sea. *Comment. Phys. Math*., 25, 1–136.

Levitus, S., T. P. Boyer, M. E. Conkright, T. OBrian, J. I. Antonov, C. Stephens, L. Stathopolos, D. Johnson and R. Gelfeld (1998). World Ocean Database 1998 - NOAA Atlas NESDID18, National Oceanographic Data Center, Silver Spring, MD.

Lindsay, R.W. and H.L. Stern, 2003, The RADARSAT geophysical processor system: Quality of sea ice trajectory and deformation estimates, J. Atmos. Ocean Tech 20 (9): 1333-1347 Sep 2003.

Lindsay, R. and Zhang, J. 2006. Assimilation of ice concentration in an ice-ocean model. J. Atmos. Ocean. Tech., 23:742-749.

Lisæter, K.A., J. Rosanova, and G. Evensen, Assimilation of ice concentration in a coupled ice–ocean model, using the Ensemble Kalman filter, *Ocean Dynamics*, *53* (4), 368-388, 2003.

Lisæter, K.A., G. Evensen and S. Laxon, *J. Geophys. Res*., 112, C07023, doi:10.1029/2006JC003786, 2007.

Madec, G., P. Delecluse, M. Imbard and C. Levy (1998). OPA 8.1 general circulation model reference manual, Notes de l'Institut Pierre-Simon Laplace (IPSL) - Universite P. et M. Curie, B102 T15-E5, 4 place Jussieu, Paris cedex 5, 91p.

Madec, G. and M. Imbard (1996). "A global ocean mesh to overcome the North Pole singularity." Clim. Dyn. 12: 381-388.

Martin, M.J., A. Hines, and M.J. Bell, 2007, Data assimilation in the FOAM operational short-range ocean forecasting system: a description of the scheme and its impact, Q. J. R. Meteorol. Soc., 133, 981-995.

Meier, W., Maslanik, J. and Fowler, C. 2000. Error analysis and assimilation of remotely sensed ice motion within an Arctic sea ice model. J. of Geophys. Res. 105(C2):3339-3356. Doi:10.1029/1999JC900268.

Mellor, G. L., 1996: User's guide for a three-dimensional primitive equation, numerical ocean model. 35 pp., Atmos. and Oceanic Sci. Program, Princeton Univ., Princeton, N. J.

Pham D. T., J. Verron and M. C. Roubaud, 1998: A singular evolutive extended Kalman filter for data assimilation in oceanography, J. Mar.Syst., 16, 323-340.

Rigor, I. 2002. IABP drifting buoy, pressure, temperature, position, and interpolated ice velocity. Compiled by the Polar Science Center, Applied Physics Laboratory, University of Washington, Seattle, in association with NSIDC. Boulder, CO: National Snow and Ice Data Center. Digital media.

Shine, K. P., D. A. Robinson, A. Henderson-Sellers, and G. Kukla, 1984: Evidence of Arctic-wide Atmospheric Aerosols from DMSP Visible Imagery. *J. Appl. Meteor*., 23, 1459–1464.

Stark, J.D., J. Ridley and F. Hilton, 2005, Synergistic Use of Remote Sensing Data in Coupled Ocean-Ice Model Data Assimilation. Final Report for ESA, under ESTEC Contract No.17334/03/NL/FF. Available from the Met. Office, Exeter, UK.

Steele, M., R. Morley and W. Ermold (2001). "PHC: A global ocean hydrography with a high quality Arctic Ocean." Journal of Climate 14: 2079-2087

Uppala, S. (2001), ECMWF Reanalysis, 1957-2001, ERA-40 - Proceedings of workshop Re-analysis, 5-9 november, ECMWF, Reading.

Weaver, A. T., and P. Courtier, 2001: Correlation modeling on the sphere using a generalized diffusion equation. *Quart. J. Roy. Meteor. Soc*., 127, 1815–1846.

Weaver, R. Steffen, K., Heinrichs, J. Maslanik, J. And Flato, G. 2000. Data assimilation in sea-ice monitoring. Ann. of Glaciol. 31:327-332.

Whitaker, J. S., and T. M. Hamill, 2002: Ensemble data assimilation without perturbed observations. *Mon. Wea. Rev*., 130, 1913–1924.

Yao, T., C. L. Tang, and I. K. Peterson, 2000: Modeling the seasonal variation of sea ice in the Labrador Sea with a coupled multicategory ice model and the Princeton ocean model. *J. Geophys. Res*., 105, 1153–1165.

Notebook

Editorial Board:

Laurence Crosnier

Secretary:

Monique Gasc

Articles:

Contact:

Please send us your comments to the following e-mail address: webmaster@mercator-ocean.fr

Next issue: April 2008